The development of an experimental system for insertion loss measurements using a truncated, transient parametric array operating in a wide bore tube

Anastasiadis, Kosmas

Award date:
1990

Awarding institution:
University of Bath

THE DEVELOPMENT OF AN EXPERIMENTAL SYSTEM FOR INSERTION LOSS MEASUREMENTS USING A TRUNCATED, TRANSIENT PARAMETRIC ARRAY OPERATING IN A WIDE BORE TUBE.

submitted by Kosmas Anastasiadis

for the degree of PhD

of the University of Bath

1990

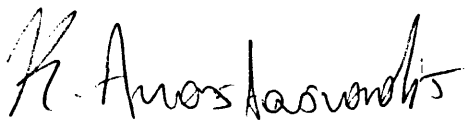

ProQuest LLC
789 East Eisenhower Parkway
P.O. Box 1346
Ann Arbor, MI 48106-1346

SUMMARY

The operation of a truncated transient parametric array in a wide bore tube was investigated both theoretically and experimentally. A 52cm long parametric array was formed by a 5cm diameter circular piezoelectric piston transducer radiating a 960kHz primary wave modulated by a 20kHz raised cosine envelope. The transmitter radiated along the axis of a 2m long plastic (ABS) tube with an internal diameter of 47cm. The inner surface of the tube was covered with neoprene rubber to avoid coupling of the wavefield into the tube wall. The experimental system and procedure used to obtain data have been described in detail. Results were presented for difference frequencies in the range 5-50kHz. The contributions to the difference frequency pressure due to the direct arrival and waves reflected once from the tube wall were considered. Although the difference frequency pressure amplitude at the tube wall was low, the focussing effect of the curved surface resulted in a significant contribution to the wavefield on the tube axis. Theoretical results predicting the strength of the single reflected wave were presented. The theoretical results confirmed experimental observations at an axial receiver that indicated a strong tail in the time waveform after the arrival of the direct signal due to reflections from the tube wall. Efforts to reduce the relative strength of the reflected signal concentrated on the use of large synthetic receivers for improved directionality and on the use of absorbing wedges on the tube wall to reduce the strength of the reflection. Insertion loss measurements indicated that the system can provide reliable results in the frequency range of interest.

ACKNOWLEDGMENTS

I would like to acknowledge the continual encouragement and support of my supervisor Dr V.F. Humphrey and also that of Professor H.O. Berktay.

Sincere thanks are extended to the technician for the underwater acoustics group Mr Brian Gay for his help in the development of the experimental system.

I would also like to thank my wife Sophia for her support and for her patience with me during the final stages of the preparation of this thesis.

This work was supported by the Procurement Executive of the Ministry of Defence.

Table of Contents

LIST OF SYMBOLS

a	:-	transmitter radius
b	:-	tube radius
c_o	:-	equilibrium sound velocity
d	:-	hydrophone-test panel separation, receiving element separation (chapter 5)
$f_{1,2}$	:-	primary frequencies
f	:-	difference frequency
F_{env}	:-	frequency of the envelope of the transmitted pulse
g,h	:-	auxilliary functions [83]
H	:-	water level in the tube
$H_o^{(1),(2)}$	:-	Hankel functions of order one and of the first or second kind
$J_{o,1}$	:-	Bessel function of the first kind and of first or second order
j	=	$\sqrt{-1}$
k	:-	difference frequency wavenumber
$K_{1,2}$	:-	primary frequency wavenumbers
R	:-	observation distance
$R(\theta)$	:-	Rutherford scattering directivity
R_{o+}	:-	Rayleigh distance at the primary frequency
$R_{1,2}$	:-	segments of the geometrical ray paths of the reflected waves
s	:-	source point-observation point separation
S_o	:-	primary beam cross-sectional area
t	:-	time variable
t	=	$\frac{R-z}{2}$
u	:-	particle velocity
Y_1	:-	Neuman function of the first kind and first order
z	:-	axial distance variable
Z	:-	acoustic impedance
α	:-	mean attenuation coefficient at the primary frequencies
β	:-	parameter of nonlinearity of water

L	:-	parametric array length, receiving aperture length (chapter 5)	ρ_o	:-	equlibrium water density
p	:-	difference frequency pressure	θ	:-	observation angle (measured from the acoustic axis)
$P_{1,2}$	:-	primary frequency pressures	ϕ, ψ, γ	:-	angle variables
$Q(\underline{r})$	:-	difference frequency source strength at field point $\underline{r}$	Φ	:-	normalised reflected wave spectrum
q	:-	difference frequency source density function	ω	:-	difference frequency angular velocity
r	:-	radial distance			

1 INTRODUCTION

There is a need in underwater acoustics to determine the transmission characteristics of limited size panels over a frequency band in the 10-50kHz region. It is also desirable to assess the performance of those materials under high hydrostatic pressure.

Tank facilities have been developed for this purpose and are in operation in several laboratories throughout the world. These are usually large tanks which are not very practical in terms of size, cost or ease of use. In contrast, the present facility is built around a tube 2m high and 50cm outside diameter which can easily be accommodated in the laboratory. The aim is to design a compact system that will enable acoustical measurements to be performed quickly but with the accuracy of the larger facilities.

Several problems are encountered in the design of such a system and they are mainly associated with the smallness of the tube diameter and the cylindrical shape of the tube wall which give rise to sound wave reflections that can lead to large uncertainties in the measured quantities.

The sound source used with this facility is a truncated parametric array. It was selected for its highly directive beam in order to reduce the insonification of the tube wall and hence minimize reflections. It was also chosen because it is capable of generating a wideband signal in the frequency range of interest. Thus it is possible to obtain results over a wide frequency range using a single transmitting transducer and a single experimental measurement. An investigation of the operation of the truncated parametric array in a wide bore tube is presented here.

In chapter 2 a survey of the relevant literature is presented. Two areas of interest are identified and investigated separately: (a) the parametric array and (b) the acoustical measurement of the material properties of samples.

The experimental system is described in chapter 3 along with the experimental procedure followed in order to obtain the data presented in later chapters.

The theoretical treatment of the operation of the truncated parametric array in a wide bore tube is presented in chapter 4. Several theoretical models are developed for this purpose and numerical and analytic results are compared with experimental results in order to assess their accuracy and the validity of the assumptions made in the derivation of these results. The appendices at the end of this thesis contain more of the mathematical details of the derivation of these theoretical results.

The theoretical results confirm experimental observations at an axial receiver, without a test panel interposed, which indicate a strong tail in the time waveform after the arrival of the direct wave from the transmitter to the receiver. This tail is attributed to reflections of the low frequency wave at the tube wall which follow a longer path and hence are delayed relative to the direct arrival. This delay, the extra path length, is determined by the position of the low frequency source point within the source volume and also on the number of reflections suffered by the wave before its arrival at the receiver. When every point within the parametric source volume is considered, we obtain quite a complicated picture even if only geometrical ray paths are considered and this investigation is restricted to the study of only single bounce waves within the tube. This is acceptable in practice because the path lengths associated with double, triple etc reflections are such that these contributions can easily be removed with an appropriate time window on the received wave.

The experimental attempts to reduce the relative strength of the single bounce reflected wave are described in chapters 5 and 6. Chapter 5 contains the results obtained by applying synthetic aperture techniques to obtain a directive receiver that has good response to the direct wave arrivals but is able to reject off axis arrivals due to reflections at the tube wall.

Chapter 6 contains details of the construction, use and results obtained with a set of absorbing wedges mounted on the tube wall in order to cover the regions where reflections seem to originate.

In chapter 7, some experimental insertion loss measurements are presented. An acoustically 'hard' and an acoustically 'soft' sample are investigated and the results obtained are compared to reliable 'free-field' experimental results obtained in a tank facility. Some of the errors associated with these measurements are identified and investigated.

The most important points arising from this investigation are recapitulated together with the discussion and conclusions in chapter 8.

2 LITERATURE REVIEW: PARAMETRIC ARRAYS, ACOUSTIC MEASUREMENTS OF MATERIALS AND IMPEDANCE TUBE SYSTEMS

The three main areas of interest in this thesis cover the development and use of the parametric array as a sound source, acoustical measurements of materials and the use of impedance and pulse tube systems to perform materials measurements.

2.1 THE PARAMETRIC ARRAY

Interest in the interaction of sound waves dates back to the 18th Century and Lamb [1] credits the first observation of difference frequency tones to Sorge (1745) and Tartini (1754). Subsequent interest in the scattering of sound by sound dates back to last century when Rayleigh [2] considered the scattering of sound from regions in which both density and compressibility were assumed to be different from the equilibrium values in the medium. Rayleigh's treatment formed the basis for the study of the case where the variation of density and compressibility in a given region of the medium is caused by a second sound wave.

Contemporary work on the generation of difference frequency sound by the nonlinear interaction of two sound waves started with two classic papers by Westervelt [3,4].

Before we go into a more detailed account of the generation of low frequency waves using Westervelt's parametric arrays and their subsequent theoretical and experimental development it may be useful to clarify the basic principles governing the behaviour of transmitting parametric arrays. In the simplest case, the parametric array consists of a primary transducer transmitting high frequency pump waves into a volume of water. The pump wave often consists of a two frequency signal (but see section 1.2) with neighbouring frequencies f_1 and f_2. If the intensity of the primary waves is sufficiently great, it is not adequate to use the equations of linear acoustics to describe the wave propagation. If the nonlinear terms appearing in the wave equation are accounted for,

additional waves appear in the medium with new frequencies that were not present in the primary radiation. Nonlinear propagation leads to the generation of second and higher harmonics $2f_1, 2f_2, 3f_1$, etc, as well as waves at the sum $(f_1 + f_2)$ and difference $f_- = f_1 - f_2$ frequencies. The region of interaction of the primary waves may be limited by absorption, saturation (see section 1.1), diffraction (spreading loss) or artificially by means of an acoustic filter. The region of interaction where the difference frequency waves are generated plays the role of a volume array radiating at the difference frequency f_- and is usually known as a parametric array.

In [4], Westervelt (1963) formulated his now classical theory for the parametric array, a name given to the collinear sound interaction region by analogy to the concept of electrical parametric amplification. He based his derivation of the wave equation for the difference frequency pressure on the following assumptions:

1) the equation of motion for an ideal fluid is used and the attenuation effect is introduced in an 'ad-hoc' way.

2) The two superimposed, high frequency, plane primary waves are assumed to form beams so narrow and so perfectly collimated that the volume distribution of sources can be assumed to be small compared with the wavelength at the difference frequency.

3) No attenuation of the difference frequency wave is assumed to occur.

4) The attenuation coefficients of the primary waves are equal, and one or more orders of magnitude less than the wavenumber of the difference frequency wave. In addition they result essentially from linear processes, i.e. nonlinear attenuation is negligible.

Allowing for the above assumptions, Lighthill's [5-7] exact equation for arbitrary fluid motion was transformed by Westervelt into the following inhomogeneous wave equation for the difference frequency pressure (p):

$$\nabla^2 p - \frac{1}{c_o^2}\frac{\partial^2 p^2}{\partial t^2} = \Box^2 p = -\rho_o \frac{\partial q}{\partial t} \qquad \ldots(2.1)$$

were:

$$q = \frac{\beta}{\rho_o^2 c_o^4}\frac{\partial P_i^2}{\partial t} \qquad \ldots(2.2)$$

Here q is the difference frequency source density function and p_i is the primary frequency pressure amplitude. β is related to the second order nonlinearity ratio B/A of the fluid through $\beta = 1 + B/2A$.

The result of applying equation (2.1) for an observation point (R,θ) in the far field of a parametric array is [4]:

$$p(R,\theta) = \frac{\omega^2 P_o^2 S_o \beta}{8\pi R \rho_o c_o^4} \frac{\exp j(kR - \omega t)}{\left(\alpha - jk \sin^2\left(\frac{\theta}{2}\right)\right)} \qquad \ldots(2.3)$$

or, in absolute value:

$$|\, p(R,\theta)\,| = \frac{\omega^2 P_o^2 S_o \beta}{8\pi R \rho_o c_o^4} \frac{1}{\sqrt{\alpha^2 + k^2 \sin^4\left(\frac{\theta}{2}\right)}} \qquad \ldots(2.4)$$

ω:- difference angular frequency

P_o:- primary pressure level (assumed equal for both primaries)

S_o:- Primary beam cross-sectional area

R:- observation distance

α:- mean attenuation coefficient of primaries

θ:- observation angle.

Two conclusions can be drawn from equation (2.4):

(1) The secondary pressure amplitude is proportional to the square of the primary pressure

amplitude (this term is really the product of the primary pressure amplitudes).

(2) The total 3dB beamwidth of the difference frequency beam is given by $2\theta_{3dB}$ were:

$$\theta_{3dB} = 2\sin^{-1}\sqrt{\left(\frac{\alpha^2}{k^2}\right)} \approx 2\left(\frac{\alpha}{k}\right)^{\frac{1}{2}} \qquad \ldots(2.5)$$

and θ_{3dB} is independent of level. The angular dependence of equation (2.4) is the same as that for Rutherford scattering in atomic theory.

Since Westervelt's publication, a great deal of theoretical and experimental work has been done to improve the understanding of the characteristics of the parametric array and find applications of this new and unique tool.

The first experimental verification of Westervelt's predictions came from Bellin and Beyer [8]. They performed experiments in water and, with limited success, in air. Using a 1in diameter 13.5MHz quartz crystal, they produced difference frequencies in the region 1-2.05MHz in water. They obtained narrower beamwidth at the difference frequency than that predicted theoretically and also lower difference frequency pressure amplitude. They attributed these discrepancies to the fact that with their experimental arrangement it was not possible to work entirely within the Fraunhofer region assumed by the theory. It was also shown that the difference frequency could not have been generated by the transducer or in the electronic equipment.

Zverev and Kalachev [9] performed experimental measurements using a truncating acoustic filter to limit the length of the interaction region to within the nearfield of the primary radiation. This was done in order to simulate more accurately the conditions adopted by Westervelt were the primary beams are well collimated. The primary frequencies were about 5MHz and the difference frequency 39kHz. This meant that the difference frequency waves were not attenuated appreciably within the distances considered and also ensured that the primary beam width was small compared with the

difference frequency wavelength, enabling the parametric array to be considered as a line source. They obtained good agreement between theory and experiment as far as the difference frequency beamwidth is concerned but the actual pressure values were lower than the theoretical ones. This was considered to be due to the finite cross-sectional area of the interaction volume.

Further investigations were performed in order to reconcile the differences between theoretical and experimental results. Berktay [10,11] and Berktay and Smith [12] discussed the effect of the finite aperture of the primary beams and arrived at the following expression for the far-field directivity of the difference frequency wavefield assuming a rectangular projector of sides 2b and 2d:

$$D(\theta)=\frac{|\,p(R,\theta)\,|}{|\,p(R,0)\,|}=R(\theta)\left|\frac{\sin(kdsin\theta)}{kdsin\theta}\frac{\sin(kbsin\theta)}{kb\sin\theta}\right| \qquad \ldots(2.6)$$

Where p is the difference frequency pressure amplitude. Experimental investigations of Berktay and Smith [12] with a rectangular transducer did provide some improvement in the agreement of theoretical and experimental estimates of the difference frequency beamwidth. Naze and Tjotta [13] treated the same problem but for primary beams with circular cross-section of radius 'a' and derived the following formula for the difference frequency field directivity:

$$D(\theta)=\frac{|\,p(R,\theta)\,|}{|\,p(R,0)\,|}=R(\theta)\left|\frac{2J_1(kasin\theta)}{kasin\theta}\right| \qquad \ldots(2.7)$$

In equations (6) and (7) R(θ) is the Rutherford scattering directivity formula predicted by Westervelt [4] which, with the inclusion of absorption becomes:

$$R(\theta)=\frac{\alpha_1+\alpha_2-\alpha_-}{\left[(\alpha_1+\alpha_2-\alpha_-)^2+4k^2\sin^4\left(\frac{\theta}{2}\right)\right]^{\frac{1}{2}}} \qquad \ldots(2.8)$$

α_1 and α_2 are the absorption coefficients at the primary frequencies and α_- that at the

difference frequency.

Both (6) & (7) reduce to R(θ) (equation (2.8)) when ka (or kb and kd) ≤1 thus showing that the assumption of a narrow perfectly collimated beam is consistent for small beam cross-sections. For wider beams, ka≥1, the directivity factor equals one on the axis (θ=0) and is smaller than one elsewhere. Formulae (6) & (7) provide stronger directivity, but still the same maximum, as that predicted by Rutherford scattering.

If divergent sound beams with Bessel directivity are assumed, then ever stronger directivity is predicted for ka≥1 [13]:

$$\frac{|p(R,\theta)|}{|p(R,0)|} = R(\theta) \cdot \begin{cases} \frac{2}{\pi}\cos^{-1}\mu - \mu(1-\mu^2)^{\frac{1}{2}} & \mu < 1 \\ 0 & \mu \geq 1 \end{cases} \qquad \ldots(2.9)$$

were:

$$\mu = \frac{ka}{4\sin\theta}$$

For ka≤1 we again obtain R(θ) (equation (2.8)).

Hobaek [14] performed experimental measurements along similar lines to those of Bellin and Beyer [8]. In order to reproduce the conditions assumed for the theoretical models that existed (equations (3), (6), (7), (9)), and eliminate any near field effects, he suggested the introduction of an acoustic filter at the Fresnel distance of the primary beams were the transition from near to far field occurs. This filter would allow the primary waves to pass unaffected but attenuate any difference frequency waves generated within the primary nearfield. Thus, any difference frequency waves present would be generated by interaction within the farfield of the primaries. Such a filter, however, could not be devised and Hobaek's measurements included the Fresnel region. He observed a

directivity sharper than that given by Rutherford scattering and in good agreement with equation (2.7) in spite of the inclusion of the Fresnel zone. His measurements also indicated that the amplitude of the difference frequency sound generated in the Fresnel zone was about a quarter of that expected theoretically for collimated plane waves in this region. He also measured the axial difference frequency pressure as a function of distance from the source. The pressure increased from zero at the source, reached a maximum and then decreased with increasing distance. The position of the maximum pressure is governed chiefly by the attenuation of the primary waves and the divergence of the generated wave. The predicted [13, 15] positions of the maxima did not agree with experimental observations and this discrepancy was again attributed to the unavoidable presence of the Fresnel region were the theoretical conditions are not met.

The quasilinear plane wave approach was extended by Berktay [11] to include the case of cylindrically or spherically spreading primary beams. He found that the 3dB beamwidth of the difference frequency waves arising from the interaction of cylindrically or spherically spreading primaries does not deviate from that given by equation (2.8) provided the 3dB beamwidth of the primary spreading waves does not exceed that given by equation (2.8). Thus, the beamwidth of the difference frequency wave will not only depend on the frequencies of the primary waves but also on their original beamwidth.

Experimental results involving spherical waves were reported by Muir and Blue [16]. By performing their experiments in a fresh water lake, they were able to perform measurements in the far field of all radiations. Primary waves at 1124kHz and 981kHz were radiated from a split face 2in x 2in piston transducer leading to a difference frequency of 143kHz. They found a broader beamwidth for the difference frequency wave than that predicted by equations (6) or (8), while earlier experiments on plane primary wave parametric arrays [8,9,12,14] found narrower half-power beamwidths than predicted by theory. This discrepancy was ascribed to deviations between the

experimental conditions under which the various experiments had been performed. A suggested explanation of the experimentally observed narrower beamwidths is that a great deal of interaction between the primary waves takes place within the Fresnel zone of the transmitting source while the theory is developed assuming that the interaction takes place in the Fraunhofer zone. This is significant for the case of plane primary waves but not very important for the cylindrically or spherically spreading waves were the majority of the interaction takes place in the Fraunhofer zone. Berktay [17] showed that if the nonlinear interaction between primary waves takes place in the Fresnel region of the projector, this may indeed cause a small reduction in the difference frequency pressure in the far field but has little effect on its directivity pattern.

Another factor which may cause a deviation between theoretical and experimental results is the measurements being performed at a position not far from the interaction region. Berktay and Shooter [18] showed that beam patterns within the nearfield of the parametric array can be substantially narrower than the far field beam patterns (equations 2.5, 2.6, 2.7, 2.8).

2.1.1 ACOUSTIC SATURATION

As can be seen from equation (2.3), the pressure amplitude of the difference frequency wave is directly proportional to the product of the pressure amplitudes of the primary waves. But, as is well known, during the propagation of finite amplitude sound waves, higher harmonics are formed, due to the inherent nonlinearity of sound transmitting media, leading to a transfer of energy from the fundamental frequencies to their higher harmonics and leading to higher absorption than that for small signals. This leads to loss of energy that would otherwise be available for the production of difference frequency sound. This phenomenon is known as acoustic saturation. The range of

publications on this subject is enormous (see, for example, [19-21] and references therein). The finite amplitude absorption effect as it relates to parametric arrays has been studied extensively [22-28].

Bartram [22,23] considered the measurements performed by Mellen, Browning and Konrad [29] who observed that the functional dependence of the difference frequency level on primary level goes over from quadratic to linear, and the beamwidth broadens, at high levels. He substituted the attenuation of a shocked wave for the simple linear attenuation used by Westervelt: The resulting Green's function integral had no closed form solution but could be expressed as an infinite hyperbolic series solution. A closed form solution was possible on axis where good agreement was obtained with previous experimental results [25,29].

Fenlon [26,27] introduced the use of Burgers' equation for a description of the influence of the nonlinear and the dissipative effects in the Fresnel and Fraunhofer regions, without including shock formation.

Childs [28] performed numerical calculations to find the beam patterns and directivity indices of saturated parametric arrays. He showed that the beamwidth increases and the directivity index decreases in agreement with experimental measurements of Mellen et Al [29].

In addition to the limitation of the array length due to saturation at high primary levels, the occurrence of cavitation and gas bubbles influences the performance of low frequency parametric arrays [30]. Some attempts to reduce bubble/cavitation problems and increase the conversion efficiency involve pressurisation of the interaction volume of the parametric array [31] or the use of more suitable media for the formation of the interaction volume. This means the use of media with high nonlinearity parameter (B/A), low density and/or low sound velocity (see equation (2.4)). Ryder et al [32] reported the use

of silicone rubber for the interaction volume, Bjorno et al [31] used ethyl alcohol and methyl alcohol suitably confined and, more recently, Jongens [33] reported the use of Freon. All such investigations led to higher difference frequency pressure levels than those obtainable in water. Also, the lower sound velocity leads to a slow waveguide antenna effect which further narrows the beamwidth of the transmitted difference frequency beam.

Woodsum [34] put forward a suggestion whereby the efficiency of the parametric conversion can be increased by saturation suppression in water, if the attenuation coefficient at the second harmonic frequency of the primary wave can be selectively increased. The introduction of microscopic air bubbles which are resonant at the second harmonic frequency was proposed. The parameter of nonlinearity also increases when the bubbles are introduced; hence, parametric efficiency should be enhanced by both these effects. Lockwood et al [35] published an investigation of the increase in the parametric array efficiency due to bubbles produced by forcing air through a microporous filter in the array showing a large pressure level increase (≈30dB) at short distances but lower gain (≈14dB) at longer distances due to increased primary absorption beyond the bubble screen.

Amplitude modulation of the primary waves, which forms the basis of the transient parametric array, is an alternative way of increasing the cavitation threshold over that for continuous waves thus leading to an increase in the difference frequency levels obtainable [31].

2.1.2 THE TRANSIENT PARAMETRIC ARRAY

The parametric array described by Westervelt and utilised in the works mentioned so far operates in what is known as the spot frequency mode. That is, a single (spot) difference frequency wave is produced by the interaction of two essentially continuous primary waves.

Berktay [11] suggested the production of transient signals by the use of a modulated primary wave. He considered a collimated and plane pulsed carrier wave travelling along the x-direction, the primary differential pressure P_i at point x and time t being represented in the form:

$$P_i(t,x) = P_1 e^{-\alpha_1 x} f\left(t - \frac{x}{c_o}\right)\cos(\omega_1 t - K_1 x) \qquad \ldots(2.10)$$

Where the subscript '1' is used to denote the primary quantities. Here f(t) represents the envelope function, which has a frequency spectrum such that the highest Fourier component occurs at a frequency very much lower than that of the carrier. This condition permits the use of α_1 as the absorption coefficient for all frequencies in this band limited signal.

In equation (2.2) it is shown that the source density for the scattered sound depends on the partial time derivative of P_i^2. Now:

$$P_i^2(t,x) = 0.5P_1^2 e^{-2\alpha_1 x} f^2\left(t - \frac{x}{c_o}\right)[1 + \cos(2\omega_1 t - 2K_1 x)] \qquad \ldots(2.11)$$

Thus, P_i^2 can be considered to be the sum of two components; one of the components will give rise to a high frequency signal that is not of interest here. Substitution of the remaining component of P_i^2 into the expression for the source density function q (equation (2.2)) gives :

$$q = \frac{P_i^2}{2\rho_o^2 c_o^4} e^{-2\alpha_1 x} \frac{\partial\left(f^2\left(t - \frac{x}{c_o}\right)\right)}{\partial t} \qquad \ldots(2.12)$$

In this case, the source density component is not a single frequency one but covers a band of frequencies determined by the form of the modulating function f(t). It turns out that the difference frequency pressure at (t,x) on the acoustic axis is given by:

$$p(t,x) = \frac{\beta P_1^2 S_o}{16\pi\rho_o c_o^4 x \alpha_1} \frac{\partial^2\left(f^2\left(t - \frac{x}{c_o}\right)\right)}{\partial t^2} \qquad \ldots(2.13)$$

where no restrictions are put on the form of f(t) except that it has a maximum value of unity. S_o is the cross-sectional area of the primary beam.

Berktay called the process of formation of the transient parametric array 'self-demodulation of a pulsed carrier'. The most important advantages to be gained by this process are:

a) the generation of a difference frequency pulse with a wide spectral band in a manner that can be predetermined by the appropriate choice of a modulating function, and,

b) by using a short pulse duration, higher transmitted power densities may be utilised with reduced cavitation problems in water (the significance of this may be seen in the discussion of acoustic saturation).

This mode of operation of the parametric array is also known in the literature as the impulse or pulse mode of operation to discern it from the spot frequency mode described by Westervelt. Both modes of parametric generation result in the generation of highly directive low frequency waves.

Throughout the work described here, a parametric array operating in the impulse mode of operation was used since it is ideal for testing the properties of a specimen as a function of frequency by spectral analysis.

The first experimental verification of Berktay's suggestion came from Moffet et al [36,37]. Since then the transient parametric array has been investigated extensively both experimentally and analytically [38-41] and has become a useful tool for the production of wideband low frequency radiation [see 42-44, 72, for a general survey of parametric array systems now in operation in the USSR see ref. 20].

For a more detailed account of the development of the parametric array since its inception along with a more precise mathematical formulation of the basic ideas discussed here the interested reader is directed to several review articles [48-52] of developments within the academic community as well as practical applications ranging from materials testing under laboratory conditions, high resolution bottom and sub-bottom profiling at sea, detection and echo ranging systems, underwater communications, fish stock estimation and location [53,20] and even the use of a parametric echoscanner for medical diagnostics [54].

2.1.3 NUMERICAL SOLUTIONS OF THE FIELD OF A PARAMETRIC RADIATOR

Closed form solutions of the inhomogeneous wave equation for the field of a parametric radiator involve various simplifications and approximations. If more sophisticated models are required in order to improve the agreement between theoretical and experimental results when the theoretical assumptions are not met, it is necessary to resort to the numerical solution of some complicated mathematical expressions.

The purpose of this section is merely to present the various sophisticated models that have been constructed and solved for parametric sound generation rather than provide

an in depth review of the available results. As will be seen in later sections dealing with the theoretical treatment of the parametric array in a wide bore tube, added complications arise due to the geometry of the experiment and fully rigourous theoretical models become prohibitive in terms of the computational effort required.

Computational difficulties are encountered when effects such as diffraction, highly nonlinear primary wave propagation, nonlinear attenuation and interaction must be accounted for consistently and simultaneously by the theoretical model.

Bartram [22] modified Westervelt's model and substituted the attenuation of a shocked wave in place of the simple linear attenuation used by Westervelt. The resulting Green's function integral no longer had a closed form solution but could be expressed in terms of a hypergeometric series solution. On axis the series converged to a closed form solution and off-axis it was quite simple to obtain results with the help of a computer.

Fenlon [26,27,55] used a numerical solution of Burgers' equation to calculate the nonlinear interaction, and hence difference frequency generation, of finite amplitude primary waves. Burgers' equation is a simplified form of the nonlinear wave equation which accounts for nonlinearity and absorption but is restricted to one dimensional progressive waves travelling in one direction only. The only diffraction effect is spreading loss which can be incorporated for plane, cylindrical and spherical waves, This approach allows dissipation effects to be accounted for in a rigourous fashion but its application to problems involving the directivity of parametric arrays is limited.

Muir and Willette [56] extended Westervelt's model to include geometric features of the interaction volume. In his original paper, Westervelt adopted a line array model for the interaction region. Muir and Willette assumed shock-free propagation and treated spherical (primary) wave interaction in the far-field of a piston source. This leads to a volume integral for the virtual sources that has to be evaluated numerically. This model

is restricted to cases when the primary frequencies are low enough to provide a diffraction (spreading loss) limited one and that means low primary frequencies in water. In fact, Muir and Willette reported good agreement with experimental results obtained in fresh water lake experiments. At higher frequencies, such as those used here, this model would prove inadequate since the interaction region is limited to within the primary nearfield.

Berktay and Leahy [57] followed the same quasilinear treatment of Westervelt and Muir and Willette and treated diffraction limited parametric arrays produced by both circular and rectangular primary transducers. Some normalised results were obtained through numerical computation of scattering integrals and were presented in the form of design curves.

Moffett and Mellen [58-61] have published extensively on the numerical computation of the field of a parametric radiator. They assume the following simple model for the primary field and thus for the virtual source volume: the nearfield is approximated by a collimated plane wave of cross-section S_o, equal to the transducer cross-section, extending to a distance $R_{o+} = \frac{S_o}{\lambda_o}$ (where λ_o is the primary wavelength), while the farfield is a spherically spreading beam confined within a cone of half angle $\theta_o = \frac{2}{K_o a}$ (where a is the piston radius). Both small signal absorption and saturation limited parametric arrays can be treated and expressions are presented for both the near ($<R_{o+}$) and far field of either an absorption or saturation limited array. Their solution is a modification of the Green's function scattering volume integral solution previously adopted by Westervelt and Berktay with modifications to allow for the geometry of the source volume and nonlinear attenuation.

A more sophisticated mathematical model was constructed and used by Tjotta and Tjotta and various co-workers [62-65]. Their model is based on a modification of Burgers' equation which in addition to nonlinearity and attenuation, accounts consistently for the

radial variation of the acoustic field and can thus tackle diffraction effects. This equation is generally known as the Khokhlov- Zabolotskaya- Kuznetsov (KZK) equation after the workers who first derived it. The field is evaluated within the quasilinear approximation, that is, the linear solution for the primaries is substituted in the nonlinear source term of the governing (KZK) equation. The expression for the strength of the virtual difference frequency source strength at a general point involves a volume integral that cannot be evaluated analytically. Garret et al [63,64] report very good agreement between numerical and experimental results at very low frequencies (0.5-5kHz). Although this model is quite sophisticated, it is not suitable for the geometry of the experiment performed here: if we consider that a volume integration has to be performed to find the field at a point on the inner tube wall and a further surface integration to find the field at a point in the tube due to the sources on the tube wall, it becomes evident that five numerical integrations of a non-trivial integrand would present unacceptable difficulty.

More recently, Foda and Ginsberg [66] used the same starting point (the KZK equation) to investigate finite-amplitude effects in dual frequency beams, treating parametric radiation as a special case within their scope. Their solution ignores the effect of absorption and accounts to the same accuracy for diffraction and nonlinearity for field point at distances less than the shock formation distance. Although an alternative mathematical treatment is used to that employed by [63-65], the resulting expressions are again not simple enough for the present purposes.

It must be said here that computational complexity is not the only factor affecting the choice of model to be used for this work. The fact that the parametric array used here operates in a simple manner similar to that originally treated by Westervelt makes most numerical models reported in the literature seem over elaborate.

2.2 ACOUSTICAL MEASUREMENT OF MATERIAL PROPERTIES- A BRIEF REVIEW OF STANDARD RESULTS

The experimental investigation of the acoustical properties of a material immersed in water usually involves the measurement of the insertion loss and/or the echo reduction of a sample of the material. The operational definition of these quantities is:

$$\text{Insertion loss} = 20\log_{10}\left[\frac{\text{Incident sound pressure}}{\text{Transmitted sound pressure}}\right] \qquad \ldots(2.14)$$

and

$$\text{Echo reduction} = 20\log_{10}\left[\frac{\text{Incident sound pressure}}{\text{Reflected sound pressure}}\right] \qquad \ldots(2.15)$$

Alternatively, the transmission and reflection coefficients are discussed and can be simply related to the quantities above (they are the reciprocals of the terms in the square brackets above, respectively).

The word 'material' is used to mean any one or a combination of acoustic filters, windows (high transmissivity), reflectors (high reflectivity), baffles (low transmissivity), anechoic coatings (low reflectivity) or sound absorbers.

Quite often, test samples come in the form of panels of limited dimensions. When measurements are performed, the dimensions, configuration and means of support of the sample influence the result. Removing the influence of those factors from the measured quantities is of the utmost importance when designing an experiment.

When the elastic properties of the sample are known, it has a simple shape and no configuration problems are encountered, it is possible to predict its insertion loss and echo reduction [67]. Experimental measurements are still required, however, in order to verify theoretical results in cases when the sample's shape and configuration prohibit theoretical calculation.

The standard experimental procedure for the determination of the transmission coefficient of a panel using an acoustical method involves the use of a directional source and a receiver in a laboratory tank, in a fresh-water lake or at sea. The change in the output of the receiver when the test panel is inserted is used to determine its transmission coefficient. The method has been described in some detail by Bobber [68] and has been used extensively by several authors [67-72] for measurements on different test materials.

One requirement for reliable measurements is the availability for a directional source radiating at the frequencies of interest. That is because the material under test often comes in the form of a panel of limited dimensions. Thus, diffraction effects may arise at the edges of the sample and interfere with the signal of interest.

The requirement for a directional acoustic source becomes harder to satisfy the lower the frequencies of the probing waves become. It is well known [73] that an acoustical beam becomes more directional as the size of the transducer increases in terms of the wavelength of the radiated frequency. For example, the farfield pressure distribution of a circular piston source operating linearly is given by:

$$P(R,\theta) = P(R,0)\frac{2J_1(ka\sin\theta)}{ka\sin\theta} \qquad \ldots(2.16)$$

were $P(R,\theta)$ is the pressure at distance R and at an angle θ to the normal to the source, $P(R,0)$ is the axial pressure at distance R, k is the wavenumber of the radiated wave, a the radius of the piston and J_1 a first order Bessel function. The first zero of the Bessel function occurs at:

$$ka\sin\theta = 3.833$$

thus, for a source radius of 2.5cm, for example, the first zero occurs at an angle of 2° when the radiated frequency is of the order of 1MHz whereas at a frequency of ≈50kHz this angle increases to ≈46.5°. In order to obtain the first zero at 2° with a 50kHz circular

source the radius of that source should be about 52cm.

Three solutions have been proposed in order to alleviate the diffraction problems associated with low frequency measurements:

a) an interferometric technique for the measurement of displacement on the panel surface,

b) the use of a small tube to confine the radiated wave and the sample under test, and

c) the use of the parametric array as the low frequency sound source.

A brief review of some of the developments concerning methods (a) and (b) mentioned above will be discussed in following sections.

The narrow beamwidth and low sidelobe level of the parametric array along with the wide bandwidth obtainable (several octaves) make it ideal for low frequency testing of the properties of limited size. A very successful system has been developed by Humphrey [44,72] for the measurement of the properties of limited size panels in a laboratory tank. This system involves the use of a truncated parametric array operating in the self-demodulation regime [11]. Reliable results have been obtained in the region of 10-100kHz using a single transducer and panels typically 45cm square.

2.3 IMPEDANCE AND PULSE TUBE SYSTEMS

An alternative method of measuring material properties in air and underwater is a system known as the impedance tube. The apparatus is so called because the measurement parameter that is usually quoted is the acoustic impedance of the material under test. The acoustic impedance can be inferred by the measurement of the reflection coefficient of the sample which, in turn, is determined from the standing wave pattern set up in the tube. Once the acoustic impedance is determined, other key parameters such as the attenuation coefficient and loss factors related to stiffness can be calculated [67].

Plane wave propagation is assumed within the tube and is usually attained by using a rigid walled tube with a diameter equal to a small fraction of a wavelength of sound in the water and test material.

Extensive investigations of aerial waves in tubes were performed by Kundt (1868) [74]. His investigations were primarily concerned with the determination of the speed of sound in various gases.

Kundt's experimental setup was substantially retained by Taylor (1913) [75] who was the first to perform experiments with a tube for the evaluation of various materials as sound absorbers. Taylor's investigations were prompted by the inadequacy of the method then used for the evaluation of various absorbers in architectural acoustics. The method then used was called the reverberation method and consisted of measuring the time of decay of the residual sound of an organ pipe with and without a known quantity of the absorbing material in a room.

Taylor devised a method whereby standing waves were set up in a tube in a similar manner described by Kundt. The sound source (an organ pipe of known frequency) was situated close to one end of the tube and the material under test at the other end. Standing waves were formed in the tube and by locating the positions of the maxima and minima inside the tube, as well as their amplitudes, it was possible to deduce the absorption (or reflection) coefficient of the test material.

By performing measurements in the tube, Taylor eliminated the effect of the interference system in a room on the absorbing power of the material under test.

Although the transduction techniques of that experiment seem primitive by today's standards (Taylor used fine powders to locate the positions of the nodes and antinodes),

and its scope unduly restrictive, the principles of the experiment are substantially retained in modern impedance tube measurements in both air and underwater measurements. The technique and some of its difficulties is well described in the literature [76-78].

Melling [79] gives a detailed account of the design, construction, calibration and performance of an impedance tube facility designed to operate over the frequency range 300-3250Hz; some of the mathematical principles involved are also presented.

Brouns [80] used a 10ft long, 30in diameter steel tube to perform low frequency (1-35Hz) measurements in air. He developed his facility to measure the performance of directional microphones at frequencies at which it is difficult to produce plane waves in anechoic chambers[1]. Because the experiment was performed in air, the inside diameter of the tube was a small fraction of a wavelength at the frequencies of interest and only plane waves propagated.

Sabin [81] described the use of a pulse tube for high hydrostatic pressure measurements of the acoustic impedance of various materials. The acoustic source and the test panel were again situated at either end of the tube. The probing pulse was recorded part-way down the tube, on the tube wall, on its way to the sample, and again, after it had been reflected by it. The magnitude of the reflection coefficient of the sample was then easily deduced from the ratio of the magnitudes of the two signals. The determination of the phase of the reflection coefficient involved the substitution of the test material by a perfect reflector (either very high or very low impedance) and comparing the phases of the reflected pulses. If the reflection coefficient as determined above is given by A,

1 For example, at 1Hz, if we consider the sound source as a point source, then in order to consider waves emanating from this source as plane waves, we must position the receiving microphone several hundred meters away (since $\lambda \approx 343m$). In that case, the experiment cannot be performed in an anechoic chamber.

and the acoustic impedance of water by Z_w, then the impedance of the test material can be determined from [67]:

$$Z = Z_w\left(\frac{1+A}{1-A}\right) \qquad \ldots(2.17)$$

Among the advantages he cites for his method over the standing wave (CW) method, Sabin includes such things as interference by tube wall coupling, extraneous modes etc. That suggests that some of the difficulties tackled in the present work where indeed identified by Sabin. In his case, however, these effects would be small since the diameter of the tube was small enough to enable it to sustain just plane longitudinal waves along the tube axis.

Impedance tubes are used extensively in marine technology laboratories throughout the world for the measurement of the acoustic properties of materials as they vary with frequency, hydrostatic pressure, temperature and angle of incidence in the region below ≈5-10kHz (and as low as a few Hz).

The extension of the impedance tube technique to higher frequencies, however, presents severe hardware problems. It has been shown [see for example 81] that the tube can be considered as a waveguide, and in order to have only the plane wave (normal) mode propagating the operating frequency f must satisfy:

$$f < \frac{0.585c}{2b} \qquad \ldots(2.18)$$

where 2b is the tube diameter and c the speed of sound. Above that frequency radial modes of vibration are excited in the tube and the nature of the wavefield becomes very complicated. It is, of course, the purpose of this work to overcome those difficulties. Using the above relationship, if measurements were required in the region of 30kHz the diameter required to enable only plane wave propagation is of the order of about 2.9cm.

A tube of such diameter would not be suitable. There would be problems with the production of such low frequencies from a transducer of this size and also, limiting the sample size to such an extent could be unacceptable.

Nicholls [42] describes the design of a pulse tube that operates in the region up to 100kHz. He does mention that 'extraneous signals' were identified which suggests that he indeed encounter some of the problems dealt with in this work. He does not present detailed experimental results so it is not possible to comment on the way he dealt with such problems. In any case, he used a conventional source and thus he did not have the broadband capability of the system used for this work.

2.4 AN INTERFEROMETRIC TECHNIQUE FOR ACOUSTIC IMPEDANCE MEASUREMENT

This technique is not used extensively and there is very little literature providing confirmation of its usefulness [42].

The technique provides direct point impedance measurement by using a laser interferometer to detect surface displacement. Since the particle velocity (u) is the first derivative of displacement, it is only necessary to determine the associated acoustic pressure (P) at a surface to obtain the impedance as:

$$Z = \frac{P}{u} \qquad \ldots(2.19)$$

The difficulties associated with this method concern the measurement of acoustic pressure as well as the acousto-optic effect on the measurement of displacement. When perfected, it could prove useful in the determination of the effects of heterogeneity of the test sample since it produces the response at a point on the sample rather than the total field response.

2.5 SUMMARY

The aim of this chapter has been to review some of the developments in two areas of interest in underwater materials characterisation, namely the parametric acoustic array and tube measurements of materials properties.

Some of the methods currently used for underwater materials characterisation have been reviewed. The inadequacy of currently available methods for such measurements in confined environments at the frequencies of interest is borne out. One promising [44-46,72] method used for materials characterisation in laboratory conditions uses a parametric acoustic array to produce wideband signals at the range of interest. The results obtained with the method are very good but to date the measurements had only been performed in a large tank where wall effects could be clearly identified and rejected. This makes operation of this facility at high hydrostatic pressure difficult.

An alternative method of materials characterisation involves the use of a conventional single frequency sound source operating in a narrow water-filled tube. The source operates in either a continuous (CW) or a pulse mode. The principle of operation relies on the assumption that only plane waves can be sustained within the tube with all other modes attenuated. Such apparatus is usually known as the impedance or pulse tube. The main advantage of the impedance tube is that it is very small and can easily be used for measurements under high hydrostatic pressures. It has, however, three drawbacks at the frequency ranges considered here:

(a) it turns out, that the diameter of a tube required to sustain normal mode operation only at the frequencies of interest is excessively small (a few cm) thus limiting the size of test sample,

(b) since a conventional source is used, in order to measure the frequency dependence

of the properties of the test sample, several sources are required,

(c) the limited size of the sample may give unrepresentative results for inhomogeneous materials.

Thus, a combination of the two methods outlined would have considerable advantages in being able to produce measurements in a confined environment over a wide frequency range. This thesis describe an investigation of such a test facility using a parametric acoustic array to produce the frequencies of interest. In this case the parametric array is formed in a wide bore tube suitable for large sample testing within a confined environment rather than in a pulse tube.

The parametric array is the most novel part of the experimental apparatus. Although its concept is not very old (Westervelt, 1960), its development has been rapid, co-ordinated and varied.

Some essential contributions to the development of the parametric array have been reviewed in section 2.1 and its most useful and relevant properties have been identified:

(a) wide frequency bandwidth,

(b) narrow beamwidth, and

(c) low sidelobe level.

Four distinct operating regimes for parametric sources have been identified:

(a) when the effective length of the parametric array volume is determined by the small signal absorption coefficient and is confined to the primary nearfield. This involves the use of relatively low-power, high-frequency primary beams. This model was considered in Westervelt's original theory and also forms the basis of the theoretical models developed here,

(b) as the primary frequencies are lowered. Small signal absorption is no longer sufficient

to confine the parametric array volume to within the primary nearfield and there is generation of the difference frequency in the farfield of the primary beams where a theoretical model for spherically spreading primaries is useful.
(c) as the primary power is increased, a third operating regime is encountered in which the array length is limited by nonlinear absorption in the primary nearfield. Such arrays are called saturation limited because their effective length is determined by the generation of harmonics and shock formation in the primary beams.
Finally, (d) the fourth extreme involves saturation limiting in the primary farfield. This regime is not frequently encountered in practise but could prove important if spherically spreading primaries are considered.

In addition, the parametric array has two modes of operation:
(a) the spot frequency mode where a single difference frequency is produced by the interaction of two primary beams. This is the concept put forward by Westervelt,
(b) the parametric array can also operate in the self-demodulation regime where a primary wave is modulated by one of lower frequency. In this mode of operation a wide band of difference frequencies is produced simultaneously. The bandwidth is determined by the shape and duration of the modulating envelope. This concept was put forward by Berktay.

The parametric array used in experiments here operates in the self-demodulation regime. The interaction volume is limited to within the primary nearfield by means of an acoustic filter that attenuates the primary frequencies substantially but leaves the difference frequencies practically unaffected. This arrangement is used to provide a source-free region in which the test panel is placed and also avoids the possibility of nonlinearities in the receiving hydrophone. The use of the acoustic filter allows the primary field to

be considered as a collimated plane beam leading to a uniformly strong source volume at the difference frequency and simplifying the theoretical treatment of the truncated parametric array in a wide bore tube considerably.

3 THE EXPERIMENTAL SYSTEM AND MEASUREMENT TECHNIQUE

3.1 MECHANICAL ARRANGEMENT

Most of the experiments described in this work were performed in a plastic (ABS) tube with an internal diameter of 47cm, 2cm thick and 2m high. When free-field tank experiments were required these were performed up in a tank 1.8m long x 1.2m wide x 1.2m deep.

Although a thick walled stainless steel tube would be required for experimental measurements under high hydrostatic pressures, a plastic tube was used for this test facility. This choice was made for several reasons:

a) there was no intention to use the facility for measurements under hydrostatic pressure,

b) the plastic tube is much lighter than an equivalent steel tube and thus presents fewer handling problems,

c) there are no corrosion problems, and

d) a plastic tube is cheaper and more easily available from local sources.

The internal diameter of the tube was largely dictated by the size of the panels that were likely to be tested in this facility. This diameter was chosen so as to allow a specimen to be cut from a 0.45m square sample so as to fill the tube cross-section.

The length of the tube was chosen so as to allow the formation of parametric arrays up to 1m long with enough room for a test panel and the hydrophone. Sufficient separation was also allowed between the water surface and the receiving hydrophone. This was necessary because the tube was not terminated with an absorber so that large reflections from the water-air interface occurred.

Since the tube wall confines the acoustic field inside the tube, its properties will affect the nature of that field. In order to disassociate the effect of the particular tube wall

material on the measured field inside the tube, a 4mm thick sheet of closed-cell neoprene rubber, mounted on a 1mm thick rolled aluminium backing sheet was used to line the inside surface of the plastic tube. The lining extended from the transducer towards the hydrophone for 1.2m. Due to the high air content of the neoprene rubber a compliant boundary was formed on the tube wall which acted as a perfect reflector for the field incident on it.

The high air content of the closed-cell neoprene rubber makes it buoyant. In order to fix the lining in position, the aluminium backing sheet was rolled to a larger bending radius to that of the tube. This coupled with the inherent flexibility of a thin metal sheet ensured that the lining could be fixed inside the tube with reasonable effort. Once inside the tube, the aluminium sheet recoiled to its original bending radius and pushed against the tube walls. Friction between the two surfaces ensured that the lining did not rise to the surface when the tube was filled with water.

In order to simplify the mechanical arrangement, tube filling procedures and prevent problems with air bubbles, the tube was positioned vertically. One end of the tube was faced off and fitted with a base plate and gasket. The tube was placed on a large aluminium base to spread the load and held in place by a frame made of aluminium angle. This frame also enabled a platform to be constructed of the same material at the top of the tube from which various items could be suspended into the tube.

The tube with its support structure and associated transmitting and receiving electronics is shown in photograph 1. Figure 3.1 shows a schematic arrangement of the various components inside the tube which are described below.

With these arrangements some problems were still encountered with air bubbles forming due to air coming out of solution. In particular air bubbles were found to form on the

neoprene lining. This problem was subsequently minimised by applying a thin coat of mild detergent (tepol) as a wetting agent onto the neoprene before filling the tube. In order to allow an equilibrium air concentration to be reached in the tube, 10-14 days were allowed between filling the tube and performing acoustic measurements.

The transducer was initially fixed to the bottom plate facing upwards. Subsequently, the transducer was placed onto a carriage that enabled the transducer position along the diameter of the tube to be adjusted from the outside. The transducer holder was mounted on two PTFE blocks which were allowed to slide on two stainless steel rails. The transducer could be moved by pulling or pushing a stainless steel rod connected to the transducer mounting plate and extended to the outside of the tube through a water tight opening near the bottom. Photographs 2 & 3 show the transducer carriage and transducer holder mounted on the base plate of the tube. In this arrangement the transducer face was 20cm above the base plate. Electrical connection to the transducer was made through an underwater connector, mounted on the inside of the tube, which can also be seen in photographs 2 & 3.

The acoustic filter that was used to truncate the parametric array was cut to a circular shape and fitted snugly inside the tube. It was suspended in a horizontal position from the top end of the tube via four nylon threads connected to screw adjusters in order to avoid diffraction complications from the mounting arrangement of the filter. The filter had neutral buoyancy so there was no stretching of the nylon lines which could change the truncation distance. Before acoustic measurements were made, care was taken so that air had not accumulated on the underside of the filter.

The receiving hydrophone was mounted at the end of a hollow stainless steel tube and immersed through the top of the tube. The hydrophone mounting was in turn fixed onto a stepper motor controlled translation stage that enabled the hydrophone to be moved

through 0.5m along a tube diameter. The stepper motor was controlled by a desktop computer via an IEEE interface. The horizontal position of the hydrophone could thus be accurately controlled. The vertical position of the hydrophone could also be manually adjusted. The hydrophone was actually mounted at the end of the tube so that its axis of symmetry was perpendicular to the transducer/tube axis. This arrangement was used because the hydrophone used (Brüel & Kjær 8103) is omnidirectional in a plane normal to its axis of symmetry.

Test panels were suspended from the top of the tube in a similar arrangement to that used for mounting the acoustic filter. Screw adjusters near the top of the tube enabled the position of the sample to be adjusted. Before the test panels were immersed, they were covered with a thin film of mild detergent that acted as a wetting agent and inhibited the seeding of air bubbles on the test panels.

The tank used for some comparative studies has been extensively used in a previous research program [88] and experimental details and results have been published [44-46, 72]. The facility comprises a tank 1.8m long x 1.2m wide x 1.2m deep with no absorbing or reflecting linings. The experimental arrangement for insertion loss measurements is shown diagrammatically in figure 3.2 (reproduced with kind permission from [88]). The transducer was mounted at one end of the tank and aligned so that its acoustic axis was parallel to an optical bench mounted along the top of the tank. The hydrophone was mounted in a vertical tube supported by a carrier on the optical bench. The micropositioner on the carriage facilitated accurate positioning of the hydrophone on the axis of the transducer while the carrier enabled the hydrophone to be easily translated along the axis and ensured accurate repositioning.

The acoustic filter was mounted vertically in a metal frame and positioned normal to the acoustic axis.

The test specimen was suspended from a rotation stage so that it could be rotated about a vertical axis in order to perform measurements at various angles of incidence. The rotation stage was placed on the optical bench so that the transducer-test panel separation could be adjusted.

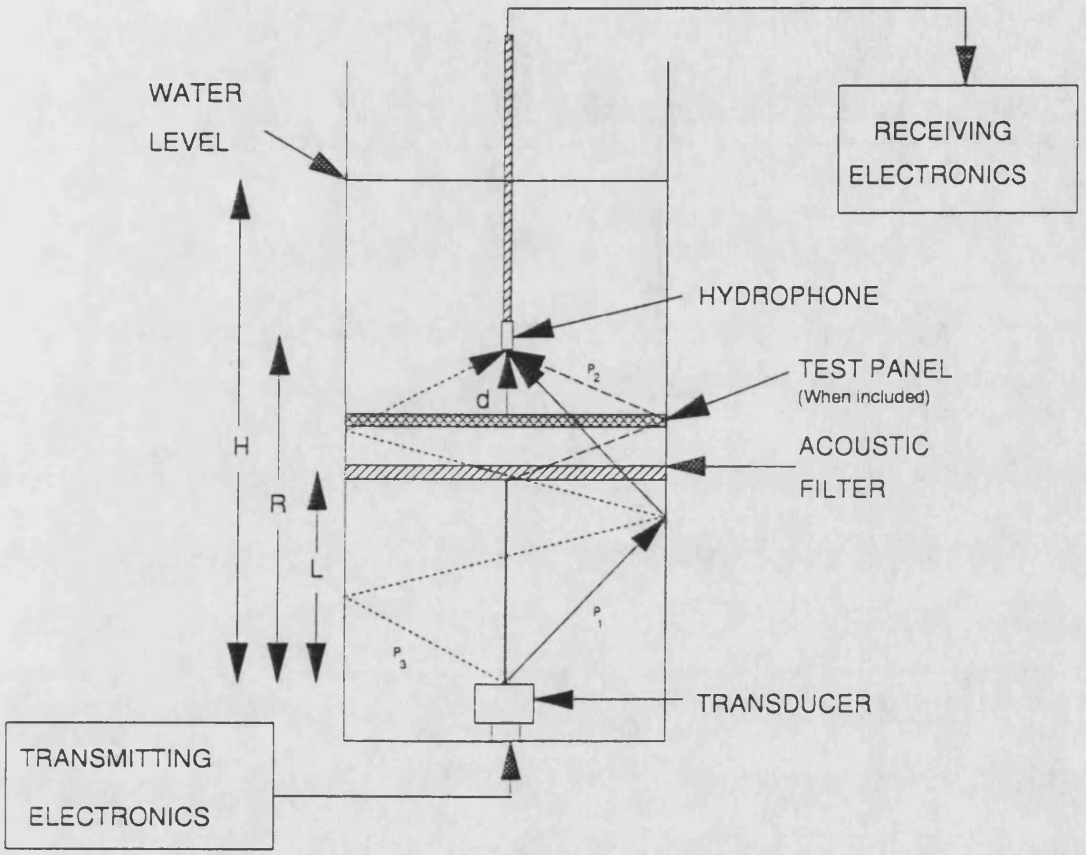

Figure 3.1 Schematic arrangement of the tube and associated electronics. Some ray paths are also shown.

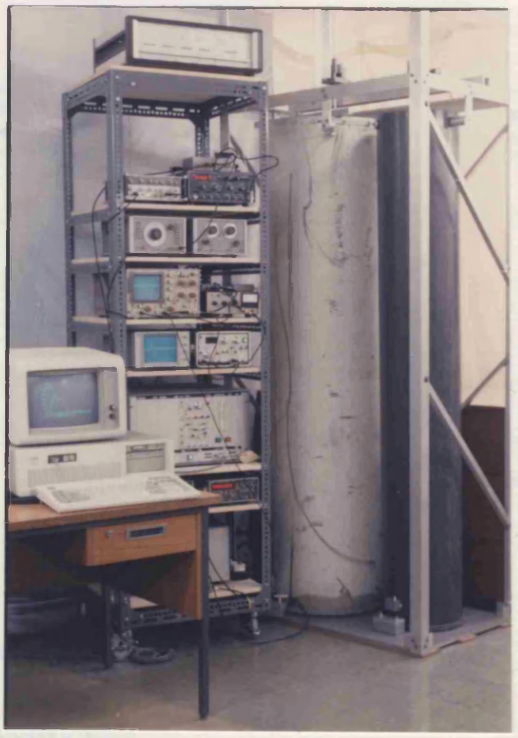

Photograph 1. The experimental system: Tube (right), electronics (centre) and computer (left).

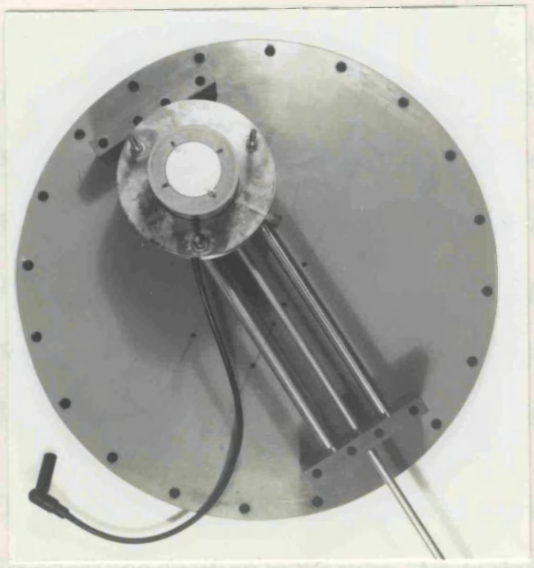

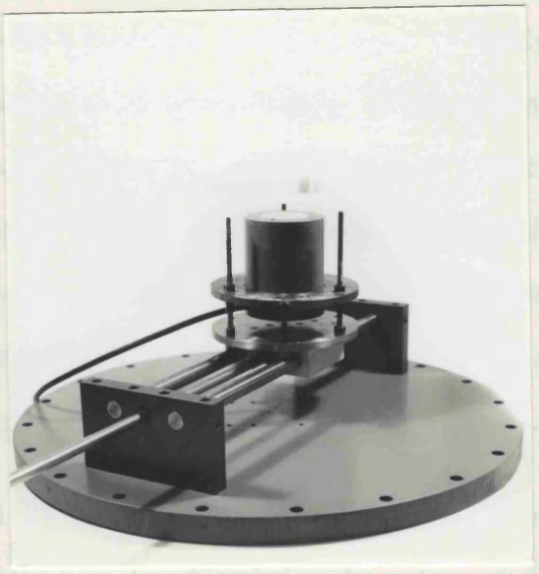

Photographs 2 & 3. The transducer carriage and transducer holder mounted on the base plate of the tube.

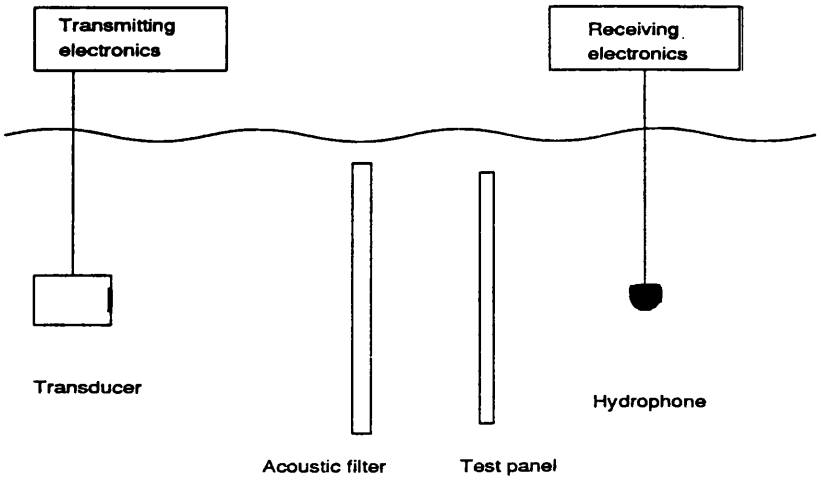

Figure 3.2 Experimental arrangement for tank measurements.

3.2 TRANSMITTING TRANSDUCERS

A single transducer (designed, constructed and tested by one of the author's colleagues) was used throughout the experiments performed with the tube. The transducer was made from a 5cm diameter disc of PZT-4 resonant at 960kHz mounted on a backing block of highly attenuating material made from glass microspheres in an epoxy matrix. It had a front matching layer of epoxy resin that was machined to a quarter of a wavelength thick in order to improve coupling into water. This resulted in the very wide bandwidth transducer with a Q of 5.3. Previous transducers of this type have an efficiency of about 40-50% [88]. The most important features of this transducer were its piston-like behaviour and its wide bandwidth that enabled a wide range of difference frequencies to be produced.

The impedance of the transducer was measured as a function of frequency when placed in its operating position in the tube. An angled reflector was placed just below the water surface to prevent reflections from the surface interfering with this measurement. A matching transformer was then made for the transducer so that it presented an impedance of 50Ω to the power amplifier.

Precise characterisation of the transmitting transducer was not necessary because all measurements were comparative. That is, measurements were made before and after a test panel was inserted. Assuming that the characteristics of the system do not change in this time interval, the exact sensitivity of the transducer was not required.

The transducer used for tank measurements was of similar construction, resonant at 920kHz with a Q of 5.8 and efficiency of 46% measured by self reciprocity.

Transducers of nominal frequency in the region of 1MHz were chosen because they have a bandwidth suitable for generating parametric signals at frequencies up to about 100kHz. A lower primary frequency would lead to reduced bandwidth for parametric generation which could perhaps be unacceptable for the present purposes. An additional problem with lower frequency primaries and the truncated parametric array is that the acoustic filter must provide good rejection (attenuation) at the primary frequencies while allowing the parametrically generated waves to pass unaffected. Such low pass filtering is difficult to achieve when the primaries are closer to the secondary frequencies.

3.3 RECEIVING HYDROPHONE

A commercially available cylindrical hydrophone, the Brüel & Kjær 8103, was used throughout this work. It has a sensitivity of about -211dB re 1V/μPa and a flat response to within ±2dB up to 100kHz and almost uniform about its axis of symmetry. The flat response of this hydrophone in the frequency range of interest, combined with its small size make it suitable for the present application.

Previous observations [89,90] suggest that there is the possibility of production of difference frequency signal within the hydrophone due to the nonlinear interaction of primary frequencies on the hydrophone. The degree of hydrophone nonlinearity depends on the primary signal level and frequency.

The effects of hydrophone nonlinearity are avoided by placing the hydrophone behind an acoustic filter that reduces the primary signal level without attenuating the difference signal level.

Thus, the use of the acoustic filter prevents the effects of hydrophone nonlinearity and provides a source free region in which the properties of a test panel can be tested without any complications.

3.4 TRANSMITTING AND RECEIVING ELECTRONICS

Block diagrams of the transmitting and receiving electronics are shown in figures 3.3 and 3.4.

A pulse generator (Lyons Instruments PG71N) with variable pulse repetition rates (typically 10-100Hz), triggers a function generator (Philips PM5134) and also provides a trigger pulse for the receiving electronics. The function generator provides a single cycle at the desired envelope frequency. Adjustment of the start phase and the D.C. offset then enables a raised cosine bell modulating envelope to be produced. This waveform is fed into a double balanced mixer (Hatfield Instruments Ltd, type 1754) along with a continuously running carrier signal (from a Krohn-Hite model 4200A oscillator running at 960kHz), and produces a modulated carrier signal. This modulated signal is then fed, via a buffer amplifier and variable attenuator, into an rf power amplifier (ENI model A150) of 55dB gain whose input voltage is restricted to 1Volt by limiting diodes. The output of the power amplifier then drives the transducer via an impedance matching transformer.

The low frequency signal is received by the hydrophone (B & K 8103) and is passed through a low pass filter to eliminate any high frequency still present. The signal is then amplified using a variable gain, low frequency amplifier (Ortek Brookdeal 9452/11). At this point, the received signal is displayed on an oscilloscope (Gould OS3300B) and is also digitized

by a transient recorder (Datalab DL905). The pulse generator in the transmitting side of the electronics also provides a trigger pulse which enables the digitization to be synchronized with each transmission.

The received signal is digitized to 8 bits precision using a Datalab DL905 transient recorder with maximum digitizing frequency of 5MHz. The digitized waveform is then passed to a Data Laboratories DL4000B signal processor which also displays it on a separate CRT.

The DL4000B is a dedicated signal processor that can perform certain tasks quite efficiently. It contains four memory channels, each 1024 words long, into which each signal from the transient recorder can be stored. The DL4000B can be programmed to perform signal averaging by adding consecutive signals from the transient recorder into one channel. This enables the signal-to-noise ratio to be improved quite significantly by averaging over a large (typically 1024) number of signals in a short time interval (less than a minute).

The DL4000B is capable of a large range of computations ranging from simple arithmetic operations, such as adding or dividing two channels, to more complex operations such as removing the D.C. component of a signal, evaluating the Fourier and inverse Fourier transform of a channel. A number of computational steps can be stored in the internal memory of the processor and performed again and again in any order.

The contents of each channel are displayed on a monitor which enables a check to be made on the progress and the results of processing.

The DL4000B is programmed via an RS-232 serial interface. The contents of each channel can also be output over the same interface.

The IBM computer is connected to the DL4000B via this interface. This allows the DL4000B to be programmed via the computer which is also capable of storing and retrieving the data,

from the built-in hard disk, for further processing and plotting. The IBM can simultaneously control the position of the hydrophone via an IEEE interface, an X-Y plotter through a serial (RS-232) interface, and a parallel printer.

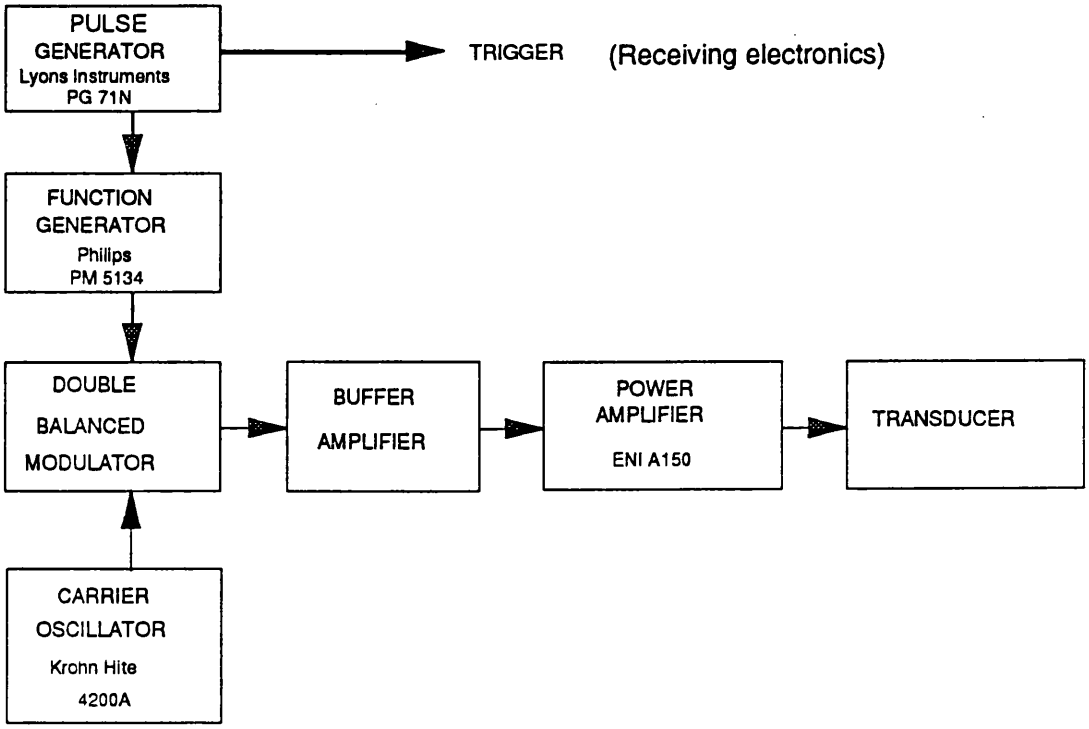

Figure 3.3 Block diagram of the transmitting electronics.

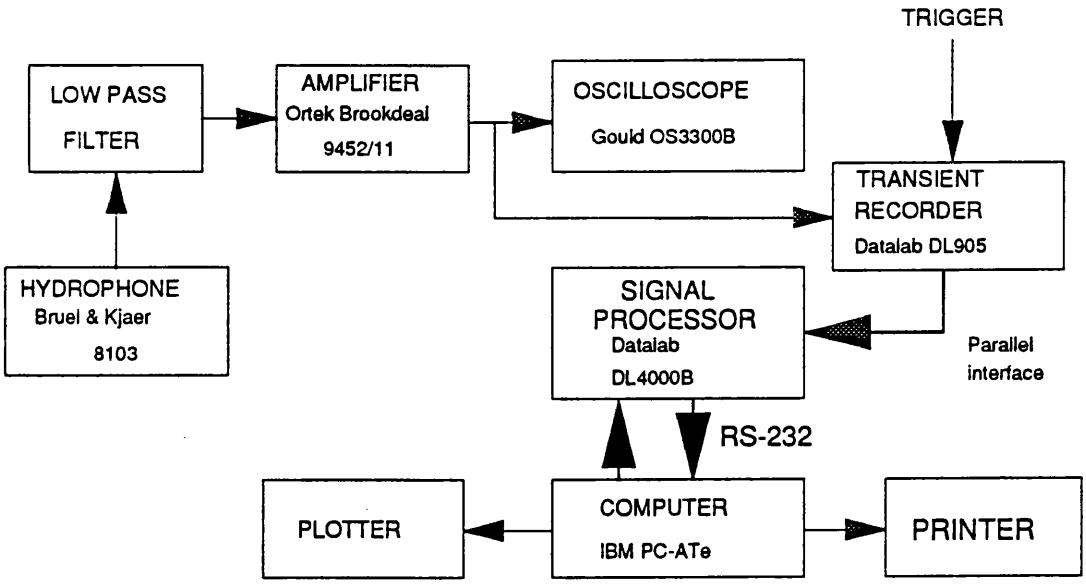

Figure 3.4 Block diagram of the receiving electronics.

3.5 EXPERIMENTAL PROCEDURE

The basic experimental procedure that was followed when measurements were made in the tube is described here.

Before reliable measurements could be made, the electronic equipment was switched on and allowed to reach a stable operating temperature. The carrier and envelope frequencies were checked using an accurate timer counter (Philips PM6671) to ensure that the nominal values were obtained and that there was no drift. The shape of the modulated carrier frequency pulse was checked against the original envelope function that was produced by the function generator to ensure that the shape of the envelope had not deteriorated in the mixing process. This is a significant step in the mixing procedure since, as discussed earlier, the difference frequency pulse envelope, and therefore the difference frequency spectrum, is proportional to the second time derivative of the square of the carrier envelope.

The carrier frequency was set to 960kHz to coincide with the resonant frequency of the transmitting transducer. The envelope frequency was usually set to 20kHz and the envelope shape was a raised cosine bell or haversine function. This set-up gives a difference frequency pulse with a smooth frequency spectrum with most of the energy concentrated in the 10-50kHz frequency band. Figure 3.5a shows the shape of the modulating envelope (20kHz), figure 3.5b shows the modulated carrier waveform that is transmitted by the transducer and figure 3.5c shows the theoretical difference frequency waveform that is recorded at the farfield of a parametric source. The frequency spectrum of the difference frequency pulse is shown in figure 3.5d. It can easily be shown that the general shape of the difference frequency spectrum will remain the same for any envelope frequency provided its shape is a raised cosine of the form of figure 3.5a. The zero crossing in the spectrum of the difference frequency pulse always occurs at $3*F_{env}$ were F_{env} is the envelope frequency used to derive the Haversine envelope. Thus, for

example, the 20kHz envelope produces a minimum at 60kHz in the difference frequency spectrum. By increasing the envelope frequency it would be possible to broaden the difference frequency spectrum at the expense of reduced signal level at lower frequencies provided the bandwidth of the transmitting transducer was sufficient. For present purposes, a 20kHz envelope was almost always used.

Every time the experiment was performed, the acoustic filter was turned over in order to release any air bubbles trapped underneath. Since the acoustic filter fitted quite snugly inside the tube, it was quite difficult for air released from the lower body of water to reach the water surface with the filter in place. Thus, every time the tube was refilled, several days were allowed for the air content of the water to stabilise before the acoustic filter was inserted. Before each set of measurements, the distance of the acoustic filter from the top of the tube was measured to insure that the parametric array length had not changed due to stretching of the nylon strings used to suspend it. The acoustic filter was usually positioned 52cm from the transducer. Screw adjusters at the top of the tube enabled a horizontal position to be attained.

The various test panels were inserted in a similar way to the acoustic filter.

The hydrophone was placed on the tube axis. A rough estimate of this position was obtained by traversing the hydrophone along a diameter of the tube using the translation stage and noting the position were the amplitude of the received signal was maximum. The waveform was then recorded at two points a fixed distance either side of the estimated position of the tube axis. Since the wavefield inside the tube is circularly symmetric, the waveforms recorded at the two points should be the same. If any differences was observed, an adjacent point was adopted as the tube centre and the process was repeated. An accurate position of the tube axis was obtained after 2-4 iterations of the above procedure. This measurement was only repeated after the tube had been emptied and

moved from its position relative to its supporting frame.

When spatial averaging of the received signal was required, the hydrophone was scanned along a range of positions on a tube diameter using the translation stage under computer control. A stepper motor controller (Digiplan CD20) was controlled by a desktop IBM PC/ATe via a general purpose interface bus connection (IEEE488 GPIB). The speed and distance of each traverse could be defined. At each position of the traverse, the waveform was digitized over 1msec and averaged over 1024 measurements to improve the signal-to-noise ratio. The averaged signal was then stored in the DATALAB 4000B signal processor for processing and later transfer to the desktop controlling computer over a serial RS-232C interface operating at 1200Baud.

3.6 OPTIMUM OPERATING POSITIONS FOR THE ACOUSTIC FILTER, HYDROPHONE AND TEST PANEL

Some of the signals present in the tube are considered here. Propagation is considered to be along geometric ray paths and diffraction effects or the relative strength of the various arrivals are not considered. The parametric array is assumed to be an axial line of virtual sources and the hydrophone is also on the tube axis.

The relative parameters that enter the discussion below are shown in figure 3.1. This figure shows a schematic diagram of the tube and approximate relative positions of the transducer, acoustic filter, test panel and receiving hydrophone. Also shown are four ray paths that waves inside the tube may follow:

1) P_0 is the direct path for the difference frequency along the tube axis,

2) P_1 is the shortest possible path a single bounce reflected wave can follow,

3) P_2 is the longest ray path for a single bounce reflected wave, and,

4) P_3 is the shortest path a double bounce reflected wave can follow.

These four waves are considered since they are the strongest and must be resolvable in time.

The parameters that are considered fixed for the purpose of this discussion are: (a) the tube radius, since it cannot be easily changed, (b) the carrier frequency envelope shape and frequency, since these are determined by the bandwidth requirement for testing purposes.

Using the notation of figure 3.1:

b:- tube radius

R:- transducer-hydrophone separation

L:- parametric array length

d:- test panel-hydrophone separation

τ:- duration of the signal transmitted by the transducer

H:- transducer-water surface separation

thus:

$$P_o = R$$

$$P_1 = 2\sqrt{\left(\frac{R}{2}\right)^{\frac{1}{2}} + b^2}$$

$$P_2 = L + 2\sqrt{\left(\frac{R-L}{2}\right)^2 + b^2}$$

$$P_3 = 4\sqrt{\left(\frac{R}{4}\right)^2 + b^2}$$

Six different, and sometimes competing, considerations enter into the calculation of the optimum values for R, L and d:

(A) In order to resolve the direct wave along P_o from that travelling along P_1 we must have:

$$P_o + \tau c \leq P_1 \qquad \ldots(3.1)$$

where τc is the path length corresponding to a pulse duration τ. This gives

$$R + \tau c \leq 2\sqrt{\left(\frac{R}{2}\right)^2 + b^2}$$

$$\therefore \quad R \leq \frac{4b^2 - \tau^2 c^2}{2\tau c} \qquad \ldots(3.2)$$

Using a=0.225m , τ=50μsec (20kHz envelope), c=1486m/sec, we get

$$R \leq 1.326m \qquad \ldots(3.3)$$

(B) We also need to resolve waves that have travelled along P_2 and P_3 since the later is a double reflection path and theoretical models do not include the double bounce contributions. This requires

$$P_2 + \tau c \leq P_3 \qquad \ldots(3.4)$$

$$\therefore \quad P_2 \leq P_3 - \tau c$$

Introducing a variable x where

$$x = P_3 - \tau c = 4\sqrt{\left(\frac{R}{4}\right)^2 + b^2} - \tau c \qquad \ldots(3.5)$$

then equation (3.4) becomes $P_2 \leq x$ $\qquad \ldots(3.6)$

$$L + 2\sqrt{\left(\frac{R-L}{2}\right)^2 + b^2} \leq x$$

$$\therefore \quad (R-L)^2 + 4b^2 \leq (x-L)^2$$

$$\therefore \quad L \leq \frac{x^2 - 4b^2 - R^2}{2(x-R)} \qquad \ldots(3.7)$$

That is, given a value for the transducer-hydrophone separation (R), equation (3.6) combined with equation (3.5) provides an upper limit for the parametric array length L.

(C) In experimental waveforms there is an identifiable contribution due to waves reflected from the water surface. We want this wave to arrive after the longest path single bounce wave (P_2) so that it can be gated out electronically. If the transducer-water surface distance is S then

$$R + 2(H - R) \geq P_2 + \tau c \qquad \ldots(3.8)$$

$$\therefore \quad P_2 \leq R + 2(H - R) - \tau c \qquad \ldots(3.9)$$

By making the substitution x'=R+2(H-R)-τc, equation (3.9) becomes identical to equation (3.6) and similarly the solution of equation (3.9) becomes (c.f. equation (3.7)):

$$L \leq \frac{x'^2 - 4b^2 - R^2}{2(x' - R)} \qquad \ldots(3.10)$$

alternatively, solving equation (3.8) for R:

$$R \leq \frac{2H^2 + (2H - \tau c)^2 - 4HL + 2\tau cL}{4H - 4L - 2\tau c} \qquad \ldots(3.11)$$

or

$$H \geq \frac{P_2 + \tau c + r}{2} \qquad \ldots(3.12)$$

In practice, the reflection from the water surface can be easily identified and isolated and does not pose a problem at the values of L and R that are commonly used with the 20kHz envelope signal. In addition, the water level is maintained at the maximum possible level by periodically adding small amounts of water to counteract evaporation.

It would be possible to use an absorber to terminate the top of the tube. This would enable restrictions imposed by equations (10)-(12) to be lifted and a shorter tube (slightly longer than R) to be used. For the present purposes, however, such an absorber would make experimentation cumbersome and was not used.

(D) We also need to distinguish between the two single bounce waves along P_1 and P_2, i.e.:

$$P_1 + \tau c \leq P_2 \qquad \ldots(3.13)$$

Equation (3.13) is similar to equations (4) and (9) and its solution similar to equations (7) and (10). Expanding P_1 and P_2 in terms of L, R and b we get:

$$L \geq \frac{R^2 + 4b^2 - x''^2}{2(R - x'')} \qquad \ldots(3.14)$$

were
$$x'' = P_1 + \tau c = 2\sqrt{\left(\frac{R}{2}\right)^2 + b^2} + \tau c \qquad \ldots(3.15)$$

Equations (14) and (7) set lower and upper limits to the length of the parametric array (L) given the hydrophone position (R), the tube radius (b) and the pulse duration (τ). That is

$$\frac{R^2 + 4b^2 - x''^2}{2(R - x'')} \leq L \leq \frac{R^2 + 4b^2 - x^2}{2(R - x)} \qquad \ldots(3.16)$$

with x given by equation (3.5) and x'' by equation (3.15).

(E) Another requirement is that we need to be able to isolate the wave that has been multiply reflected between the hydrophone and the test panel, from the direct wave. If the test panel-hydrophone separation is d, then:

$$2d > \tau c$$

$$\therefore \quad d > \frac{\tau c}{2} \sim 3.7cm \qquad \ldots(3.17)$$

This is the minimum value of d for which the two waves considered do not overlap. In practice, a larger (5-10cm) panel-hydrophone separation is used to allow for the delay of internally reflected waves in the panel which would effectively lengthen the duration of the direct signal.

Finally, (F), it is desirable to restrict the range of R to <1.0m on the basis of overall size but still leave enough room for a test panel without generating strong multiple reflections (R>0.7m). That is:

$$0.7 \leq R \leq 1.0m \qquad \ldots(3.18)$$

This satisfies the condition imposed by equation (3.3) on R and further restricts the range of values it can take.

Equation (3.18) along with equation (3.16) are sufficient for the determination of the range of suitable values for R and L; a minimum value for d is suggested by equation (3.17). The resulting values are

$$0.31 \leq L \leq 0.60 \qquad (R = 0.7m)$$

$$0.49 \leq L \leq 0.76 \qquad (R = 1.0m)$$

Therefore, in general, $0.7 \leq R \leq 1.0m$, $0.5 \leq L \leq 0.6m$ and d>5cm would be satisfactory for the conditions set out in (A)-(F) above.

(a) envelope of the transmitted signal

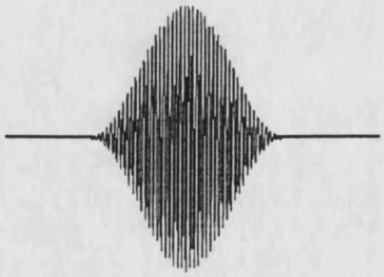

(b) modulated carrier waveform

(c) difference frequency waveform

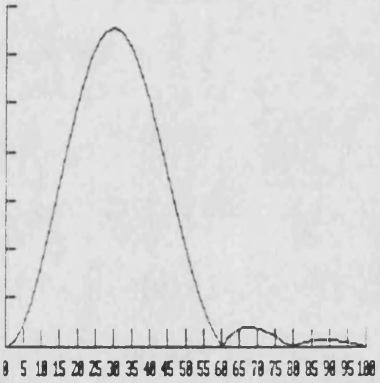

(d) frequency spectrum of difference frequency wave (c)

Figure 3.5. System waveforms of interest. These waveforms have been derived theoretically and do not represent waves obtained in the tube.

4 THEORY

4.1 INTRODUCTION

In this chapter some fundamental principles concerning the formation of a parametric array in water are reviewed. The distinctive features of the parametric array operating in a wide bore tube are identified and distinguished from the unconfined parametric array. The special geometry of this configuration introduces an extra term in the expression for the field at an axial point receiver due to wave reflection from the inner tube surface. The theoretical treatment of the confined parametric array begins with a simple treatment of the fundamental mechanism of reflection of the wave field from a point source and its detection by a point receiver within the confined environment of the tube. The results of this treatment form the basis of more complex and refined models for the parametric array volume which is just a conglomeration of point sources. Three models for the parametric array volume are considered and treated separately.

(1) The simplest model that can be adopted for the parametric array is that of a line array of sources with negligible transverse dimensions and thus no transverse aperture effects (as opposed to longitudinal aperture effects associated with the length of the interaction region and truncation effects). In this case, the expression for the field at a point receiver due to a point difference frequency source has to be integrated along a straight line to find the reflected wave strength at a point receiver due to a line array.

(2) The column array model represents the virtual source volume as a cylindrical column of the same radius as the primary piston source extending from the piston face to the truncating filter. The transverse distribution of virtual sources is uniform and the axial distribution is the same as that of the line array in the above model. Two aperture effects are identified: (a) the transverse aperture effect which introduces a Bessel function directivity function for the difference frequency, and, (b) a longitudinal aperture factor which is the same as that for the line array and mainly depends on the parametric array

length in terms of the difference frequency wavelength.

(3) The most rigourous model for the distribution of the virtual sources takes the structure of the primary field in the interaction region into account. Since the virtual source strength at a particular point in the interaction region depends on the product of the primary pressures generating the difference frequency wave, the distribution of virtual sources will be affected by the structure of the primary frequency field. A closed form expression is used to describe the primary field structure. Since the detail in the primary field is too small in terms of the difference frequency wavelength (except at the high end of the difference frequencies of interest) the inclusion of this refinement is not expected to lead to big improvements over the column array model described above. In fact, a comparison of theoretical results supports that view.

The results obtained with the above models for the field on the tube axis are integral expressions that cannot be evaluated analytically unless some simplifying assumptions are made.

Numerical and analytic results are presented in terms of the normalised difference frequency spectrum of the reflected wave. That is, the expression for the reflected wave strength at the receiver is divided by the expression for the direct wave (the wave that travelled along the tube axis) at a each frequency. By repeating this process, the normalised reflected wave amplitude at the receiver as a function of frequency can be obtained. Such graphical representation makes it very easy to determine the relative strength of the direct and reflected waves at the receiver at specific frequencies. Inter-comparison of the normalised reflected wave spectra obtained using different theoretical models and results facilitates the evaluation of the effects of the various assumptions and refinements leading to those results. By including experimental data presented in the same form, it is possible to compare the theoretical models with the experiment. In terms of materials test measurements, the normalised reflected wave

spectrum provides a measure of the relative contributions from the direct and reflected waves observed behind the test panel. If, for example, the normalised reflected wave spectrum at a particular frequency has a value much smaller than unity, then the direct wave at that frequency can be considered much stronger than the reflected one. In this case, the wave recorded behind a test panel can be used for transmission coefficient measurement at normal incidence (provided, of course, that it is suspended normal to the acoustic axis). If, on the other hand, the normalised reflection spectrum has a value close to, or greater than, unity then a significant proportion of the wavefield has undergone reflection at the tube wall. In this case an accurate prediction of the transmission coefficient cannot be made unless it is known *a priori* that the transmission coefficient does not vary appreciably with the angle of incidence of the interrogating wave.

In section 4.3.1, it will become clear that the reflected waves can be assumed to propagate along ray paths. These paths can be classified according to the number of reflections off the tube wall they suffer before they arrive at the receiver. Thus, we can have single bounce reflected wave which, after it is generated, it suffers a single reflection before arriving at the receiver, double bounce reflected waves, etc. It will be shown that there is some propagation delay associated with the waves along the various ray paths and the delay associated with double, triple, etc bounce waves enables them to be easily separated experimentally with suitable time gating of the received signal. It turns out, however, that the time delay associated with single bounce waves is not large enough to enable them to be safely separated from the direct (axial) wave. In all the theoretical models and graphs that follow, the term reflected wave is used to refer to single bounce wave rather than the complete field at the receiver.

Two questions may arise at this point. The first concerns the operational characteristics of the parametric array used in the experiment. As seen in the literature review, absorption, diffraction and nonlinearity (saturation) are all potentially very important

effects. In the present case, small signal absorption is not included for either the primary or the difference frequency radiation although it is quite easy to do so in an *ad-hoc* way at any stage in the theoretical treatment. That is because, for the distances involved, the small signal attenuation is very small. For example, if we consider the small signal absorption to follow a functional relationship of the form [73]

$$\alpha = 2.5 \cdot 10^{-15} f^2 Np\,m^{-1}$$

then, for a 1MHz signal, the attenuation suffered in a path x=1.5m long is $e^{-\alpha x}$=0.9962, i.e. less than 0.4% which is negligible. At the difference frequency that figure would be even lower.

As far as diffraction effects are concerned, these are accounted for to various degrees of complexity and rigour for both the primary and the difference frequency beams in the rest of this chapter.

It is assumed that the parametric array works in the quasilinear manner assumed by Westervelt [4]. That is, the generation of difference frequency waves does not affect the propagation of the primary waves. The primary waves propagate linearly and no finite amplitude effects such as nonlinear distortion, attenuation and saturation are present in the primary beams.

Another point that merits clarification is the fact that the theoretical treatment provides essentially a single frequency solution. This is again the case treated originally by Westervelt and, subsequently, by many more. This approach is adopted because of the relative ease with which results can be obtained and interpreted despite the fact that the experimental parametric array operates in the self-demodulation regime as described by Berktay [11]. Thus, the experimental difference frequency spectrum that is modelled by the theory possesses a wide bandwidth rather than being a single frequency line spectrum

as that in Westervelt's model. The initial pulse is analysed into its constituent frequencies using the Fourier transform, each frequency is then propagated independently and the waveform at the receiver is then obtained through an inverse Fourier transformation.

4.2 FUNDAMENTAL PRINCIPLES OF OPERATION OF THE TRUNCATED PARAMETRIC ARRAY

The basic theory concerning the formation of the parametric array was developed by Westervelt [3,4]. The parametric array relies on the nonlinear interaction of high frequency propagating primary waves to generate lower frequency secondary waves that can be considered to emanate from pseudo sources distributed throughout the interaction region of the primary waves. It is the phasing of these virtual sources that gives the parametric array its characteristic narrow beamwidth; each of the virtual sources has the same phase as that of a difference frequency wave that has been propagated from the transducer face to the source point. The result is that, although the difference frequency wave emanating from any one point within the interaction region is very small, all the virtual sources are phased in such a way that their signal is coherently added when it propagates along the acoustic axis.

Let us now consider a circular transducer of radius a, at the origin of a cylindrical co-ordinate system (z,r,ϕ) as shown in figure 4.1, radiating at the primary frequencies. A primary wavefield $p_i(\underline{r})$ is generated at a point $\underline{r}$. As a result of nonlinear interaction, a pseudo source of strength $Q(\underline{r})$ is formed at that point.

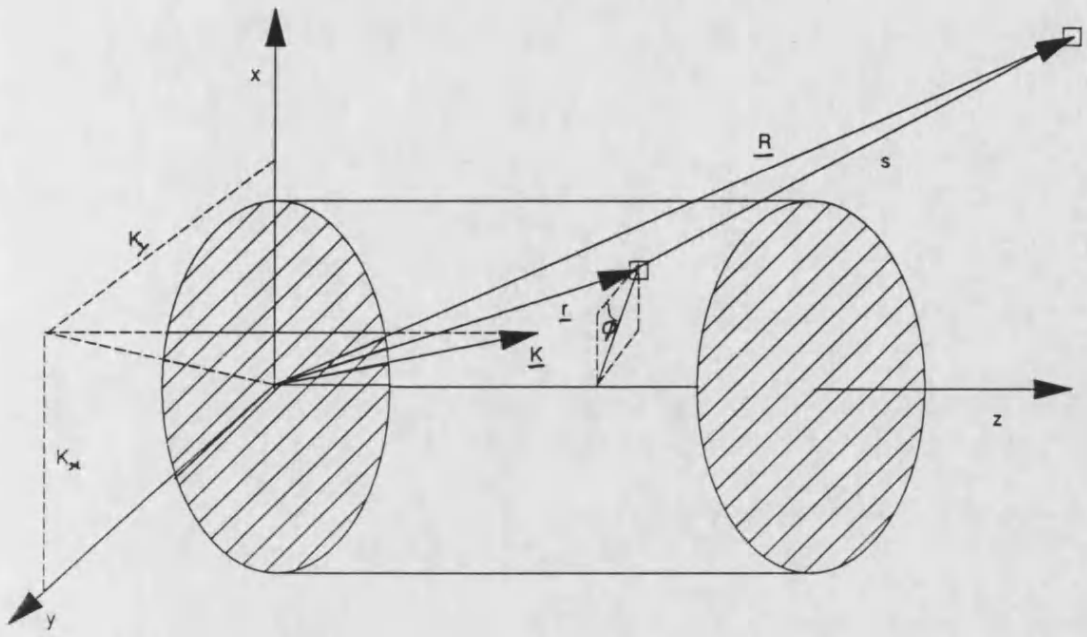

Figure 4.1 Schematic diagram of the source volume and some useful quantities.

If $p_i(\underline{r})$ is the primary field at $\underline{r}$, then the strength of the virtual difference frequency source at that point is given by [4]:

$$Q(\underline{r}) = \frac{\beta}{\rho_o^2 c_o^4} \frac{\partial p_i^2(\underline{r})}{\partial t}$$

for plane, collimated primary waves:

$$p_{1,2} = P_{1,2} e^{jk_{1,2}z}$$

and the difference frequency source function becomes:

$$Q(\underline{r}) = -j \frac{k \beta P_1 P_2^*}{\rho_o^2 c_o^3} e^{jkz} \qquad \ldots(4.1)$$

Here, β is the nonlinearity parameter (β=3.5 in water), ρ_o is the water density and c_o the wave velocity in water. z is the normal distance from the transducer to the source point and a term exp(-jωt) has been dropped for simplicity.

Each point within the primary beam radiates uniformly (spherically) with strength $Q(\underline{r})$. Thus, in order to find the total difference frequency field at some observation point $\underline{R}$ (see figure 4.1), we have to evaluate the appropriate scattering integral over the interaction volume. The difference frequency field $p(\underline{R})$ at $\underline{R}$ is thus given by [4]:

$$p(\underline{R}) = -\frac{j\omega}{4\pi}\rho_o \iiint_{\text{Interaction Volume}} Q(\underline{r})\frac{e^{jk|\underline{R}-\underline{r}|}}{|\underline{R}-\underline{r}|}dV. \qquad \ldots(4.2)$$

In the present application, the interaction volume extends from z=0 to z=L, thus the above integral takes the form:

$$p(\underline{R}) = -\frac{j\omega}{4\pi}\rho_o \int_0^{2\pi} d\phi \int_0^{\infty} r\,dr \int_0^{L} Q(\underline{r})\frac{e^{jk|\underline{R}-\underline{r}|}}{|\underline{R}-\underline{r}|}dz. \qquad \ldots(4.3)$$

If the primary beams are assumed to be well collimated in the region z=0 to z=L with radius a, then the limits of the integral over r will extend from r=0 to r=a.

If the radius a is a small fraction of the difference frequency wavelength, then the distribution of virtual sources can be likened to a line array of sources situated on the acoustic axis. In that case, the integrals over ϕ and r need not be performed provided $Q(\underline{r})=\pi a^2 Q(z)$ now represents the source strength per unit length (elementary volume):

$$p(z) = -\frac{j\omega}{4\pi}\rho_o \int_0^{L} Q(z)\frac{e^{jks}}{s}dz \qquad \ldots(4.4)$$

$$= -\frac{j\omega}{4\pi}\rho_o q_o S_o \int_0^{L} \frac{e^{jk(z+s)}}{s}dz \qquad \ldots(4.5)$$

where $$q_o = -j\frac{kP_1P_2^*\beta}{\rho_o^2 c_o^3} \qquad \ldots(4.6)$$

and $S_o dz$ represents the elementary volume of the source density.

4.2.1 THE AXIAL NEARFIELD OF THE PARAMETRIC ARRAY

An expression for the axial nearfield of the parametric array is needed for the subsequent analysis of the array in the tube in order to use it as a normalising expression for the reflected wave strength on the tube axis. As mentioned above, theoretical and experimental results are presented in the form of a comparative study of the strengths of the direct and reflected wave spectra (the normalised reflected wave spectrum), rather than absolute pressure or velocity potential values.

A simplified model of the truncated parametric array that is used here has been considered by Berktay and Shooter [18]. They found, by integration of equation (4.5), that the axial nearfield at a distance z , of a truncated line array of length L is given by:

$$p(z) = -\frac{j\omega}{4\pi}\rho_o q_0 S_o \; e^{jkz} \ln\left(\frac{z}{z-L}\right) \qquad \ldots(4.7)$$

Berktay and Shooter also showed that the above expression is valid for observation points in the paraxial region, i.e. at small off-axis distances.

If the column array model is used to obtain a more accurate estimate of the nearfield of the truncated parametric array, then it can be shown that the expression for the axial nearfield changes very little. The integrals in equation (4.3) cannot be evaluated analytically but it is possible to obtain an expression for the plane wave spectrum of the truncated parametric array using both the line array and the column array models. In appendix A it is shown that when a column array of radius a is considered then the angular dependence of the plane wave spectrum consists of the product of an aperture factor $2J_1(ka\sin\theta)/ka\sin\theta$ and that due to a line end-fire array. Here θ is the angle to the z-axis. Thus, provided ka is not very large, this factor is not very important and the line array model is adequate.

In all theoretical results, equation (4.7) is used to normalise the reflected wave. It is assumed that it provides a reasonably accurate representation of the axial field within the tube, and as shown here, it changes very little when different models are considered.

4.3 THE PARAMETRIC ARRAY IN THE TUBE

The theoretical treatment of the parametric array in a wide bore tube will be concerned with the difference frequency field. As mentioned in the introduction to this chapter, in view of the fact that the tube diameter is much larger than that of the transmitting transducer, and also, that the interaction volume is limited to the primary nearfield, it is assumed that the primary wavefield is totally unaffected by the presence of the tube wall.

In the investigation of the difference frequency field, the material properties of the tube wall will affect the waves reflected by it. If waves are allowed to penetrate into the tube wall, then they will suffer a phase shift upon reflection depending on the frequency of the wave and its angle of incidence. In the present application, it is assumed that the tube wall forms a pressure release boundary that acts as a perfect reflector which introduces a phase inversion at all frequencies and angles of incidence. In practise, this condition is easily met by coating the inside of the tube with closed cell neoprene rubber. The high air content of neoprene ensures a large impedance mismatch at the tube wall and enables this theoretical assumption to be matched experimentally [see section 3].

4.3.1 PRESSURE ON THE TUBE AXIS DUE TO A POINT SOURCE

In order to calculate the effect due to the presence of the tube wall, we want to calculate the pressure at an observation point on the axis of the tube, due to waves reflected from the tube wall. For simplicity, we first consider the field on axis due to a point source of difference frequency waves and only investigate the field due to a single reflection. This result can subsequently be used to construct models of the difference frequency source

volume by integrating over suitable spatial limits.

Figure 4.2 shows a point source S and a point receiver P within the confines of the tube. The two points are separated by distance s and the tube radius is b. The source point may lie a small distance y off the tube axis.

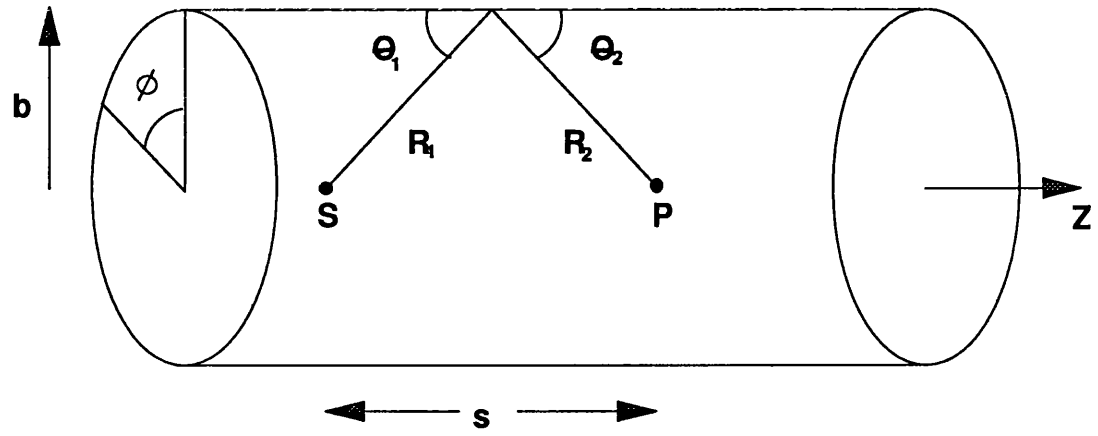

Figure 4.2 Point source S and point receiver P within the tube.

The pressure at P can be obtained from Huygen's diffraction integral over the tube surface [82, page 370]:

$$p = -\frac{j\omega\rho_o}{2\pi} Q(S) e^{j\pi} \int_0^{2\pi} \int_{-\infty}^{+\infty} b \frac{e^{jk(R_1+R_2)}}{R_1 R_2} \frac{(\sin\theta_1 + \sin\theta_2)}{2} d\phi dz \qquad \ldots(4.8)$$

where Q(S) is the strength of the point source S and is given by equation (4.1), k is the difference frequency wavenumber and the rest of the symbols are defined in figure 4.2. The term $e^{j\pi}$ represents the phase reversal suffered by the wave at the wall.

Equation (4.8) cannot be evaluated analytically but a good asymptotic approximation

can be obtained using the method of stationary phase[1]. A full exposition of the mathematical analysis is given in Appendix B. It is shown that the pressure at an axial point receiver at P due to a point source at S is given approximately by:

$$p \approx \rho_o c_o Q(S) b \frac{e^{j\frac{3\pi}{4}}\sqrt{\pi k}}{\left(b^2+\left(\frac{s}{2}\right)^2\right)^{\frac{3}{4}}} e^{j2k\sqrt{b^2+\left(\frac{s}{2}\right)^2}} J_o\left(\frac{kyb}{\sqrt{b^2+\left(\frac{s}{2}\right)^2}}\right) \qquad \ldots(4.9)$$

In the derivation of equation (4.9) it is assumed that the source S is located only a small distance y off axis compared to the tube diameter. In addition, the method of stationary phase requires k in the exponential of equation (4.8) to be large. This condition is fulfilled at the higher end of the difference frequency range of interest, whereas agreement may deteriorate at lower frequencies (f≤5kHz, k≤20).

When the first of the above conditions is satisfied, it turns out (Appendix B), that the major contributions to the reflected waves at the receiver come from specular reflections from two points on the tube wall, half way between the source and the receiver (equations (B25)).

Equation (4.9) can consistently account for source points located a small distance off axis as well as axial source points.

One interesting feature that must be noted in equation (4.9) is the form of the spreading loss factor. The distance travelled from the source point to the receiver via the stationary phase point on the tube wall is equal to:

$$2\left[\left(\frac{s}{2}\right)^2+b^2\right]^{\frac{1}{2}} \qquad \ldots(4.10)$$

---

1 This method has been used extensively for the asymptotic evaluation of diffraction integrals similar to that in equation (4.8). The stationary phase method identifies regions in the vicinity of critical points, within the region of integration, that give rise to the major contributions to the asymptotic expansion, and an approximation is obtained by summing those contributions. For a fuller exposition of this method see [82, p.752-754].

and the expression of a spherical wave emanating from the same point and travelling the same distance under free field conditions would be proportional to:

$$\frac{e^{j2k\sqrt{\left(\frac{s}{2}\right)^2+b^2}}}{2\sqrt{\left(\frac{s}{2}\right)^2+b^2}} \qquad \ldots(4.11)$$

The corresponding term in equation (4.9) has the same form for the exponential term but the spreading term no longer has the 1/(distance) dependence but is given by:

$$\frac{1}{\left(\left(\frac{s}{2}\right)^2+b^2\right)^{\frac{3}{4}}} \qquad \ldots(4.12)$$

Unless a large radius (b) tube and a large source-receiver separation (s) are used, equation (4.12) implies slower spreading than ordinary spherical spreading. That is, some form of focussing of the indirect radiation from the source can be said to occur to waves propagating in a practical tube.

The rest of the terms in equation (4.9) indicate diffraction effects due to the geometry of the situation.

Equation (4.9) will form the basis for the development of most models of the parametric array operating in the tube. As mentioned in the beginning of this chapter, the basic difference of the various mathematical models lies in the geometry of the parametric array source volume.

4.3.2 THE LINE PARAMETRIC ARRAY ON THE TUBE AXIS

The line array model has been used extensively throughout the literature and it has been shown that it generally provides a good compromise in terms of the accuracy of the results it provides and the simplicity of the analysis required.

The output of the line array can be found by adding together the effect of point sources with the appropriate phase. For an axial line array and an axial point receiver, the pressure at the receiver can be obtained using equation (4.9) and setting the off-axis source distance y=0, and integrating over the array length (i.e. z=0 to z=L).

By setting y=0, the zeroth order Bessel function in equation (4.9) becomes equal to unity. Also, if the receiver is situated at a distance R from the transmitting transducer (origin), and a general source point is at z, then s, which represents the source-receiver separation in equation (4.9), should be replaced by R-z. The reflected field at an axial point receiver due to an axial line array is thus given by:

$$p(R) = \rho_o c_o \sqrt{\pi k}\, bQ e^{j\frac{3\pi}{4}} \int_0^L \frac{e^{j2k\sqrt{b^2+\left(\frac{R-z}{2}\right)^2}}}{\left(b^2+\left(\frac{R-z}{2}\right)^2\right)^{\frac{3}{4}}} e^{jkz} dz \qquad \ldots(4.13)$$

where Q is the difference frequency source strength per unit length and is assumed constant throughout the length of the array. The extra term (e^{jkz}) within the integrand accounts for the phase of the virtual source at distance z (see equation 6).

By changing the variable of integration to $t = \frac{R-z}{2}$, equation (4.13) becomes:

$$p(R) = \rho_o c_o \sqrt{\pi k}\, Qbe^{j\frac{3\pi}{4}} e^{jkR} 2 \int_{\frac{R-L}{2}}^{\frac{R}{2}} \frac{e^{j2k\left(\sqrt{b^2+t^2}-t\right)}}{(b^2+t^2)^{\frac{3}{4}}} dt \qquad \ldots(4.14)$$

The integral of equation (4.14) will be evaluated analytically later, under the more general case of the cylindrical parametric array with the help of simplifying assumptions. At present, however, it is quite easy to evaluate equation (4.14) numerically using a Numerical Algorithms (NAG) library routine to perform the numerical integration. The solution is a single frequency solution.

In practise, equation (4.14) is normalised with respect to the on-axis wave to obtain a simple and quick measure of the strength of the unwanted contribution. The normalising equation is equation (4.7) and the final (normalised) result of the line array model is:

$$\Phi(k) = \frac{\text{Reflected signal spectrum}}{\text{Direct signal spectrum}} =$$

$$= \sqrt{\pi k}\,\frac{e^{j\frac{3\pi}{4}}}{\ln\left(\frac{R}{R-L}\right)}\,2b\int_{\frac{R-L}{2}}^{\frac{R}{2}}\frac{e^{j2k\left(\sqrt{b^2+t^2}-t\right)}}{(b^2+t^2)^{\frac{3}{4}}}\,dt \qquad \ldots(4.15)$$

Results obtained using the line array model are compared with experimental results and other theoretical results in figure 4.7.

4.3.3 THE UNIFORM CYLINDRICAL PARAMETRIC ARRAY ON THE TUBE AXIS

The line array model of the previous section can be improved by considering the pseudo-sources to be distributed uniformly in a cylindrical volume equal in diameter to that of the active element of the transducer and extending to the acoustic filter. This is equivalent to assuming that the high frequency transducer produces collimated plane waves, confined to a cylindrical volume, and that the secondary sources are also confined within this volume. These assumptions represent an improvement over the line array model but they are clearly not true since it is well known [84] that the nearfield of the transducer has a complicated structure at the primary frequencies. The structure of the primary field, however, is of the order of the primary wavelength and it appears quite smooth at the scale of the difference frequency wavelength since their ratio is of the order of 1:100 (at about 10kHz) to 1:20 (at about 50kHz). In addition, the acoustic filter limits the interaction volume to well within the primary nearfield where, it can be shown [84], that the primary field is fairly well collimated. Thus, the uniform cylindrical array model is expected to give reasonable results.

The pressure at an axial point receiver due to a cylindrical source on the tube axis can be obtained by integrating equation (4.9) within the limits of the interaction volume. Before this expression is formally written, we must clarify one point in equation (4.9), Q(S) represents the virtual source strength per unit length per unit solid angle of a point source at point S, and it is assumed that, apart from a positional phase factor, this is a constant. In the present geometry, the source strength per unit length per unit area (i.e. per unit volume) per unit solid angle is required. Thus, instead of Q(S) we shall use $Q(S)/(\pi a^2)$ where a is the transducer radius (see equation (4.6)). Thus, the field on the tube axis, distance R from the origin is given by:

$$p(R) = \rho_o c_o \frac{Q}{\pi a^2} \sqrt{\pi k}\, b e^{j\frac{3\pi}{4}} \cdot$$

$$\int_0^L \int_0^{2\pi} \int_0^a \frac{e^{j2k\sqrt{b^2+\left(\frac{R-z}{2}\right)^2}}}{\left(b^2+\left(\frac{R-z}{2}\right)^2\right)^{\frac{3}{4}}} e^{jkz} J_o\left(\frac{kyb}{\sqrt{b^2+\left(\frac{R-z}{2}\right)^2}}\right) y\, dy\, d\theta\, dz \qquad \ldots(4.16)$$

Performing the integration with respect to θ and substituting $t = \frac{R-z}{2}$

$$p(R) = \rho_o c_o \frac{Q}{\pi a^2} \sqrt{\pi k}\, b e^{j\frac{3\pi}{4}} e^{jkR} 2\pi \cdot 2 \cdot$$

$$\int_{\frac{R-L}{2}}^{\frac{R}{2}} \int_0^a \frac{e^{j2k\left(\sqrt{b^2+\left(\frac{R-z}{2}\right)^2}-t\right)}}{\left(b^2+\left(\frac{R-z}{2}\right)^2\right)^{\frac{3}{4}}} J_o\left(\frac{kyb}{\sqrt{b^2+t^2}}\right) y\, dy\, dt \qquad \ldots(4.17)$$

Now consider the integration with respect to y. Let

$$I = \int_0^a J_o\left(\frac{kyb}{\sqrt{b^2+t^2}}\right) y\, dy \qquad \ldots(4.18)$$

with

$$u = \frac{kyb}{\sqrt{b^2+t^2}},$$

then

$$\frac{\partial u}{\partial y} = \frac{kb}{\sqrt{b^2+t^2}}$$

and
$$I = \int_0^{\frac{kab}{\sqrt{b^2+t^2}}} J_o(u) \frac{\sqrt{b^2+t^2}}{kb} u \frac{\sqrt{b^2+t^2}}{kb} du. \qquad \ldots(4.19)$$

Hence
$$I = \frac{(b^2+t^2)}{(kb)^2} \frac{kab}{\sqrt{b^2+t^2}} J_1\left(\frac{kab}{\sqrt{b^2+t^2}}\right) \qquad \ldots(4.20)$$

which can be written as

$$I = \frac{(b^2+t^2)^{\frac{1}{2}}}{kb} a J_1\left(\frac{kab}{\sqrt{b^2+t^2}}\right) \qquad \ldots(4.21)$$

Substituting equation (4.21) into equation (4.17) we get

$$p(R) = \rho_o c_o \frac{Q}{\pi a^2} \frac{\sqrt{\pi k}\, b e^{j\frac{3\pi}{4}}}{kb} e^{jkR} 2\pi.2a \int_{\frac{R-L}{2}}^{\frac{R}{2}} \frac{e^{j2k\left(\sqrt{b^2+t^2}-t\right)}}{(b^2+t^2)^{\frac{3}{4}}} \sqrt{b^2+t^2} J_1\left(\frac{kab}{\sqrt{b^2+t^2}}\right) dt. \qquad \ldots(4.22)$$

Dividing equation (4.22) by equation (4.6) we obtain the normalised reflected wave at R due to a cylindrical array:

$$\Phi_c(k) = \left(\frac{\text{Reflected signal spectrum}}{\text{Direct signal spectrum}}\right)_{\text{cylinder}} =$$

$$= \frac{e^{j\frac{3\pi}{4}}}{\ln\left(\frac{R}{R-L}\right)} 4\sqrt{\frac{\pi}{ka^2}} \int_{\frac{R-L}{2}}^{\frac{R}{2}} \frac{e^{j2k\left(\sqrt{b^2+t^2}-t\right)}}{(b^2+t^2)^{\frac{1}{4}}} J_1\left(\frac{kab}{\sqrt{b^2+t^2}}\right) dt \qquad \ldots(4.23)$$

with $t = \frac{R-z}{2}$ as before.

Equation (4.23) is directly comparable to equation (4.15) which gives the normalised reflected wave at R due to a line array. The only difference between the two results is an extra factor in equation (4.23) of the form:

$$\frac{2J_1\left(\frac{kab}{\sqrt{b^2+t^2}}\right)}{\frac{kab}{\sqrt{b^2+t^2}}} \qquad \ldots(4.24)$$

This term accounts for the directivity of the pseudo source cross-sectional area at an angle

$$\theta = \sin^{-1} \frac{b}{\sqrt{b^2 + t^2}}$$

to the tube axis corresponding to the geometric ray path from the source point to the observation point via the tube wall. This result shows that for low difference frequencies the Bessel function term (equation (4.24)) will have a value very close to unity and the difference between the column array model (equation (4.23)) and the line array model (equation (4.15)) will be very small.

Equation (4.23) does not have a simple analytical solution. It can, however, be easily evaluated numerically in a similar fashion to equation (4.15) using a digital computer running a NAG software package to perform both the numerical integration and the evaluation of the first order Bessel function for discrete frequency steps in the range of interest.

Equation (4.23) was used to obtain the variation of the reflected wave due to a line array along the tube axis for two different frequencies within the range of interest and two different array lengths. Figures 4.3 to 4.6 show the axial variation of the normalised reflected wave (given by ln(R/(R-L)) for frequency f=20 or 50kHz and L=0.52 or 1.0m (see figure caption for the particular values applying in each case). Figures 4.3-4.6 reveal two interesting features: (a) that the reflected wave does not follow the monotonic fall-off of the direct axial wave but exhibits oscillations in amplitude. As will be seen later, these oscillations originate from interference of the waves from the two ends of the parametric array. And, (b) that the reflected wave strength is comparable or greater than that of the direct wave on the axis of the parametric array. This turns out to be the most troublesome feature of the parametric array in the tube.

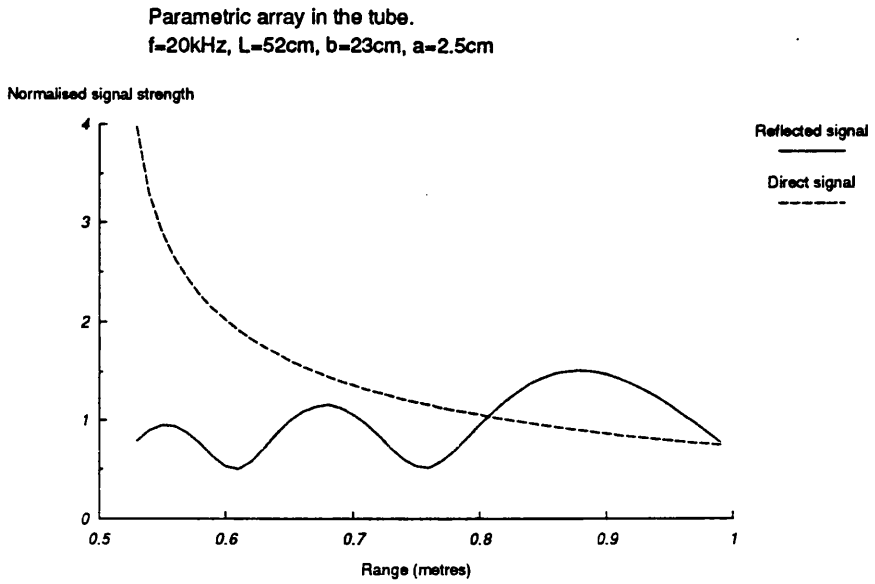

Figure 4.3 The axial variation of the normalized reflected wave in the tube at 20kHz due to a parametric array 52cm long. The normalising (direct) wave variation is also shown (dotted line: ln(R/[R-L])).

Figure 4.7 shows the normalised reflected wave calculated using equation (4.15) (line array model) and equation (4.23) (cylindrical array model) along with experimental results. The receiver position is R=90cm from the origin, L=52cm and the frequency range extends up to 50kHz. It can be seen that the line array model predicts a much stronger reflected wave contribution due to a combination of the focussing effect of the tube wall and the fact that the source is concentrated on the tube axis which is reinforcing that effect. The cylindrical array model gives fairly good agreement with the experimental result.

Although the computational effort required to evaluate equation (4.23) is well within the capabilities of even personal computers, it may be instructive to attempt to approximate analytic solutions of equation (4.23) to obtain a closed form solution and

also, a different insight into the formation of the reflected difference frequency field. In the subsections that follow, three attempts at obtaining an approximate closed form solution to equation (4.23) are described.

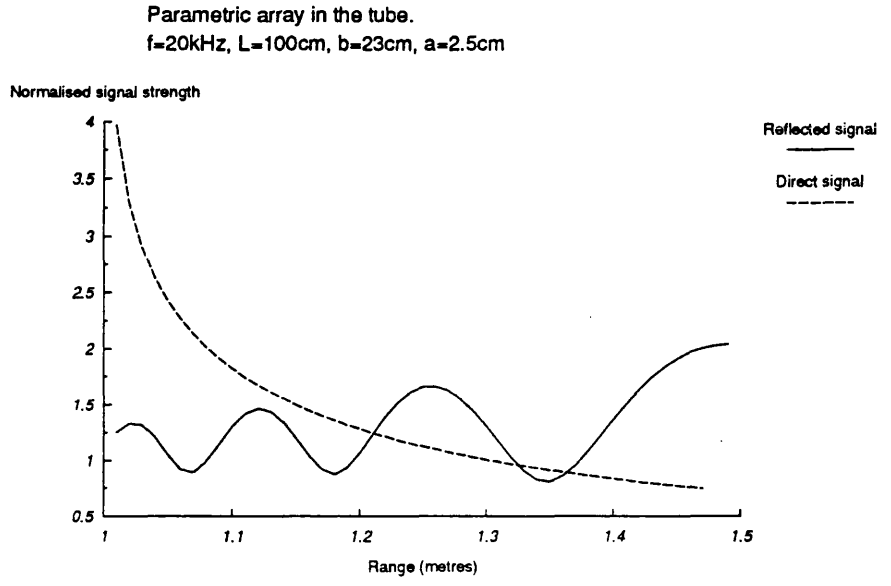

Figure 4.4 The axial variation of the normalised reflected wave in the tube at 20kHz due to a parametric array 100cm long.

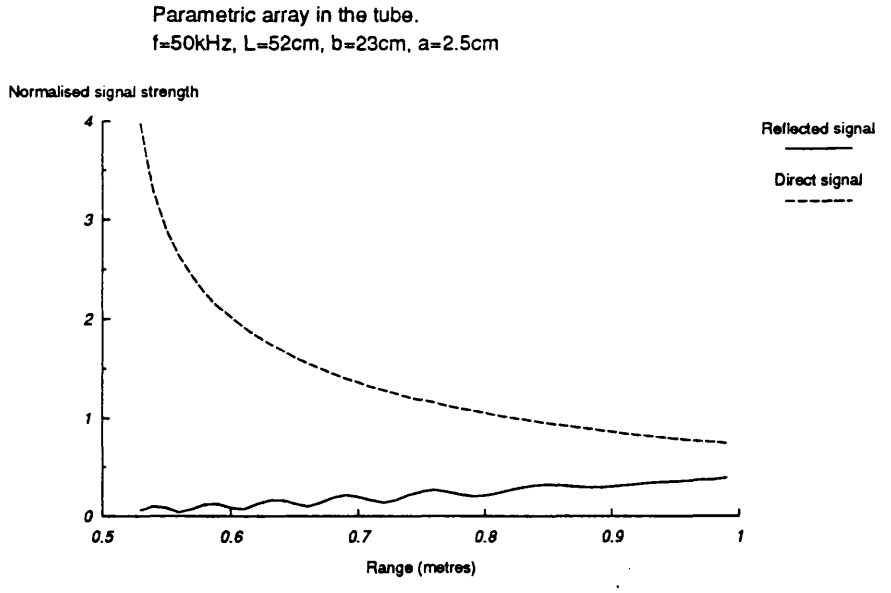

Figure 4.5 The axial variation of the normalised reflected wave in the tube at 50kHz due to a parametric array 52cm long.

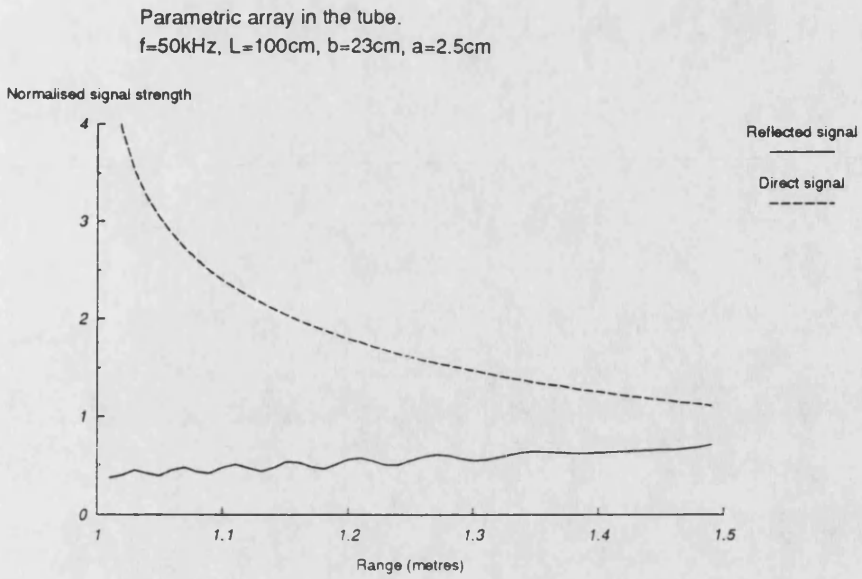

Figure 4.6 The axial variation of the normalised reflected wave in the tube at 50kHz due to a parametric array 100cm long.

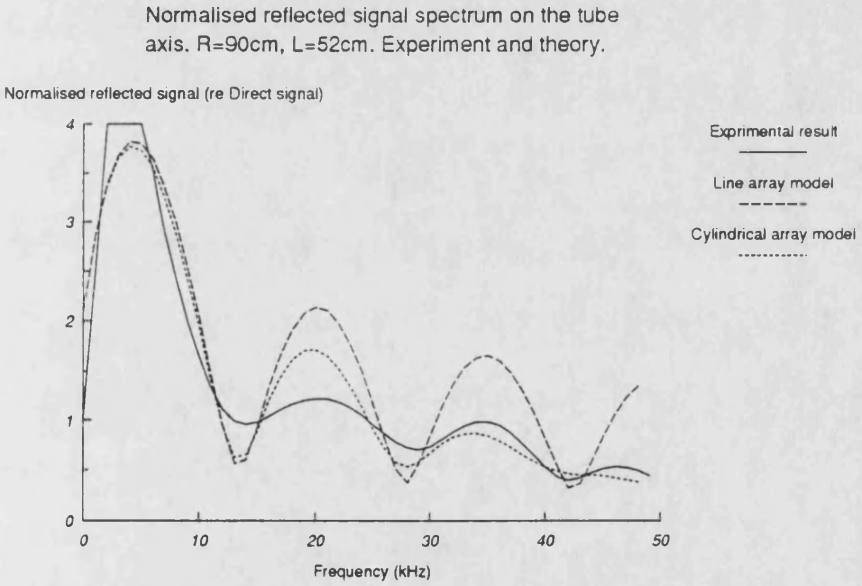

Figure 4.7 Theoretical (equations (4.15) & (4.23)) and experimental estimates of the normalised reflected wave spectrum obtained on the tube axis at R=90cm with a parametric array 52cm long.

4.3.3.1 STATIONARY PHASE SOLUTION OF EQUATION (4.23)

An alternative to the numerical computation of equation (4.23) is to obtain an asymptotic approximation to the integral using the method of stationary phase (see section 4.3.1). This would enable much faster calculation of the reflected wave spectrum.

Two problems, however, arise with this approach. First, as mentioned previously, the stationary phase method relies on the assumption that the value of the wavenumber k in the exponential within the integral is large. This condition leads to large fluctuations of the value of the exponential which eventually cancel out except in the region of the critical (stationary phase) point(s) where the major contribution(s) to the integral come from. This condition is obviously not satisfied at lower difference frequencies. In addition, a second problem arises due to the fact that, as can be shown (Appendix C), there is no stationary phase point within the region of integration. Although the method is still capable of providing an asymptotic approximation to the solution of equation (4.23), the accuracy of this approximation will be impaired by the two factors mentioned above.

The algebraic manipulation required to obtain the stationary phase approximation to equation (4.23) is given in Appendix D. Here, it will suffice to give the final expression for the normalised reflected wave strength on axis (equation (D6)):

$$\Phi(R) = \frac{1}{\ln\left(\frac{R}{R-L}\right)} \frac{2}{a} \sqrt{\frac{\pi}{k}} e^{j\frac{\pi}{4}} \frac{1}{k} \cdot \left[\frac{(b^2+t_1^2)^{\frac{1}{4}}}{\sqrt{b^2+t_1^2}-t_1} e^{j2k\left(\sqrt{b^2+t_1^2}-t_1\right)} J_1\left(\frac{kab}{\sqrt{b^2+t_1^2}}\right) - \frac{(b^2+t_2^2)^{\frac{1}{4}}}{\sqrt{b^2+t_2^2}-t_2} e^{j2k\left(\sqrt{b^2+t_2^2}-t_2\right)} J_1\left(\frac{kab}{\sqrt{b^2+t_2^2}}\right) \right] \quad \ldots(4.25)$$

where

$$t_1 = \frac{R-L}{2} \text{ and } t_2 = \frac{R}{2}$$

This solution suggests that the main contributions to the reflected wave at the receiver come from the two end points of the parametric array represented here by t_1 and t_2. The two sources are in phase opposition and hence they subtract when they interfere.

A comparison of the result obtained using equation (4.25) to the numerical result from equation (4.23) is shown in figure 4.8. The input parameters are R=90cm, L=52cm and the frequency range extends to 50kHz. It can be seen that, as expected, the agreement between the two results is very good except at low frequencies were the stationary phase approximation does not hold (small k).

4.3.3.2 APPROXIMATE ANALYTIC SOLUTION OF EQUATION (4.23)

In the previous section, the stationary phase method was used to obtain an asymptotic approximation to the integral in equation (4.23). It is well known that for the stationary phase approximation to be valid, k (the difference frequency wavenumber) in the exponent inside the integral should be large. This is clearly not true at the lower end of the frequency range of interest and the results obtained using equation (4.25) begin to deviate from numerical predictions of equation (4.23). In this section, a different approach is attempted in order to avoid the stationary phase approximation and its drawbacks.

Attention is again drawn to the integral within equation (4.23):

$$\Phi = \frac{e^{j\frac{3\pi}{4}}}{\ln\left(\frac{R}{R-L}\right)} 4\sqrt{\frac{\pi}{ka^2}} \cdot I \qquad \ldots(4.23)$$

where

$$I=\int_{\frac{R-L}{2}}^{\frac{R}{2}} \frac{e^{j2k\left(\sqrt{b^2+t^2}-t\right)}}{(b^2+t^2)^{\frac{1}{4}}} J_1\left(\frac{kab}{\sqrt{b^2+t^2}}\right)dt. \qquad \ldots(4.26)$$

Making two substitutions:

$$i)\quad u=\sqrt{b^2+t^2}-t \qquad \ldots(4.27A)$$

$$ii)\quad v=\frac{u}{b} \qquad \ldots(4.27B)$$

and expanding $J_1(z)$ (here $z=\frac{2kav}{1+v^2}$) as an asymptotic series [83] gives

$$J_1=\frac{1}{2}\{H_1^{(1)}(z)+H_1^{(2)}(z)\}=$$

$$=\frac{1}{\sqrt{2\pi z}}\left\{e^{j\left(z-\frac{3\pi}{4}\right)}F_1(z)+e^{-j\left(z-\frac{3\pi}{4}\right)}F_2(z)\right\} \qquad \ldots(4.28)$$

where $F_1(z)$ and $F_2(z)$ are hypergeometric series [83].

After some considerable algebraic manipulation equation (4.23) becomes:

$$\Phi=\frac{1}{\ln\left(\frac{R}{R-L}\right)}\sqrt{\frac{2\pi}{kb}}\frac{1}{ka}\cdot$$

$$\left[\frac{1+v_1^2}{v_1^{\frac{3}{2}}}e^{j\left(2kbv_1+\frac{\pi}{4}\right)}\left\{\frac{J_1\left(\frac{2kav_1}{1+v_1^2}\right)-j\frac{a}{b\left(1+v_1^2\right)}Y_1\left(\frac{2kav_1}{1+v_1^2}\right)}{1-\left(\frac{a}{b\left(1+v_2^2\right)}\right)^2}\right\}\right]-$$

$$\left[\frac{1+v_2^2}{v_2^{\frac{3}{2}}}e^{j\left(2kbv_2+\frac{\pi}{4}\right)}\left\{\frac{J_1\left(\frac{2kav_2}{1+v_2^2}\right)-j\frac{a}{b\left(1+v_2^2\right)}Y_1\left(\frac{2kav_2}{1+v_2^2}\right)}{1-\left(\frac{a}{b\left(1+v_2^2\right)}\right)^2}\right\}\right] \qquad \ldots(4.29)$$

where

$$v_1=\sqrt{1+\left(\frac{R}{2b}\right)^2}-\frac{R}{2b}$$

$$v_2=\sqrt{1+\left(\frac{R-L}{2b}\right)^2}-\frac{R-L}{2b}$$

and $J_1()$ and $Y_1()$ represent, respectively, Bessel and Neuman functions of the first

kind and order one.

A detailed mathematical derivation of equation (4.29) is given in appendix E. Here, it will suffice to say that due to the considerable complexity of the expressions that appear in the derivation of equation (4.29), it has to be assumed that the value of 2kb is much larger than one. Thus, again, the validity of this solution is restricted at the lower end of the difference frequency range of interest.

The restrictions that have to be imposed on the difference frequency wavenumber k have the same effect as the stationary phase approximation. Thus, a comparison of the results obtained using equation (4.29) with numerical results from equation (4.23) reveal good agreement except at lower frequencies, as expected.

The solution, is again the sum of contributions from two points represented by v_1 and v_2 which represent the end-points of the parametric array in transformed co-ordinates.

Figure 4.8 shows the results obtained using equation (4.29) along with numerical results from equation (4.23) approximate results from equation (4.25) derived in the previous section and experimental results. It can be seen that only at low frequencies there is some discrepancy between the theoretical results. This is due to the assumptions made in the derivation of equations (4.25) and (4.29) which forfeit their validity at low frequencies.

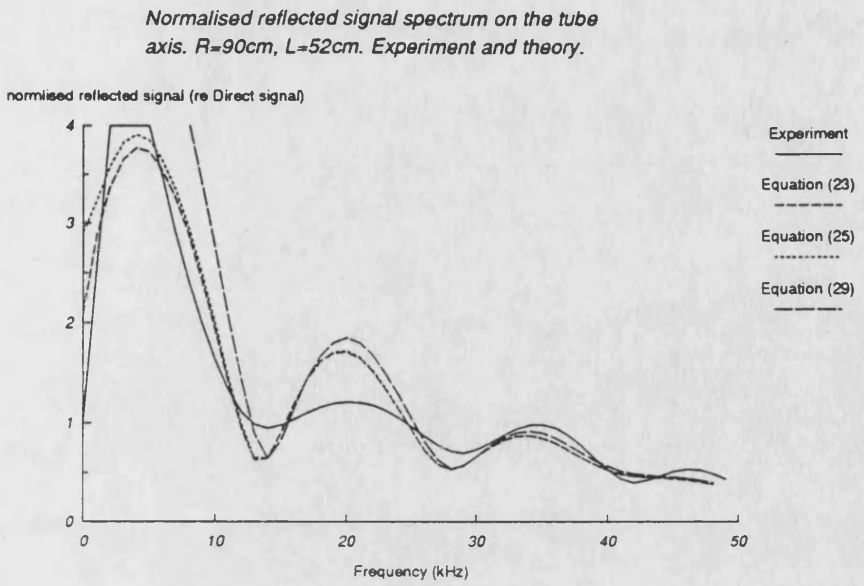

Figure 4.8 Experimental and theoretical (equations (4.23),(4.25) & (4.29)) estimates of the reflected wave spectrum on the tube axis.

4.3.4 THE NORMALISED DIFFERENCE FREQUENCY FIELD AT AN AXIAL RECEIVER DUE TO AN EXTENDED PARAMETRIC ARRAY WITH THE PRIMARY FIELD ACCOUNTED FOR.

So far, it has been assumed that the difference frequency sources are distributed either along a line or, more realistically, uniformly throughout a cylindrical volume with a radius equal to that of the transducer and extending from the transducer to the acoustic filter. The latter model is fairly well justified provided the array length L does not exceed the nearfield distance at the primary frequency.

Since, as will be seen at a later chapter, there is some discrepancy between experimental results and those given by the models described in the previous sections, it was decided to include the primary field structure within the model in order to weigh the contributions from the different parts of the array. There are, however, difficulties associated with the exact analytical description of the primary sound field generated by the transducer.

The nature of the radiated field from a planar piston transducer has been studied widely and approaches are diverse. Zemanek [84] has presented numerical results for the nearfield of such an acoustic source. A similar approach would not be suitable here because extra numerical integrations would be required to the ones that are already performed. A review of other solutions can be found in [85] and [86]. It turns out that although the approaches to this problem are diverse, most efforts can be traced to a few fundamental methods of analysis. Principal among these solutions are those by Rayleigh, King and Schoch [86]. The expressions used for this analysis are analytic (stationary phase) approximations derived by Lancaster [87] and based on a solution of King's integral. These expressions were derived as part of a quasilinear analysis of the nonlinear field of an ultrasonic radiator and as such would not apply if the parametric array was saturating. The difference frequency strength of a parametric source point within the array turns out to be:

$$\text{Source strength} \quad q' = q_o \cdot q_{1,2}(y,s) \qquad \ldots(4.30)$$

where

q_o:- is the difference frequency source strength due to unit amplitude primary strength (equation 6)

y:- radial distance of source point

s:- axial distance of source point

$q_{1,2}$:-the product of the normalised primary field amplitude at one of the generating frequencies with the complex conjugate of the normalised primary field at the other generating primary frequency , at a point (y,s); (both normalised with respect to that on the transducer face). q_1 for y<a and q_2 for y>a

With [87]:

$$q_1 = e^{jks}\left\{1 + \frac{R_o \pi}{2s}\Gamma\Gamma^* e^{j\frac{R_o}{s}(1+\mu^2)}\right\} \qquad \ldots(4.31)$$

$$q_2 = e^{jks}\frac{R_{o+}\pi}{2s}\Lambda\Lambda^* e^{j\frac{R_o}{t}(1+\mu^2)} \qquad \ldots(4.32)$$

where * denotes a complex conjugate and

$$\mu = \frac{y}{a}$$

$$R_{o+} = \frac{Ka^2}{2} = \text{ Rayleigh distance at the primary frequency}$$

$$R_o = \frac{ka^2}{2} = \text{ Rayleigh distance at the difference frequency}$$

and

$$\Gamma = H_o^{(1)}\left(\frac{2R_{o+}\mu}{s}\right)(g+jf)\left((1+\mu)\sqrt{\frac{2R_{o+}}{\pi s}}\right)+$$
$$+H_o^{(2)}\left(\frac{2R_{o+}\mu}{s}\right)(g+jf)\left((1-\mu)\sqrt{\frac{2R_{o+}}{\pi s}}\right) \qquad \ldots(4.33)$$

$$\Lambda = H_o^{(1)}\left(\frac{2R_{o+}\mu}{s}\right)(g+jf)\left((1+\mu)\sqrt{\frac{2R_{o+}}{\pi s}}\right)-$$
$$-\sqrt{\mu}H_o^{(2)}\left(\frac{2R_{o+}\mu}{s}\right)(g+jf)\left((\mu-1)\sqrt{\frac{2R_{o+}}{\pi s}}\right) \qquad \ldots(4.34)$$

In equations (4.33) and (4.34), $H_o^{(1)}$ and $H_o^{(2)}$ represent zeroth order Hankel functions of the first and second kind respectively, and g & f are Fresnel functions that can be computed using a polynomial approximation [83].

Using equations (4.30)-(4.34) and following the same procedure used in section 4.3.3 for the derivation of equation (4.23), we get the following result for the normalised reflected wave spectrum at an axial receiver:

$$\Phi(R) = \frac{\sqrt{\pi k}}{\ln\left(\frac{R}{R-L}\right)}4\frac{b}{a^2}\int_{\frac{R-L}{2}}^{\frac{R}{2}}\frac{e^{j2k\left(\sqrt{b^2+t^2}-t\right)}}{(b^2+t^2)^{\frac{3}{4}}}dt \cdot (I_1+I_2) \qquad \ldots(4.35)$$

where

$$I_1 = \int_0^a q_1(y,t) J_o\left(\frac{kby}{\sqrt{b^2+t^2}}\right) y\,dy \qquad \ldots(4.36)$$

$$I_2 = \int_a^b q_2(y,t) J_o\left(\frac{kby}{\sqrt{b^2+t^2}}\right) y\,dy \qquad \ldots(4.37)$$

$$\text{and} \quad t = \frac{R-s}{2}$$

In practise, the upper limit in the radial integral in equation (4.37) does not have to extend to the tube radius since the primary field is confined to small off axis distances. Figure 4.9 shows the radial distribution of the primary field close to the transducer (at ≈3 transducer radii) and also at a distance of L=0.52m which is the usual parametric array length. It can be seen from figure 4.9 that the primary field (and consequently the difference frequency field) does not exhibit the step distribution assumed for the uniform array model, although, by definition, the total primary field energy is the same. Also, it can be seen that the radial limit of the integral in equation (4.37) can be safely set to about 2 transducer radii. This is especially true at smaller distances from the transducer and enables faster numerical computation of equation (4.37). Figure 4.9 also reinforces the assumption of the uniform array model that postulates a collimated primary beam.

As far as the axial distribution of the primary and difference frequency radiation is concerned, figures 4.10 and 4.11 may enable the formulation or justification of a model for the parametric array source distribution. Figure 4.10 shows the axial variation of the normalised primary field (1MHz) produced by a transducer of radius 0.025m in the range 0m-0.52m. At distance smaller than two transducer radii the field is set equal to unity to avoid the rapid fluctuations brought about by diffraction effects. It would seem at first sight that a uniform cylindrical array model could not be based on these findings. Figure 4.11, however, shows the product of the normalised primary field amplitudes that

give rise to the difference frequency point sources (equations (4.30) or (4.31) depending on the radial distance). The variation of the difference frequency source strength, at 30kHz, in the direction of propagation is plotted along the acoustic axis, at a radial distance of 0.025m (=transducer radius) parallel to the acoustic axis, and at a radial distance of 0.05m which is equal to twice the transducer radius. Figure 4.11 has several interesting features: (a) the axial difference frequency field is almost constant and bears no resemblance to the primary field variation along the acoustic axis (figure 4.10).
(b) In addition, the off-axis difference frequency wave modulation is much smoother than that of the primary field, and,
(c) at radial distances larger than the transducer radius, along a path parallel to the acoustic axis, the difference frequency source strength is very low (provided, of course, that we are confined to the primary nearfield).

Thus, in view of the above, we may conclude that in the difference frequency range of interest and for the parametric array length used here, the uniform cylindrical array model can be a very good approximation to the actual difference frequency source distribution.

Equation (4.35) has been evaluated using a desk-top computer to perform the double integration numerically. The results obtained using equation (4.23) are compared to those obtained using equation (4.35) in figure 4.12. These results seem to support the cylindrical wave approximation of the uniform array models. The main difference between the uniform array model and the present one which accounts for the fine structure of the primary field is due to the fact that the radial distribution of difference frequency sources turns out to be smoother than the step-like distribution of the uniform array models. Thus interference effects from the two ends of the parametric array models, as seen in figure 4.12 are stronger when the uniform array model is used.

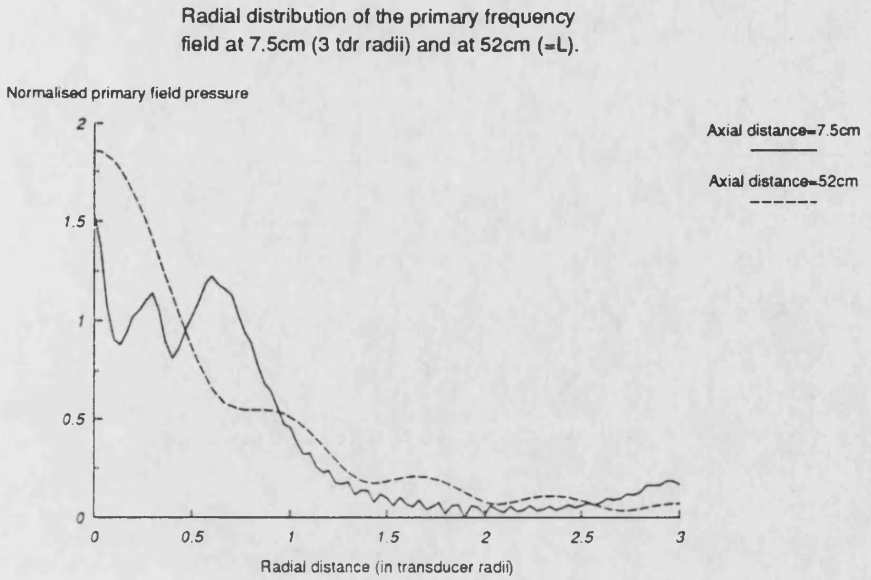

Figure 4.9 The radial distribution of the normalised primary field (1MHz) close to the transducer (≈3 transducer radii) and at a distance of 52cm.

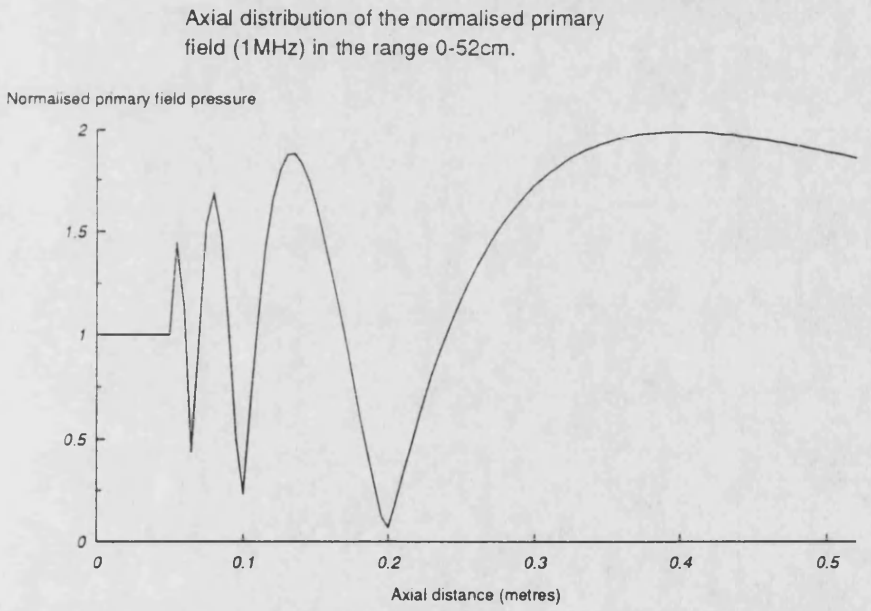

Figure 4.10 The axial variation of the normalised primary field (1MHz)

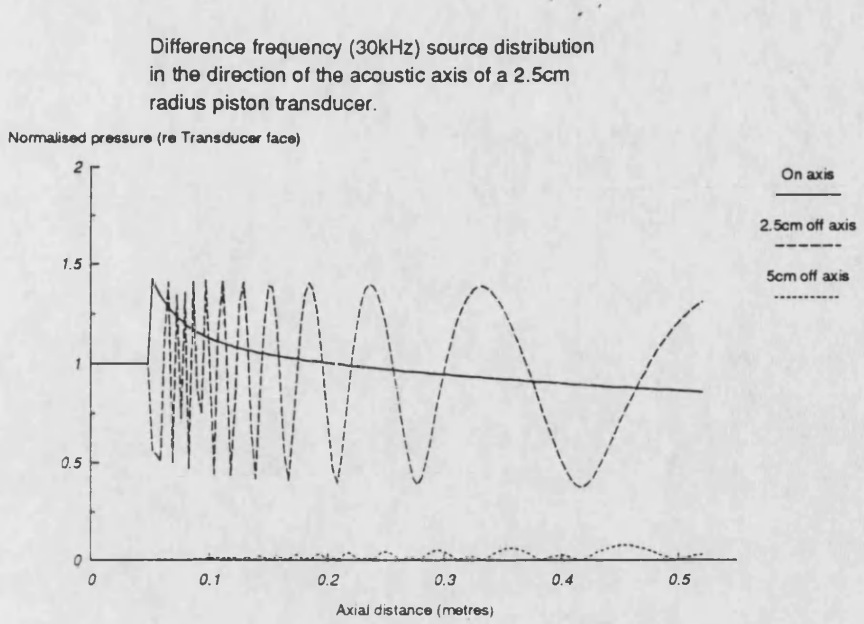

Figure 4.11 The product of the normalised primary field (960kHz) amplitudes that give rise to difference frequency point sources at 30kHz. (a) along the transducer axis, (b) 2.5cm off axis and (c) 5cm off axis.

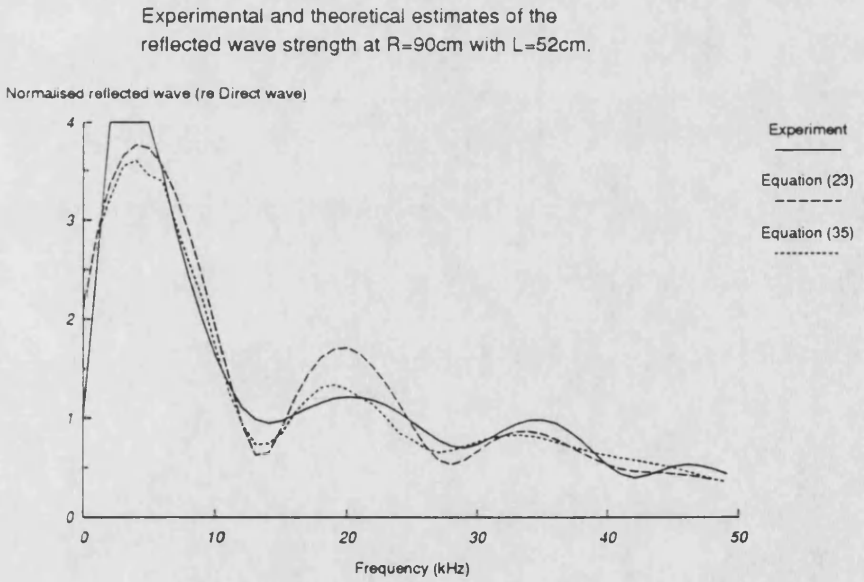

Figure 4.12 Theoretical (equations (23) & (35)) and experimental estimates of the reflected wave spectrum on the tube axis.

4.4 SUMMARY

In this chapter, a theoretical investigation of a truncated parametric array in a wide bore tube has been presented. It is useful to construct a mathematical model in order to understand the physical processes that give rise to the experimental observations and to obtain accurate estimates of the strength of the signals involved. Two principle contributions to the field inside the tube have been considered; one due to direct propagation along the tube axis and another due to a reflected waves that have undergone a single bounce. The direct wave strength has been evaluated by using a free field solution.

The analysis begins with the presentation of some fundamental results relating to the parametric array under free field conditions. An expression is obtained for the direct axial wave generated by the parametric array in the tube. This expression is subsequently used to normalise other extraneous waves in order to measure clearly their relative importance.

The geometry of the experiment has been taken into account in order to calculate the field at a point on axis due to a general off-axis point source. In this case, it is the indirect contributions to the wave at the receiver that are of interest. It turns out that the tube wall confines the indirect radiation from the source and redirects it back towards the tube axis. This effect can be likened to focussing of the reflected wave back onto the tube axis. Thus, although the indirect wave generated by the parametric array is weak compared to the axial wave, the focussing effect of the tube wall leads to very strong reflected contributions on the tube axis.

Another result of the treatment of the point source and receiver within the tube is that the most significant contributions to the reflected wave at the receiver follow geometrical ray paths via the tube wall. This simplification is very useful at later stages when it

comes to identifying the various components of the reflected wave from more complicated source geometries. The propagation delay associated with different ray paths enables various contributions to be identified.

The results of the treatment of the point source and receiver in the tube form the basis for the construction of more complex and refined models for the parametric array which is just considered as a conglomeration of point sources. Three models have been considered here: the simplest one is the line array model which considers the difference frequency sources to be distributed along the axis of the primary frequency transducer. This model is commonly justified in view of the small transverse dimensions of the primary frequency interaction volume in terms of the difference frequency wavelength. In the present geometry, however, this is not a satisfactory model due to the 'focussing' of the tube wall. The estimated strength of the reflected wave is too high.

A more realistic model of the parametric array source volume is a cylinder of uniform strength point sources extending from the transducer to the truncation filter and of radius equal to that of the transducer. Several expressions for the normalised reflected wave strength at an axial receiver have been derived using both numerical and analytic approximations for this case.

The most rigourous model of the parametric source volume takes into account the structure of the primary field that gives rise to the difference frequency sources. Numerical results are obtained using this model but, it turns out, that the results are very similar to those obtained with the uniform cylindrical array model. Thus, the latter is preferred since it is much easier and faster to compute. This agreement can also be taken as a justification of the uniform array model for the parametric source distribution in the present case. It would, however, be necessary to include the influence of the primary field structure if the parametric array volume was allowed to extend to the farfield of

the primary radiation.

It has not been possible to construct a mathematical model of the parametric array in the tube that would give rigourous analytic or even numerical results with reasonable computational effort. The various approximations and assumptions that must be made in each model have been discussed within the individual sections. Most of the theoretical models do not yield analytic expressions for the reflected wave strength. Thus, can either be obtained by performing a numerical integral or by making further approximations to obtain an analytic solution. In the cases presented, however, the difference between the numerical and approximate analytic results was very small. In addition, the numerical solutions were not very hard to obtain even with a moderately powered digital computer. Thus, numerical solutions would be preferable in view of the fewer approximations required to obtain them. The analytic results indicate clearly, that the most significant contributions to the reflected wave at an axial receiver come from the two ends of the truncated parametric array which seem to radiate in phase opposition. This effect can be clearly seen in the interference pattern obtained when a plot of the normalised reflected wave of a particular frequency is plotted along the tube axis.

5 SYNTHETIC APERTURE RECEIVER MEASUREMENTS

5.1 INTRODUCTION

It has been shown, both theoretically and experimentally, that a fundamental characteristic of the operation of a parametric array in a wide bore tube is the presence of difference frequency waves reflected from the tube wall. These give rise to a long and complicated tail after the direct wave arriving at the receiver (figure 5.1). With appropriate choice of observation distance, parametric array length and tube diameter the different arrivals can just be separated. However, the separation of arrivals would not be satisfactory if the direct signal was lengthened as it would be, for example, by multiple reflections within the sample.

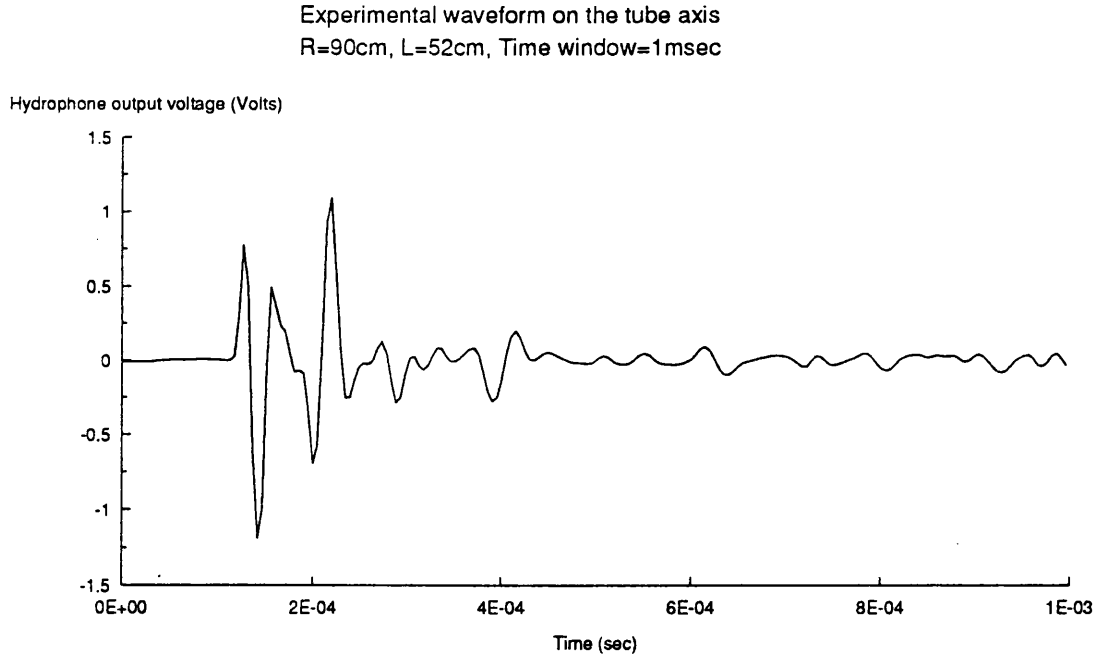

Figure 5.1. A typical experimental waveform recorded on the axis of the tube.

Two ways of reducing the importance of the reflected wave contribution were identified and pursued. The first method relied on the use of an absorbing lining on the inside surface of the tube. Several problems are associated with this approach which will be

described in chapter 6. The second method used to reduce the reflected wave strength aimed to reduce the sensitivity of the receiver to off-axis arrivals by synthesizing a directional receiving aperture. In this respect, the Brüel & Kjær 8103 hydrophone used is not ideal since its omnidirectional response means that there is no directional selectivity built into the receiver. The receiver synthesis techniques used here employ linear processing to reduce the directivity of the receiving aperture and no nonlinear techniques are employed.

It is well known that in order to obtain good directionality from a receiver, its aperture should be as large as possible in terms of the wavelength of the radiation it is supposed to detect.

In this case it was not realistic to use a hydrophone with the physical size required. Hence a large aperture receiver was synthesized by scanning a point receiver (the B&K hydrophone) across the aperture plane. The signal was recorded at several points and subsequently added with appropriate weighting for each signal. This assumed that the field is effectively stationary over the measurement period; an assumption easily satisfied over a period of a few minutes that a typical run took.

This technique is by no means new and was first used in Radio Astronomy [91]. Synthetic Aperture Radar (SAR) has been under development for many years and SAR is now a routine technique that produces high quality imagery at microwave frequencies [92]. The implementation of SAR techniques in underwater acoustics is usually associated with Synthetic Aperture Sonar (SAS) and is usually less successful than SAR due to three complicating factors:
First, the low (sound) velocity and low frequency range associated with sonar require the sonar to be towed slowly to ensure adequate sampling of the aperture. Second, the scanning speed as well as tidal and wave motion make it difficult to assess the sonar

position within the aperture accurately. Third, the underwater medium is not as stable and homogeneous as air and problems with sonar are more severe than those in SAR [93].

The above complications, however, do not affect the use of the technique for the purpose of the present application.

Griffiths and Gida [94] have performed synthetic aperture measurements in a laboratory tank and obtained improved spatial resolution of two point sources in their efforts to develop a system for underwater target classification. Their work, however, concentrates on the synthesis of linear apertures with no account of the different weighting schemes that are possible for the improvement of synthetic aperture characteristics.

The various techniques used in aperture design have been primarily developed for electromagnetic wave transmission and detection and are usually described in the literature for antenna, aperture or array design [95-98]. Some of the literature available on those subjects was utilised in the synthesis of a directional receiver.

As described in chapter 3, the hydrophone could be scanned along the diameter of the tube under computer control using a stepper motor and a screw thread. This enabled the signal to be recorded at several points along a line offered the possibility of synthesizing a line array of point receivers.

In the following section, the general principles of array design are presented and the optimum weightings for a line array are discussed.

When, however, we consider the confined acoustic field in the wide bore tube more closely, we find that the results of the linear array theory do not apply in a straight forward

manner (section 5.3). Instead of considering a planar wavefield incident on the receiver we must investigate its response to a field with cylindrical symmetry such as that reflected from the inner surface of the tube.

The directional response of various synthetic apertures in such a wavefield are considered in order to assess their usefulness for the purposes of this work. The pre-requisite qualities of the receiver are narrow beamwidth and low sidelobe levels at the frequency range of interest.

In section 5.2 the general principles or receiver array design are reviewed and some designs are presented. In section 5.3 the operation of a synthetic receiving aperture in the tube is investigated. The response of the synthetic receiver to reflected waves from the tube walls as well as that due to an axial line source is calculated. Experimental results using receiver synthesis in the tube are presented in section 5.4 and a discussion of the theoretical and experimental results is presented in section 5.5.

5.2 PRINCIPLES OF RECEIVER ARRAY DESIGN

The basic principles involved in the design of a linear receiving array are treated here. Although this treatment can be found in several textbooks, it is briefly presented here in order to provide a grounding for the more complex situation encountered in this work.

We begin by considering an array of N point receivers equally spaced on the x-axis as shown in figure 5.2.

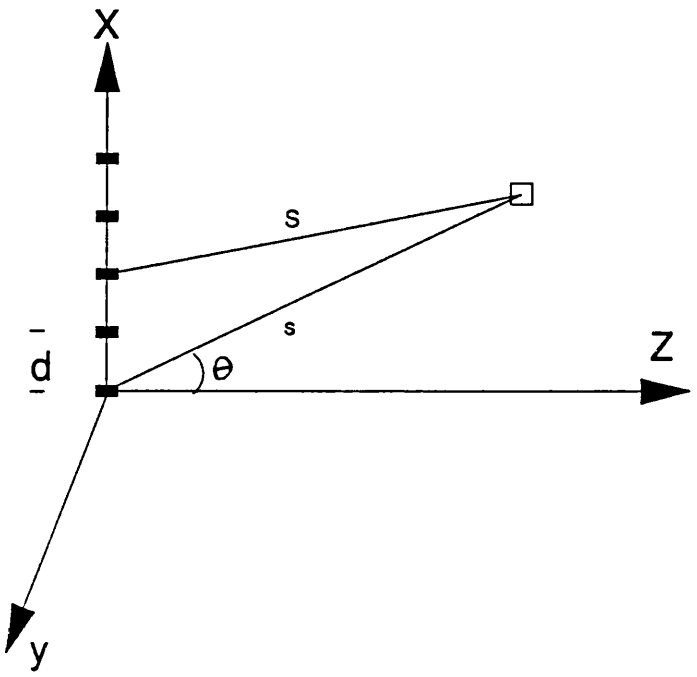

Figure 5.2. Receiving elements arranged regularly along the x-axis with spacing d and a source point at S in the far-field.

This distribution may be represented by

$$J = \delta(z)\delta(y)\sum_{n=0}^{n=N-1} A_n \delta(x - nd) \qquad \ldots(5.1)$$

where A_n is the weighting given on the n^{th} receiver (i.e. on the receiver when it occupies that position).

The overall received field A due to a point source at (s,θ) is given by the following diffraction integral

$$A = \int\int\int \frac{e^{-jkS}}{S} J dx dy dz =$$

$$= \int\int\int \frac{e^{-jkS}}{S} \delta(z)\delta(y)\sum_{n=0}^{n=N-1} A_n \delta(x - nd) dx dy dz \qquad \ldots(5.2)$$

If the source is in the far field of the receiving aperture, S may be approximated by (Fraunhoffer approximation)

$$S \approx s - x\sin\theta \qquad \text{in the exponent}$$

$$\text{and} \quad S \approx s \qquad \text{in the denominator}$$

$$\therefore \quad A = \int \frac{e^{-jkS}}{S} e^{jkx\sin\theta} \sum_{n=0}^{n=N-1} A_n \delta(x - nd)dx \qquad \ldots(5.3)$$

$$\therefore \quad A = \frac{e^{-jks}}{4\pi s} \sum_{n=0}^{n=N-1} A_n e^{jknd\sin\theta} \qquad \ldots(5.4)$$

The array factor (A.F.) is defined as

$$A.F. = \sum_{n=0}^{n=N-1} A_n e^{jknd\sin\theta} \qquad \ldots(5.5)$$

The element weights A_n do not have to be real. They may be complex and differ in both amplitude and phase[1].

Two important concepts in array design are those of the grating lobes and of the visible region. Consider equation (5.5)

Let

$$\psi = kd\sin\theta \qquad \ldots(5.6)$$

then, equation (5.5) becomes

$$A.F. = \sum_{n=0}^{n=N-1} A_n e^{jn\psi} \qquad \ldots(5.7)$$

Since the angle θ is a polar angle its range of values extends in the region $-\frac{\pi}{2} \le \theta \le \frac{\pi}{2}$. Thus, although the array factor is defined for all ψ, only the portion of the array factor in the range $-kd \le \psi, \le kd$ is associated with actual physical angles θ and shows up in an actual radiation or reception pattern. This range of A.F.(ψ) is called the visible region.

1 A linear intra-element phase variation forms the basis of operation of phase array beam steering. A quadratic phase variation leads to beam focussing.

Also, since exp(j2nπ)=1 the exponent in equation (5.7) is periodic with respect to ψ with period 2π and

$$A.F.(\psi) = A.F.(\psi \pm 2\pi) \qquad \ldots(5.8)$$

That is, the directivity pattern is repeated every

$$\psi = \pm 2\pi = kd \sin\theta \qquad \ldots(5.9)$$

This expression leads to a criterion for the spacing of the receiving elements in order to avoid the presence of grating lobes in the range of θ that is of interest. If, for example, we want the first grating lobe to appear at just the edge of the visible region, then $|\sin\theta| = 1$ and equation (5.9) gives

$$kd \leq 2\pi$$

$$\therefore d \leq \lambda \qquad \ldots(5.10)$$

The inequality in the above equation signifies that all grating lobes will be outside the visible region.

A common simplification of equation (5.7) is obtained by considering an odd number of elements N symmetrically distributed about the centre of the array so that $A_n = A_{-n}$, the array factor becomes

$$A.F.(\psi) = \sum_{n=-\frac{N-1}{2}}^{n=\frac{N-1}{2}} A_n e^{jn\psi} \qquad \ldots(5.11)$$

$$\therefore \quad A.F.(\psi) = A_o + 2\sum_{n=1}^{n=\frac{N-1}{2}} A_n \cos(n\psi) \qquad \ldots(5.12)$$

Different designs of linear array receivers may be obtained by using different functional dependences for the weighting (A_n) applied to the various elements comprising the array.

5.2.1 THE UNIFORM LINE ARRAY

The simplest weighting scheme that can be applied to the receiving elements is to give every one the same amplitude response A_o; then, the array factor (equation (5.8)) becomes

$$A.F. = A_o \sum_{n=-\frac{N-1}{2}}^{n=\frac{N-1}{2}} e^{jn\psi}$$

$$= A_o \frac{\sin\left(\frac{N\psi}{2}\right)}{\sin\left(\frac{\psi}{2}\right)} \qquad \ldots(5.13)$$

In many cases it is more appropriate to plot the square of the array factor as defined here multiplied by the constant at the front of equation (5.4) which accounts for spherical spreading.

The directional response of a uniform line array of overall length 2L=N.d, normalised with respect to its peak mainlobe value is plotted in figure 5.3 versus $N\psi/2=kL\sin\theta$. Thus the ordinate values in figure 5.3, for a given element separation d, represent different real angles θ at different frequencies (k). That is, the higher the field frequency, the narrower the directivity of this receiver. This is actually true for any aperture excitation.

The first zero in the response of the array shown in figure 5.3 occurs at

$$\frac{N\psi}{2} = \pi \qquad \therefore \qquad \sin\theta = \frac{\lambda}{Nd} \qquad \ldots(5.14)$$

That is, the beamwidth of the uniform line array decreases as its overall length (Nd) increases.

The first sidelobe of the array factor is -6.7dB lower than the main lobe (i.e. the sidelobe of the square modulus of the A.F. is -13.4dB). Although this difference is quite large, it may not be sufficient for some applications.

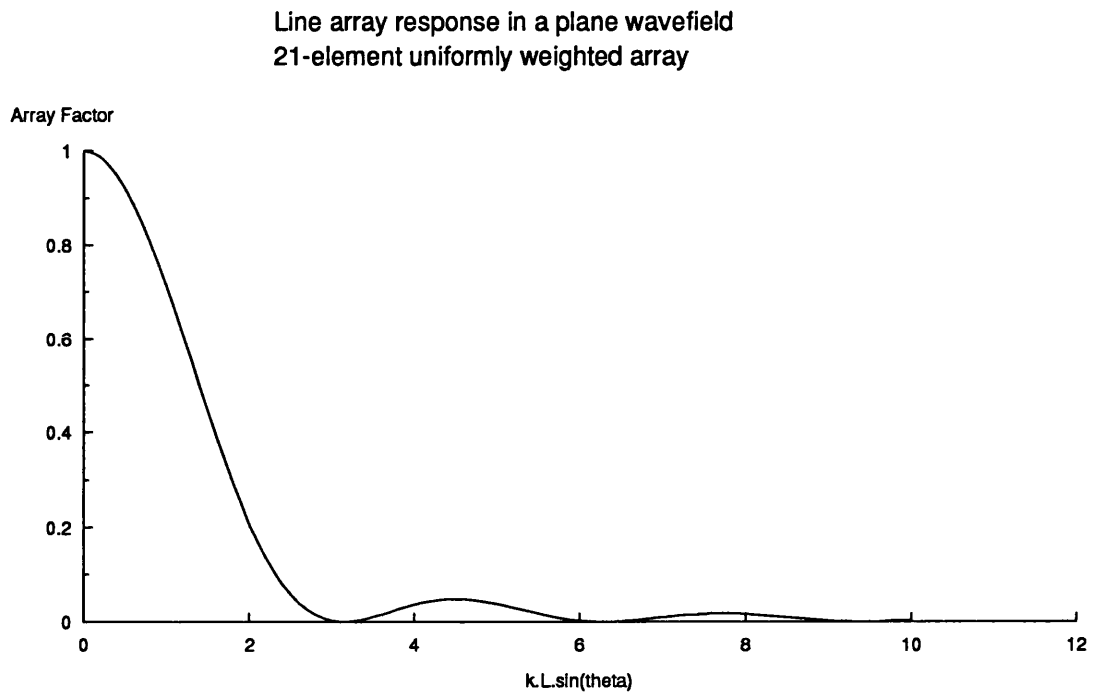

Figure 5.3. The array factor of a uniformly weighted line array consisting of 21 elements symmetrically arranged about the z-axis plotted versus kLsin(θ).

5.2.2 THE SCHELKUNOFF ARRAY

S. A. Schelkunoff [99] recognized that the array factor for discrete line arrays, given by equation (5.7), could be thought of as a polynomial in the complex variable z

$$z = e^{j\Psi} \qquad \ldots(5.15)$$

i.e.

$$A.F. = \sum_{n=0}^{n=N-1} A_n e^{jn\Psi} = A_o + A_1 z + A_2 z^2 + A_3 z^3 + .. + A_{N-1} z^{N-1} \qquad \ldots(5.16)$$

This is an important observation because it allows the use of polynomial algebra for the design of arrays.

Every linear array can be represented by a polynomial and every polynomial can be interpreted as the array factor of some linear array. The significance of this observation will also be shown at a later stage where the Chebyshev array is discussed.

An array of N elements is represented by a polynomial of degree N-1. Thus, this polynomial has N-1 roots and can be factored into the form

$$A.F. = A_{N-1}(z - z_1)(z - z_2)\ldots(z - z_{N-1}) \qquad \ldots(5.17)$$

where z_1, z_2, etc are the zeros of the A.F. This form of the array factor is interesting because it displays explicitly the zeros in the array factor since they are at the values of ψ corresponding to z_1, z_2, etc. It is thus very easy to construct arrays with zeros in the array factor at the specified directions; a feature that would be especially useful in single frequency operations although there is no provision for the optimization of the array factor in terms of minimising the sidelobe level and the mainlobe beamwidth.

5.2.3 THE BINOMIAL ARRAY

Using Schelkunoff's result that any polynomial can be thought of as an array factor, we can construct what is known as the binomial array from the following polynomial

$$A.F. = (1 + z)^n \qquad \ldots(5.18)$$

where z is defined by equation (5.15) and n is an arbitrary integer determined by the number of array elements: n=N-1.

The name of the array stems from the fact that the amplitude ratios of the various array coefficients as given by equation (5.16) are in the ratios of the binomial coefficients; that is, the coefficient of the term z^r in this binomial array is

$$nC_r = \frac{n!}{r!(n-r)!} \qquad \ldots(5.19)$$

The binomial array could be useful since it exhibits no sidelobes in its array factor. The first zero occurs at z=-1, i.e. $\psi = \pm\pi$. Subsequent zeros occur outside the visible region and are of little interest.

Figure 5.4 shows the square modulus of the binomial array factor for arrays consisting of 5, 11 and 21 elements. The ordinate axis is in units of ψ rather than $kL\sin\theta$ shown in figure 5.3. Here, the visible region extends out to $\psi = \pi$, the extra lobes shown do not appear in the visible region. It can be seen that the higher the number of elements the narrower the 3-dB beamwidth of the array factor becomes (but the array becomes longer also). As the number of elements N approaches infinity, the array factor assumes a Gaussian form.

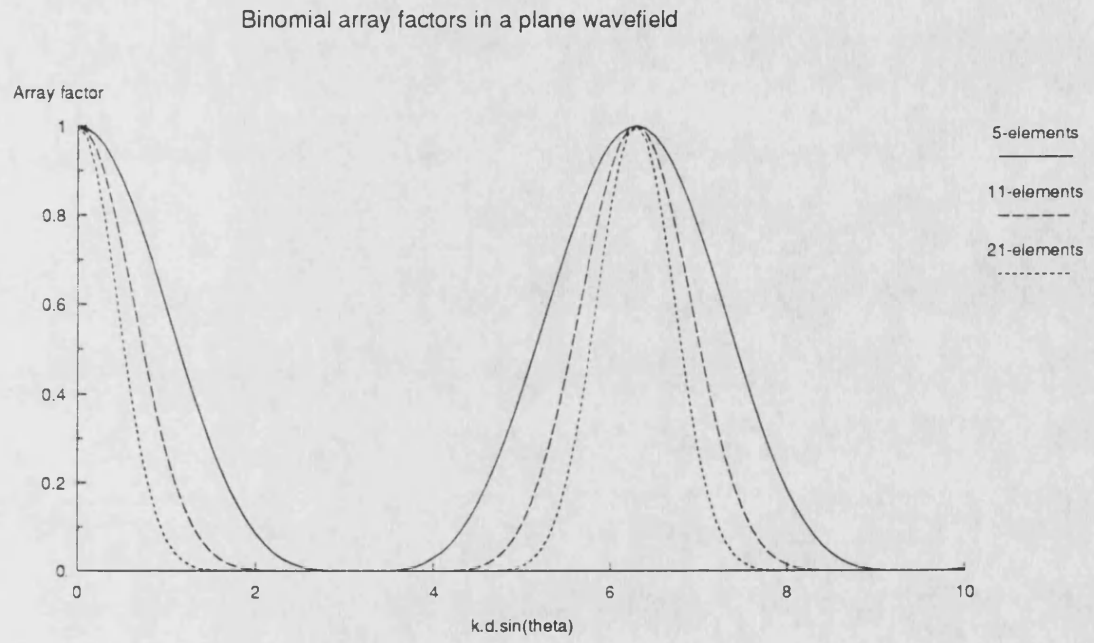

Figure 5.4. Binomial array factors of 5, 11, and 21-element arrays. The sibelobe s do not appear in the visible region which only extends out to $k.d.\sin(\theta)/2=\pi$.

5.2.4 THE CHEBYSHEV ARRAY

Various array weightings described so far attempt to increase the spatial selectivity of a synthesized receiving aperture and reduce the significance of off-axis signals by reducing the sidelobe level of the synthesized array factor. This is achieved by selecting an appropriate weighting distribution of the various receiving positions within the synthetic aperture.

Unfortunately, a narrow beamwidth and low sidelobe level are requirements and usually a compromise solution must be adopted. Low sidelobe levels can be obtained by choosing a weight distribution that falls off gradually towards the edges of the aperture. Such a distribution, however, causes the width of the main lobe to increase.

Dolph [100,101] proved that it is possible to synthesize an optimized aperture, the main lobe width of which is minimum for a given sidelobe level, or conversely, for a given beamwidth the sidelobe level is minimised. In his work, Dolph utilised Schelkunoff's [99] conclusion that any polynomial can be considered to represent an array factor. In fact, it turns out that an optimum array factor in the sense described above, can be obtained when the array factor is described by a Chebyshev polynomial which is defined by

$$T_m(x) = \cos(m \cos^{-1} x) \qquad |x| \leq 1$$
$$= \cosh(m \cosh^{-1} x) \qquad |x| \geq 1 \qquad \ldots(5.20)$$

In the range $-1 \leq x \leq 1$ the polynomials oscillate between ± 1. The m_{th} order polynomial $T_m(x)$ crosses the x-axis m times in the range $|x| \leq 1$. In the range $|x| > 1$ the polynomials increase without limit at a rate proportional to x^m.

The object of identifying an array factor with a Chebyshev polynomial is to arrange that the sidelobe levels are all equal and that either (a) the sidelobe level is specified relative to the mainlobe level, or (b) the main lobe has a specified angular width.

The problem is to find the weighting coefficients in an array such that over a restricted range $x_1 < x < x_2$, a Chebyshev polynomial is equal to the array factor

$$T_m(x) = \sum_{n=0}^{n=N-1} A_n e^{jn\psi} \qquad x_1 < x < x_2 \qquad \ldots(5.21)$$

Where x must be some function of ψ. In the case of a symmetrical array consisting of N (odd) elements

$$T_m(x) = A_o + 2\sum_{n=1}^{n=\frac{N-1}{2}} A_n \cos(n\psi) \qquad x_1 < x < x_2 \qquad \ldots(5.22)$$

The problem is to choose the functional relationship between x and ψ so that equations (5.21) and (5.22) can be satisfied in the range of interest.

A good exposition of the design procedure for Chebyshev arrays can be found in [95, pp.101-115]. Pritchard [102] discussed Chebyshev array synthesis in the context of acoustics and the effect of the number and spacing of the elements was discussed in detail.

Here it would suffice to say that, although the functional relationship between x and ψ is not unique, there is a general form of it which guarantees that the Chebyshev polynomial can be expressed in a finite cosine series

$$x = \zeta \cos\psi + \eta \qquad \ldots(5.23)$$

It turns out that the fundamental relationship between the order of the Chebyshev polynomial m and the number of array elements N is

$$N = 2m + 1 \qquad \ldots(5.24)$$

Several worked examples of the design of Chebyshev arrays appear in the literature [95,96,102].

In order to illustrate the improvements over uniform weighting obtainable with a Chebyshev array, two Chebyshev arrays were designed. The first was weighted in such a way that the first null in the array factor appears at the same place as the first null of the uniform array (i.e. at $kL\sin\theta=\pi$). The second was designed to give the same sidelobe level as that of the uniform line array. Figure 5.5 shows the Chebyshev array factors along with that obtained with uniform weighting. It can be seen that both Chebyshev designs offer an improved array factor by providing either a narrower mainlobe or a lower sidelobe level.

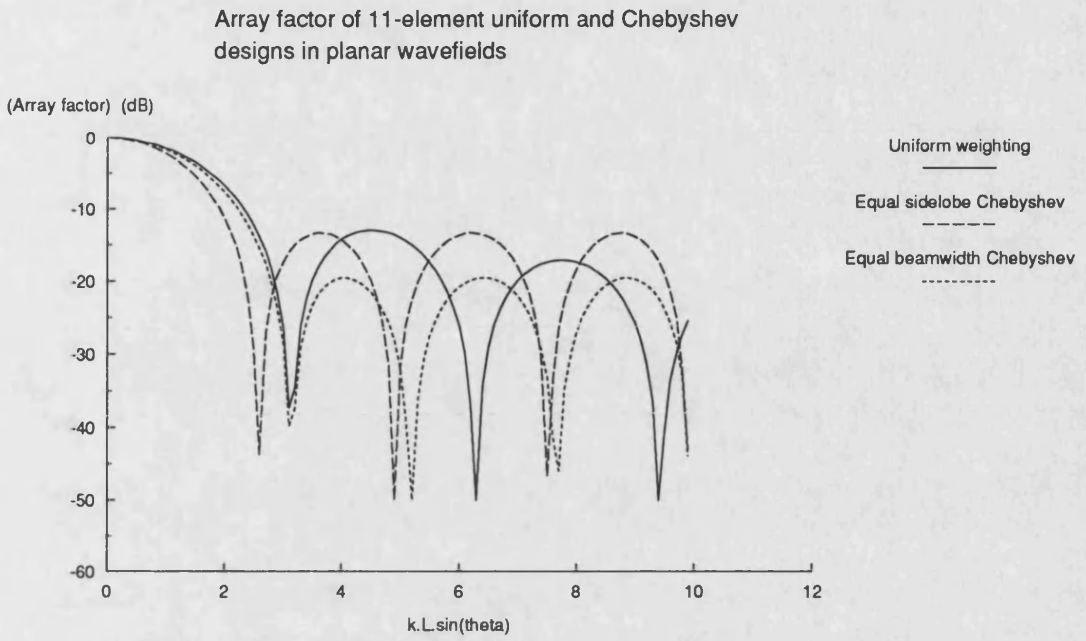

Figure 5.5. Comparison of the uniform array and two Chebyshev arrays specifically designed to give, respectively, the same beamwidth between nulls and the same sidelobe level as the uniform line array.

5.3 SYNTHETIC APERTURE RECEIVER IN THE TUBE

5.3.1 THE RESPONSE OF SYNTHETIC RECEIVING APERTURES TO REFLECTED WAVES FROM A RING ON THE TUBE WALL

In the previous section, it was shown that a line array consisting of point receivers exhibits optimum spatial selectivity when the individual elements are weighted according to the Dolph-Chebyshev method of array synthesis. That is, in the presence of two plane waves travelling, respectively, along the acoustic axis of the array and at an angle to it; immunity from interference from the off-axis wave is maximised with appropriate design.

The structure of the wavefield within the tube is considerably more complex than those considered in the previous sections. In analogy with the above example, we have the direct wave travelling along the tube (and receiver) axis. The aim is to reduce interference

from waves that arrive at the receiver after being reflected by the tube wall. A number of such arrivals at the same off axis angle arise from reflections at a ring shaped section of the inner surface of the tube wall. The 'ring' of sources can be visualised using figure 5.6 which shows a section of the tube with a point source close to the transducer and two possible ray paths from this source to an axial receiver; one along the tube axis and one through a single reflection from the tube wall. The reflected wave appears to originate from a ring on the tube wall formed by rotating figure 5.6 by 2π about the tube axis.

Thus, in this case, it may be more useful to consider the response of a synthetic linear aperture to the signal from a ring source centred on the receiver's axis rather than the classical array factor.

The most troublesome reflected wave contributions originate from difference frequency sources at the start of the parametric array. Reflected waves from these sources travel a path of similar length to the direct wave and thus cannot be easily separated in time using time-of-flight measurements. Thus, array synthesis is required to produce a synthetic receiving aperture capable of rejecting off axis signals. The off axis signal due to the sources at the start of the array arrives at the receiver at the smallest off axis angle (compared to other reflected wave contributions) and is thus hardest to eliminate. For a source-receiver separation R, the normal distance of the ring source from the receiver is z=R/2 according to a ray construction such as figure 5.6. In order to assess the usefulness of various weighting schemes used in the synthesis of a directional receiver, the normalised response to this ring source as a function of frequency will be considered with the help of figure 5.7 as the design parameter to be minimised rather than the array factor.

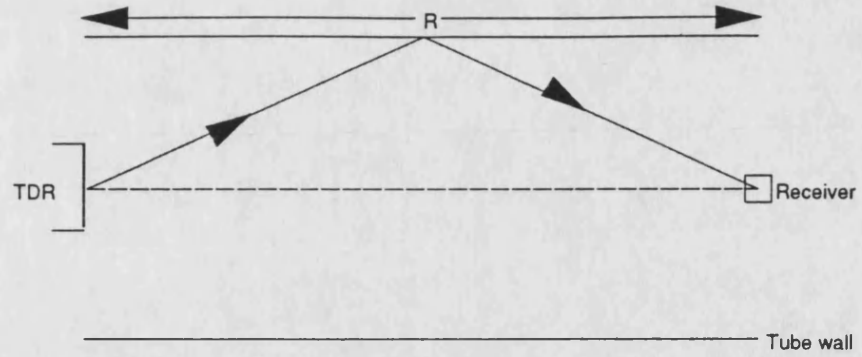

Figure 5.6 Geometric ray path of the reflected difference frequency signal generated near the transmitting transducer travelling to an axial receiver.

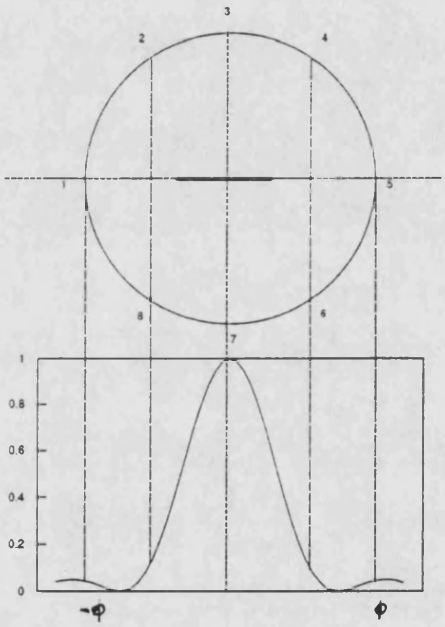

Figure 5.7 The receiving aperture in the tube looking end-on. Some source points (1-8) are identified on the tube wall forming a ring source. The response of the receiving aperture to signal from those points is indicated at the bottom.

Consider figure 5.8 which shows a ring source of radius b is situated at a normal distance z from the origin. A point receiver lies on the x-axis at distance x=nd. The ring source can be considered to be made up of point sources. The total field at the receiver is then

$$\Psi = \int_0^{2\pi} A_n \frac{e^{-jkS}}{S} d\phi \qquad \ldots(5.25)$$

where

A_n:-is an amplitude response factor associated with the receiver

s :-is the distance from the origin to an arbitrary source point

S :-is the distance from the receiver to an arbitrary source point and is given by

$$|S| = \sqrt{(b\cos\phi - nd)^2 + b^2\sin^2\phi + z^2} = \sqrt{b^2 + z^2 + n^2d^2 - 2nd\cos\phi}$$

$$\text{therefore} \quad |S| = s\sqrt{1 + \frac{nd^2}{s^2} - \frac{2ndb\cos\phi}{s^2}},$$

$$\text{or} \quad |S| \approx s + \frac{(nd)^2}{2s} - \frac{ndb\cos\phi}{s} \qquad \ldots(5.26)$$

$$\text{assuming} \quad nd << s$$

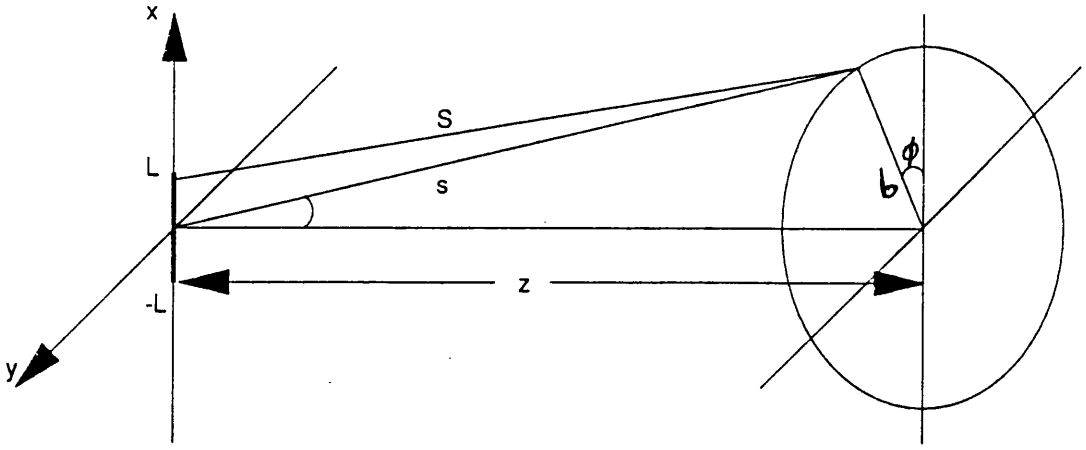

Figure 5.8 Relevant quantities used to calculate the response of a synthetic line array aperture to a ring source.

If we assume that the source receiver separation is large compared to the off axis distance of the receiver (effectively making the far-field approximation); equation (5.26) shows that S can be replaced as follows in equation (5.25):

$$|S| = s - \frac{ndb\cos\phi}{s} \quad \text{in the exponential}$$

$$\text{and} \quad \frac{1}{|S|} = \frac{1}{s} \quad \text{in the denominator} \qquad \ldots(5.27)$$

$$\text{provided that} \quad (nd)^2 \ll 2s$$

Using equation (5.27) equation (5.25) gives

$$\Psi = A_n \int_0^{2\pi} \frac{e^{-jks}}{s} e^{j\frac{kndb\cos\phi}{s}} d\phi \qquad \ldots(5.28)$$

from figure 5.8

$$\frac{b}{s} = \sin\theta$$

$$\therefore \quad \Psi = A_n \frac{e^{-jks}}{s} \int_0^{2\pi} e^{jknd\sin\theta\cos\phi} d\phi \qquad \ldots(5.29)$$

Equation (5.29) can be used to obtain the response of large synthetic apertures. The response of a linear receiving array symmetrically arranged about the origin on the x-axis, consisting of N (odd) elements is

$$\Psi_T = \frac{e^{-jks}}{s} \sum_{n=-(N-1)/2}^{n=(N-1)/2} \int_0^{2\pi} A_n e^{knd\sin\theta\cos\phi} d\phi$$

$$= \frac{e^{-jks}}{s}\left[2\pi A_o + 2\sum_{n=1}^{n=(N-1)/2} \int_0^{2\pi} A_n \cos(knd\sin\theta\cos\phi) d\phi\right] \qquad \ldots(5.30)$$

If a single point receiver situated at the origin is considered, its response to the ring source is

$$\Psi_{point} = \frac{e^{-jks}}{s} 2\pi \qquad \ldots(5.31)$$

Thus, by taking the ratio of equation (5.30) to equation (5.31) we obtain a measure of the improvement in response obtained by using the synthesized receiver rather than an axial point receiver. The improvement obtained in practice is found by considering the square modulus of the normalised response function

$$\Psi^2_{T\,norm} = \left| \frac{\Psi_T}{\Psi_{point}} \right|^2 = \left(A_o + \frac{1}{\pi} \sum_{n=1}^{n=(N-1)/2} \int_0^{2\pi} A_n \cos(knd \sin\theta \cos\phi) \right)^2 \quad \ldots(5.32)$$

As before, the sum of the coefficients is set equal to unity (ΣA_n=1.0) to provide normalisation with a maximum output value of 1.

Equation (5.32) can be used to evaluate the usefulness of the various weighting schemes that have been developed in the previous sections, in the tube geometry. Figure 5.9 shows the normalised response of a linear synthetic receiving aperture, 22cm long (N=11, d=2cm), distance z=45cm from a ring source of radius 23cm, as a function of frequency. Four weighting schemes were used: (a)all the elements of the receiving aperture uniformly weighted (solid line), (b)elements weighted according to the area they represent (this is equivalent to the synthesis of a circular receiver of the same diameter) (dashed line), and (c)elements weighted according to the Chebyshev schemes described previously for linear arrays in a plane wavefield.

In the second weighting scheme above, the amplitude weight of element ±n in an array consisting of N=2n+1 elements symmetrically arranged about the axis is given by

$$2A_n = \frac{\pi\left[\left(n+\frac{1}{2}\right)d\right]^2 - \pi\left[\left(n-\frac{1}{2}\right)d\right]^2}{\pi\left(\frac{Nd}{2}\right)^2} = \frac{8n}{N^2} \qquad \text{for} \quad n \geq 1 \qquad \ldots(5.33)$$

Where the factor of 2 on the left arises from the fact that $A_n = A_{-n}$. The central element weighting is given by

$$A_o = \frac{\pi\left(\frac{d}{2}\right)^2}{\pi\left(\frac{Nd}{2}\right)^2} = \frac{1}{N^2}$$

Due to the rotationaly symmetric field distribution inside the tube, it is the radial distance at which the receiver is placed rather than its angular position that determines its output. In fact, if we had a ring shaped receiver centred on the tube axis, its response would be identical with that obtained by multiplying the output of a point receiver on the ring circumference by the area of the ring receiver. Thus, the weighting scheme described by equation (5.33), when used to synthesize a receiving aperture in the tube, simulates the presence of a circular receiver centred on the tube axis with diameter 2l=Nd. The weights A_n represent the fractional area of the overall synthesized aperture corresponding to element n on the array.

The Chebyshev weighting schemes were those developed for a synthetic line array in a planar wavefield. That is, they were designed to give either the same sidelobe level (dotted curve, figure 5.9) or the same first null in the array factor (dot-dash curve, figure 5.9) as that obtained with a uniform line array in a planar field (equation 5.13).

It can be seen from figure 5.9 that the circular area weighting scheme gives essentially the lowest response for frequencies below about 10kHz but at higher frequencies the 'equal sidelobe' Chebyshev design described previously gives optimum response for the setup parameters used in this example.

All the weighting schemes used provide good immunity against interference from off axis waves and, in the present case, there is an improvement of more than 10dB above 5kHz over the response of a point receiver.

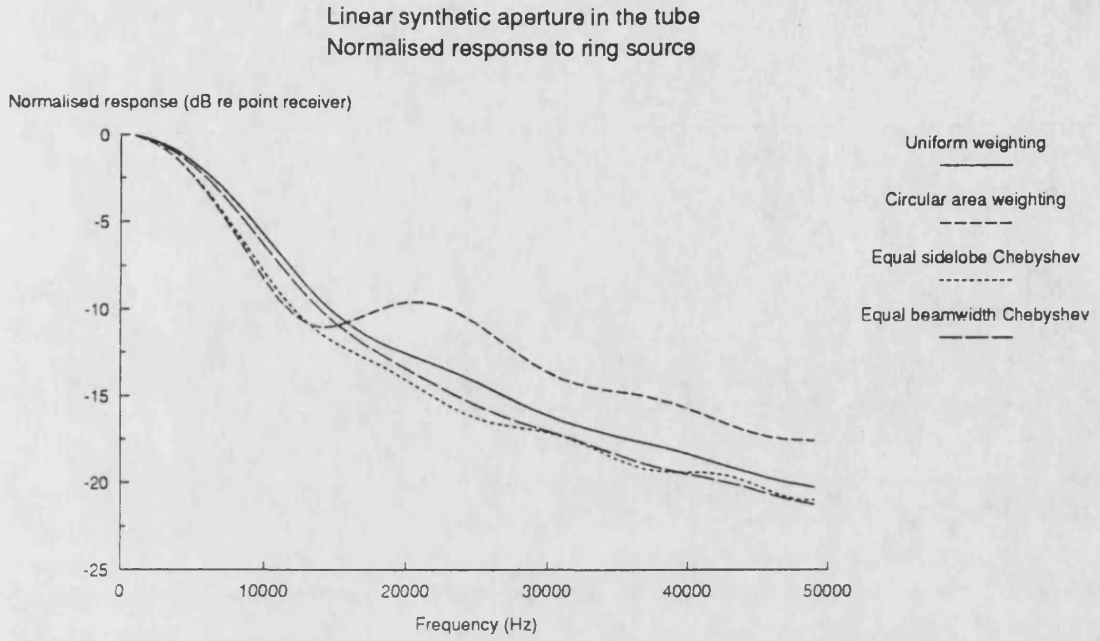

Figure 5.9. The response of a synthesized linear receiving aperture of length 2l=22cm in the tube due to a ring source on the tube wall, 45cm away obtained using equation (5.32). The receiving element separation is 2cm (i.e.N=11); (a)uniform weighting (—), (b) circular area weighting (---), (c) & (d)Chebyshev weighting for equal sidelobe level (...) and equal beamwidth (._.) as the uniform line array (equation 5.13).

Figure 5.10 shows the response of a circular area weighted line array consisting of 11 elements symmetrically arranged about the tube axis due to a ring source of radius of 23cm, 45cm away. Three element spacings are used: (a) d=2cm, i.e. 2L=22cm (solid line), (b) d=3cm, i.e. 2L=33cm (dashed line) and (c) d=4cm, i.e. 2L=44cm (dotted line). It can be seen that the off axis signal response is reduced by increasing the overall synthetic aperture length. Figure 5.11 shows the response of a uniform line array receiver. The effect of the receiver size is demonstrated.

In general, the response of a synthetic linear receiving array to off axis waves can be reduced by increasing the overall length of the synthetic aperture. If, however, the element separation d is increased, the Chebyshev weighted arrays suffer due to the

appearance of grating lobes in the response curve. The Chebyshev arrays are more sensitive to the choice of element separation than the uniform and the circular area weighted arrays. Thus, if a 'thinned' receiving array is desired, the uniform and circular area weighting schemes must be considered.

In practise, it is advantageous to have a large receiving element separation in order to minimise inter-element coupling and simplify the receiving electronics (if several receiving elements are employed simultaneously), or reduce the data acquisition storage and processing time (when a single receiver is scanned to form the synthetic aperture).

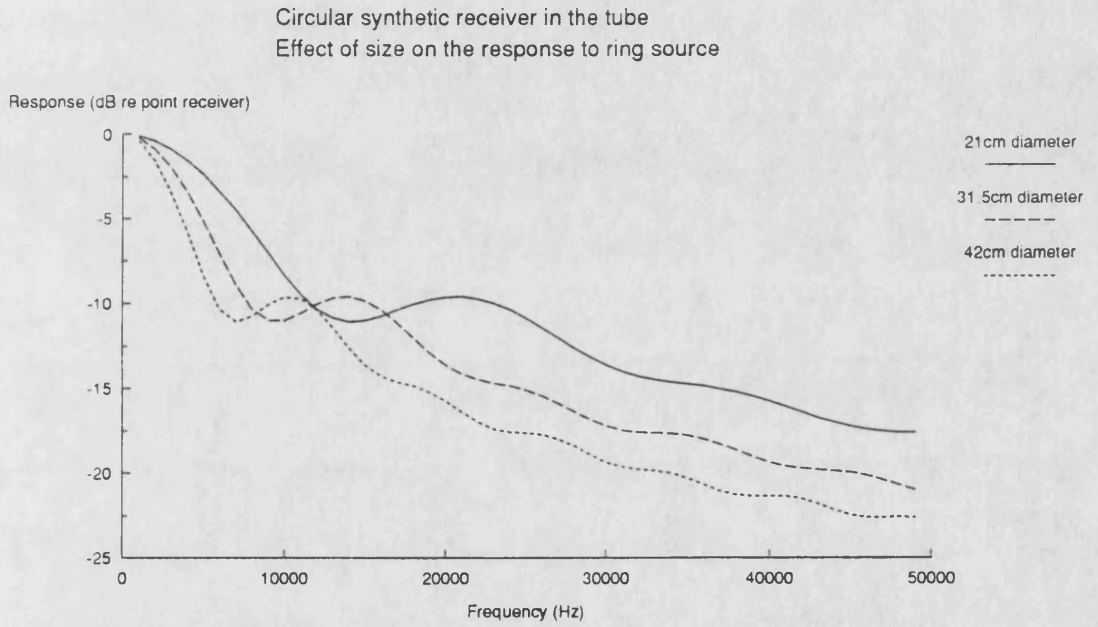

Figure 5.10. Normalised response of a circular area weighted synthetic receiver consisting of 11 elements, due to a ring source of radius=23cm, 45cm away: (—) d=2cm, (---) d=3cm, (...) d=4cm.

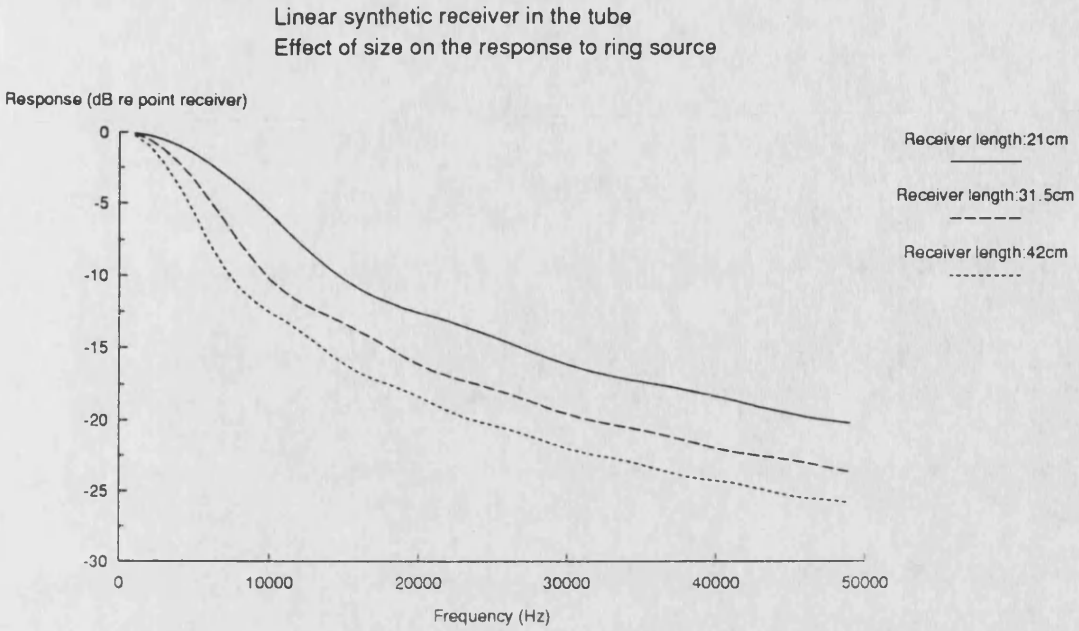

Figure 5.11. Normalised response of a uniformly weighted synthetic line receiver consisting of 11 elements, due to a ring source of radius=23cm, 45cm away: (—) d=2cm, (---) d=3cm, (...) d=4cm.

5.3.2 THE RESPONSE OF SYNTHETIC RECEIVING APERTURES TO DIRECT WAVES FROM AN EXTENDED LINE SOURCE ON THE TUBE AXIS

An additional factor that has to be taken into account in the choice of a suitable receiver weighting scheme is its response to the axial waves. The present case is again rather special in the way the difference frequency sources are distributed throughout the interaction volume rather than forming a simple aperture on a plane. Thus, the direct wavefield is not planar but it has amplitude and phase variations across its wavefront that may lead to a reduction in the response of the synthetic receiver to the direct wave.

In order to simplify this treatment, the line array model of the parametric array source distribution is adopted here. In addition, only the uniform line receiver and the circular receiver are considered.

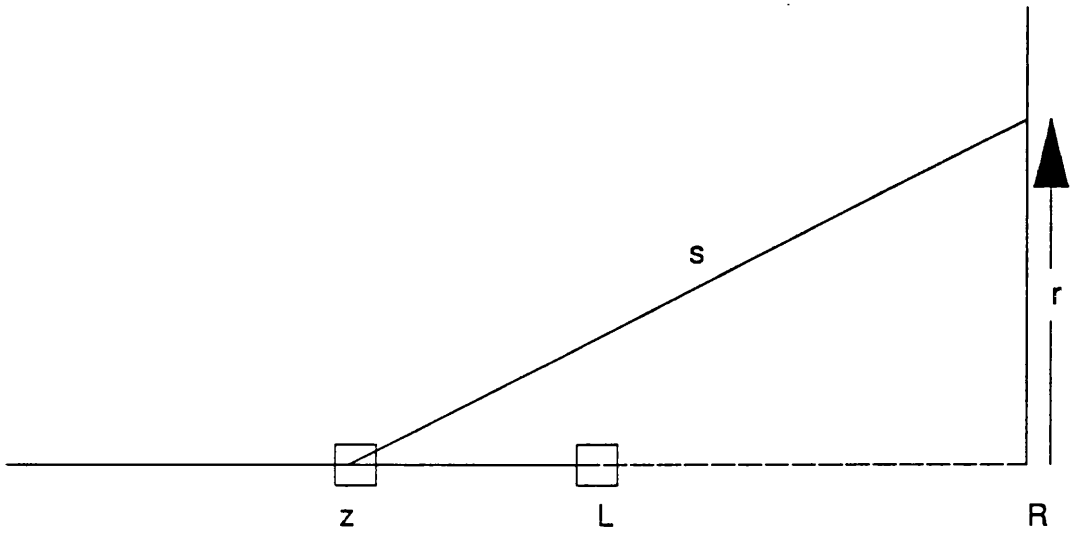

Figure 5.12. Relevant quantities for the calculation of the response of an extended receiver to an axial line source of length L originating at a distance R away.

Consider figure 5.12. The aim is to find the normalised response of an extended receiver at R due to an end-fire line source on its axis. If the source strength per unit length at a frequency specified by ω is Q(ω), then the velocity potential at a point (R,r) on the receiver is given by

$$\Phi(R,r,\omega)=\frac{Q(\omega)}{4\pi}\int_0^L \frac{e^{jk(z+s)}}{s}dz. \qquad \ldots(5.34)$$

It can easily be shown [18] that the velocity potential on the axis (r=0) is

$$\Phi(R,r=0,\omega)=\frac{Q(\omega)}{4\pi}e^{jkR}\ln\left(\frac{R}{R-L}\right). \qquad \ldots(5.35)$$

Thus, the velocity potential at (R,r) in terms of its on-axis value is

$$\Phi(R,r,\omega)=\frac{\Phi(R,o,\omega)}{\ln\left(\frac{R}{R-L}\right)}\int_0^L \frac{e^{jk(z+s-R)}}{s}dz \qquad \ldots(5.36)$$

Let $\quad u=z+s-R=\sqrt{(R-z)^2+r^2}-(R-z)$

$$\text{then} \quad z=0 \rightarrow u=u_1=\sqrt{R^2+r^2}-R$$

$$z=L \rightarrow u=u_2=\sqrt{(R-L)^2+r^2}-(R-L)$$

$$\text{and} \quad \frac{du}{dz}=\frac{u}{s}$$

Equation (5.36) becomes:

$$\Phi(R,z,\omega)=\frac{\Phi(R,o,\omega)}{\ln\left(\frac{R}{R-L}\right)}\int_{u_1}^{u_2}\frac{e^{jku}}{u}du \qquad \ldots(5.37)$$

Equation (5.37) gives the response of an off-axis point receiver in terms of the response of an axial point receiver due to an end-fire line source. For the range of R that we are concerned with, it can be written in the form:

$$\Phi(R,r,\omega)=\Phi(R,0,\omega).I \qquad \ldots(5.38)$$

I can easily be identified from equation (5.37) and it is I that changes when more complicated receiver arrangements are used. I is the transfer function of the receiver which, when multiplied by the normally incident (input) signal on axis gives the output signal of the receiver. Two cases will be considered here: (a) the case of a uniform linear receiver extending from r=-l to r=l, and (b) the circular receiver of radius l.

A) Uniform line receiver

In this case:

$$I=\frac{1}{\ln\left(\frac{R}{R-L}\right)}\frac{2}{2l}\int_0^l\int_{u_1}^{u_2}\frac{e^{jku}}{u}dudr \qquad \ldots(5.39)$$

The factor 1/2l is a normalising constant and the factor of 2 in the numerator is obtained by restricting the region of integration to $0 \le r \le l$.

Integrating by parts:

$$I=\frac{1}{\ln\left(\frac{R}{R-L}\right)}\frac{1}{l}\left[l\int_{v_1}^{v_2}\frac{e^{jku}}{u}du-\int_0^l r\left[\frac{du_2}{dr}\frac{e^{jku_2}}{u_2}-\frac{du_1}{dr}\frac{e^{jku_1}}{u_1}\right]dr\right] \qquad \ldots(5.40)$$

where $v_1=u_1(l)=\sqrt{R^2+l^2}-R$

$$v_2=u_2(l)=\sqrt{(R-L)^2+l^2}-(R-L)$$

also $u_1=\sqrt{R^2+r^2}-R \qquad \therefore \frac{r}{u_1}=\sqrt{1+\frac{2R}{u_1}} \qquad \ldots(5.41)$

and similarly $\frac{r}{u_2}=\sqrt{1+\frac{2(R-L)}{u_2}} \qquad \ldots(5.42)$

Thus, substitution of equations (5.41) and (5.42) into equation (5.40) gives:

$$I=\frac{1}{\ln\left(\frac{R}{R-L}\right)}\frac{1}{l}\left[l\int_{v_1}^{v_2}\frac{e^{jku}}{u}du-\int_0^{v_2}e^{jku_2}\sqrt{1+\frac{2(R-L)}{u_2}}du_2+\int_0^{v_1}e^{jku_1}\sqrt{1+\frac{2R}{u_1}}du_1\right] \qquad \ldots(5.43)$$

Now let $\tau=\frac{u}{c}, \qquad du=cd\tau,$

$$u=v_1 \rightarrow \tau=\frac{v_1}{c},$$

and $u=v_2 \rightarrow \tau=\frac{v_2}{c}$

$$I=\frac{1}{\ln\left(\frac{R}{R-L}\right)}\frac{1}{l}\left[l\int_{\frac{v_1}{c}}^{\frac{v_2}{c}}\frac{e^{jk\tau c}}{\tau}d\tau-\int_0^{\frac{v_2}{c}}e^{jkc\tau_2}\sqrt{1+\frac{2(R-L)}{c\tau_2}}cd\tau_2-\int_0^{\frac{v_1}{c}}e^{jkc\tau_1}\sqrt{1+\frac{2R}{c\tau_1}}cd\tau_1\right] \qquad (5.44)$$

Equation (5.44) provides the transfer function (frequency response) of the receiver. The Fourier transform of equation (5.44) gives the impulse response of this receiver; using k.c=ω:

$$FT\{I\} = \frac{1}{2\pi}\int_{-\infty}^{\infty} e^{-j\omega t} d\omega . I =$$

$$\frac{1}{\ln\left(\frac{R}{R-L}\right)}\frac{1}{2\pi l}\left[l \int_{\frac{v_1}{c}}^{\frac{v_2}{c}} \frac{e^{j\omega\tau}}{\tau} d\tau \int_{-\infty}^{\infty} e^{-j\omega t} d\omega - \int_0^{\frac{v_2}{c}} \sqrt{1+\frac{2(R-L)}{c\tau_2}}\, d\tau_2 \int_{-\infty}^{\infty} e^{-j\omega(t-\tau_2)} d\omega + \int_0^{\frac{v_1}{c}} \sqrt{1+\frac{2R}{c\tau_1}}\, d\tau_1 \int_{-\infty}^{\infty} e^{-j\omega(t-\tau_1)} d\omega \right]$$

$$\therefore \quad FT\{I\} = \frac{1}{\ln\left(\frac{R}{R-L}\right)}\frac{1}{l}\left[l \int_{\frac{v_1}{c}}^{\frac{v_2}{c}} \frac{\delta(t-\tau)}{\tau} d\tau - \right.$$

$$\left. \int_0^{\frac{v_2}{c}} \delta(t-\tau_2)\sqrt{1+\frac{2(R-L)}{c\tau_2}}\, c\, d\tau_2 + \int_0^{\frac{v_1}{c}} \delta(t-\tau_1)\sqrt{1+\frac{2R}{c\tau_1}}\, c\, d\tau_1 \right] \qquad \ldots(5.45)$$

$$\therefore \quad FT\{I\} = \frac{1}{\ln\left(\frac{R}{R-L}\right)}\frac{1}{l}\left[\frac{l}{t} p_1(t) - \sqrt{1+\frac{2(R-L)}{ct}}\, c\, p_2(t) + \sqrt{1+\frac{2R}{ct}}\, c\, p_3(t) \right] \qquad \ldots(5.46)$$

where $p_1(t)$, $p_2(t)$ and $p_3(t)$, are time window functions defined by:

$$p_1(t) = \begin{cases} 1 & \frac{v_1}{c} \le t \le \frac{v_2}{c} \\ 0 & \text{otherwise} \end{cases}$$

$$p_2(t) = \begin{cases} 1 & 0 \le t \le \frac{v_2}{c} \\ 0 & \text{otherwise} \end{cases}$$

$$p_3(t) = \begin{cases} 1 & 0 \le t \le \frac{v_1}{c} \\ 0 & \text{otherwise} \end{cases}$$

Two details are worth investigating at this point: (1) the form of the impulse response function at the limit when delayed time (with reference to the direct arrival) approaches zero, and (2) the normalised value of the transfer function I (equation (5.39)) when the frequency approaches the asymptotic limit of $\omega = 0$ (or k=0).

(1) The impulse response of the receiving aperture, as given by equations (5.45) and (5.46) has a singularity at time τ=0 due to a $1/\tau$ term appearing in the second and third integrals in equation (5.45). In order to find the limiting value of the impulse response at time t=0 consider:

$$I_1 = \int_0^{\frac{v_1}{c}} \delta(t-\tau_1)\sqrt{1+\frac{2R}{c\tau_1}}\,c\,d\tau_1$$

$$\text{and} \qquad I_2 = \int_0^{\frac{v_2}{c}} \delta(t-\tau_2)\sqrt{1+\frac{2(R-L)}{c\tau_2}}\,c\,d\tau_2 \qquad \ldots(5.47)$$

We are interested in the values of the integrals at arbitrarily small times ε and E:

$$\varepsilon = \frac{v_1}{c} = \frac{1}{c}(\sqrt{R^2+l^2}-R) \approx \frac{l^2}{2Rc}$$

$$\mathrm{E} = \frac{v_2}{c} = \frac{1}{c}(\sqrt{(R-L)^2+l^2}-(R-L)) \approx \frac{l^2}{2(R-L)c}$$

$$\therefore \quad \mathrm{E} \approx \varepsilon\frac{R}{R-L} \qquad \text{or,} \qquad \sqrt{\mathrm{E}} \approx \sqrt{\varepsilon}\sqrt{\frac{R}{R-L}} \qquad \ldots(5.48)$$

From equations (5.46)-(5.48):

$$I_1 = \int_0^{\varepsilon} \delta(t-\tau_1)\sqrt{1+\frac{2R}{c\tau_1}}\,c\,d\tau_1 \approx \sqrt{2Rc}\int_0^{\varepsilon}\frac{d\tau_1}{\tau_1} \approx 2\sqrt{2Rc}\,\sqrt{\varepsilon}$$

and, similarly

$$I_2 = \int_0^{\mathrm{E}} \delta(t-\tau_2)\sqrt{1+\frac{2(R-L)}{c\tau_2}}\,c\,d\tau_2 \approx 2\sqrt{2(R-L)c}\,\sqrt{\mathrm{E}} = 2\sqrt{2Rc}\,\sqrt{\varepsilon}$$

Therefore, $I_1 - I_2 = 0$ as it appears in equation (5.45). Thus, the limiting value of the impulse response function, at delayed time t=0 is equal to zero and this facilitates both the calculation of the impulse response and the numerical inverse Fourier transformation required for the calculation of the transfer function of the uniform line receiver due to an end-fire line source.

(2) Another point of interest emerges from equation (5.39) that describes the transfer function of the extended uniform line receiver when the limiting case of k=0 is considered. The asymptotic value of the transfer function I does not tend to 1 as k→0 as would normally be expected with an ordinary point source but, instead, it reaches a somewhat lower value. That is an amplitude effect and should not be confused with the phasing effect across the receiving aperture that reduces the output at higher frequencies. Since each point on the receiver is a different distance away from the source(s), the 1/(distance) amplitude factor for each point on the receiver changes and the integrated effect gives a value lower than unity (effectively a nearfield effect).

Consider equation (5.39) which, after some algebraic manipulation gives equation (5.43). Setting k=0 in equation (5.43) we get:

$$I_{k=0} = \frac{1}{\ln\left(\frac{R}{R-L}\right)}\left[\ln\frac{v_2}{v_1} - \frac{1}{l}\int_0^{v_2}\sqrt{1+\frac{2(R-L)}{u_2}}\,du_2 + \frac{1}{l}\int_0^{v_1}\sqrt{1+\frac{2R}{u_1}}\,du_1\right] \quad \ldots.(5.49)$$

Designate the first integral within equation (5.49) as G_0 and the second as G_1:

$$G_1 = \frac{1}{l}\int_0^{v_1}\sqrt{1+\frac{2R}{u_1}}\,du_1$$

$$\text{let} \qquad t = \sqrt{u_1} \qquad v_1 \to t_1^2$$

$$du_1 = 2\sqrt{u_1}\,dt$$

$$\therefore \qquad G_1 = \frac{2}{a}\int_0^{t_1^2}\sqrt{t^2+2R}\,dt$$

$$\text{let} \qquad t = \sqrt{2R}\sinh x \qquad t = t_1^2 = 2R\sinh^2 x_1$$

$$\therefore \quad x_1 = \sinh^{-1}\left(\frac{t_1}{\sqrt{2R}}\right)$$

$$\text{and} \qquad \frac{dt}{dx} = \sqrt{2R}\cosh x$$

$$\therefore \quad G_1 = \frac{2}{l}\int_0^{x_1} \sqrt{2R}(1+\sinh^2 x)\sqrt{2R}\cosh x\,dx = 2\frac{2R}{l}\int_0^{x_1}\cosh^2 x\,dx$$

$$\therefore \quad G_1 = \frac{R}{l}(2x_1 + \sinh 2x_1) \qquad \ldots(5.50)$$

$$\text{with} \qquad x_1 = \sinh^{-1}\sqrt{\frac{v_1}{2R}} \qquad \ldots(5.51)$$

Similarly

$$G_o = \frac{1}{l}\int_0^{v_2}\sqrt{1+\frac{2(R-L)}{u_2}}\,du_2 = \frac{(R-L)}{l}(2x_0 + \sinh 2x_0) \qquad \ldots(5.52)$$

$$\text{with} \qquad x_0 = \sinh^{-1}\sqrt{\frac{v_2}{2(R-L)}} \qquad \ldots(5.53)$$

$$\therefore \quad I_{k=0} = \frac{1}{\ln\left(\frac{R}{R-L}\right)}\left[\ln\frac{v_2}{v_1} - \frac{(R-L)}{l}(2x_0 + \sinh 2x_0) + \frac{R}{l}(2x_1 + \sinh 2x_1)\right] \ldots(5.54)$$

with v_1 and v_2 defined for equation (5.40), x_1 and x_0 by equations (5.51) and (5.53) respectively. It turns out, that I(k=0) is smaller than unity. Using typical values R=0.9m, L=0.52m and considering a linear receiver 2l=0.42m long:

$$I_{k=0} \approx 0.9775$$

Both the impulse response and the transfer function of a typical uniform line receiver will be shown along with the corresponding quantities calculated for a circular receiver in the same configuration which is now considered.

(B) Circular receiver of radius l.

All the relevant variables are again shown in figure 5.12. A circular receiver of radius l is centred on the axis of an end-fire line source.

Equation (5.38) derived for the case of the uniform line receiver is equally valid here:

$$\Phi(R, r, \omega) = \Phi(R, 0, \omega).I \qquad \ldots(5.38)$$

That is, the transfer function I of the receiver, multiplied by the incident signal gives the total output of the receiver. In the present case, the form of the impulse response function can be written in a similar fashion to that derived for the uniform line receiver:

$$I = \frac{1}{\ln\left(\frac{R}{R-L}\right)} \frac{1}{\pi l^2} \int_0^l 2\pi r\, dr \int_{u_1}^{u_2} \frac{e^{jku}}{u} du \qquad \ldots(5.55)$$

Following the same procedure as in the case of the uniform line receiver, we find the Fourier transform of I:

$$FT\{I\} = \frac{1}{\ln\left(\frac{R}{R-L}\right)} \left[\left[\frac{1}{t} - \frac{t + 2(R-L)/c}{(l/c)^2} \right] p_1(t) + \left[\frac{2Lc}{l^2} \right] p_2(t) \right] \qquad \ldots(5.56)$$

where

$$p_1(t) = \begin{cases} 1 & \frac{v_1}{c} \le t \le \frac{v_2}{c} \\ 0 & \text{otherwise} \end{cases}$$

$$p_2(t) = \begin{cases} 1 & 0 \le t \le \frac{v_1}{c} \\ 0 & \text{otherwise} \end{cases}$$

It can be seen that equation (5.56) is well behaved at time t=0 and none of the problems associated with equation (5.45) arise here. The impulse response at time t=0 is:

$$FT\{I\}_{t=0} = \frac{2Lc}{l^2} \frac{1}{\ln\left(\frac{R}{R-L}\right)} \qquad \ldots(5.57)$$

In addition, the transfer function of the circular receiver in the present configuration when the frequency approaches zero (k→0) can be found using equation (5.55) and setting k=0:

$$I = \frac{1}{\ln\left(\frac{R}{R-L}\right)} \frac{2}{l^2} \left[\int_0^l r\, dr \int_{u_1}^{u_2} \frac{e^{jku}}{u} du \right]$$

$$= \frac{1}{\ln\left(\frac{R}{R-L}\right)} \frac{2}{l^2} \left[\frac{l^2}{2} \int_{v_1}^{v_2} \frac{e^{jku}}{u} du \right] = \frac{1}{2} \int_0^l r \left[\frac{du_2}{dr} \frac{e^{jku_2}}{u_2} - \frac{du_1}{dr} \frac{e^{jku_1}}{u_1} \right] dt \Bigg].$$

So $$I_{k=0}=\frac{1}{\ln\left(\frac{R}{R-L}\right)}\frac{2}{l^2}\left[\frac{l^2}{2}\ln\frac{v_2}{v_1}-\frac{1}{2}\int_0^{v_2}(u_2+2(R-L))du_2+\frac{1}{2}\int_0^{v_1}(u_1+2R)du_1\right].$$

$$\text{Hence}\quad I_{k=0}=\frac{1}{\ln\left(\frac{R}{R-L}\right)}\left[\ln\frac{v_2}{v_1}-\frac{1}{l^2}\left(\frac{v_2^2}{2}+2(R-L)v_2\right)+\frac{1}{l^2}\left(\frac{v_1^2}{2}+2Rv_1\right)\right],\quad \ldots(5.58)$$

which, for R=0.9m, L=0.52m and l=0.21m gives

$$I_{k=0}=0.9665.$$

Figure 5.13 shows the transfer functions of a uniform and a circular receiver on the axis of an end-fire line source. They were obtained by calculating the impulse response of each aperture using equations (5.46) and (5.56) respectively and subsequently inverse fast Fourier transforming them numerically to obtain the corresponding transfer functions in the frequency domain. The usual values of R=0.9m and L=0.52m were used for the figure and two receiver sizes were investigated: overall lengths of 0.42m and 0.21m.

An alternative way of interpreting the results shown in figure 5.13 is to consider them as a measure of the deterioration in the frequency response of the receivers compared to that of an axial point receiver which would be expected to have a steady response equal to unity over the entire frequency range.

It can be seen that when a receiver 0.21m long (diameter) is considered there is very little difference in the calculated frequency response of the uniform line and circular receivers. When larger receivers are considered, the uniform line receiver seems to offer superior high frequency (>15kHz) response. The impulse response of the receivers considered in figure 5.13 are shown in figure 5.14.

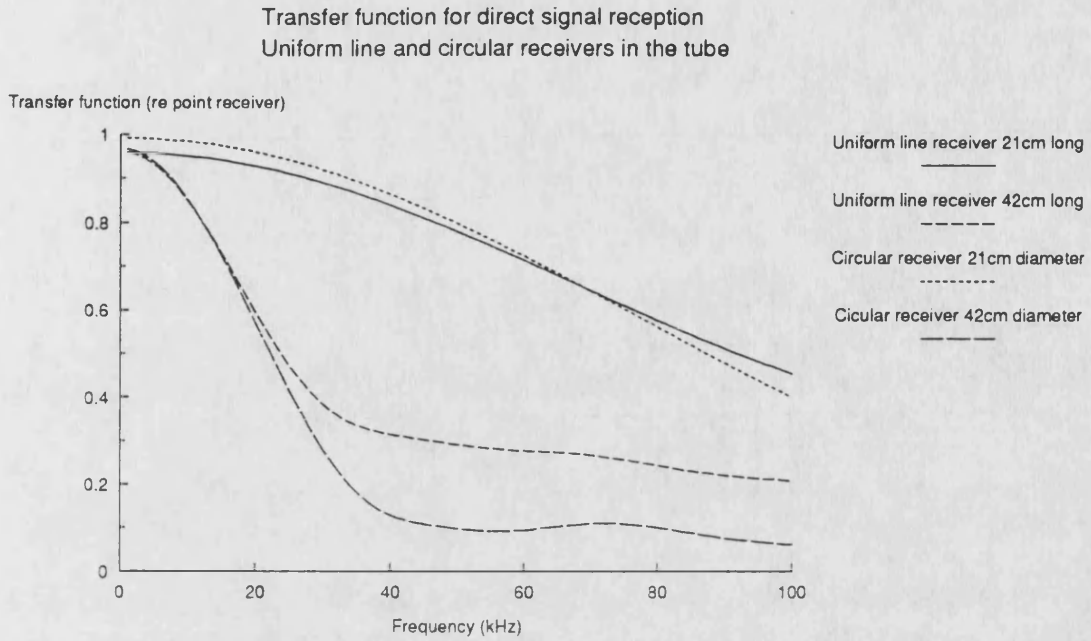

Figure 5.13. Theoretical transfer function of uniform line and circular receivers with respect to an axial end-fire source in the tube.

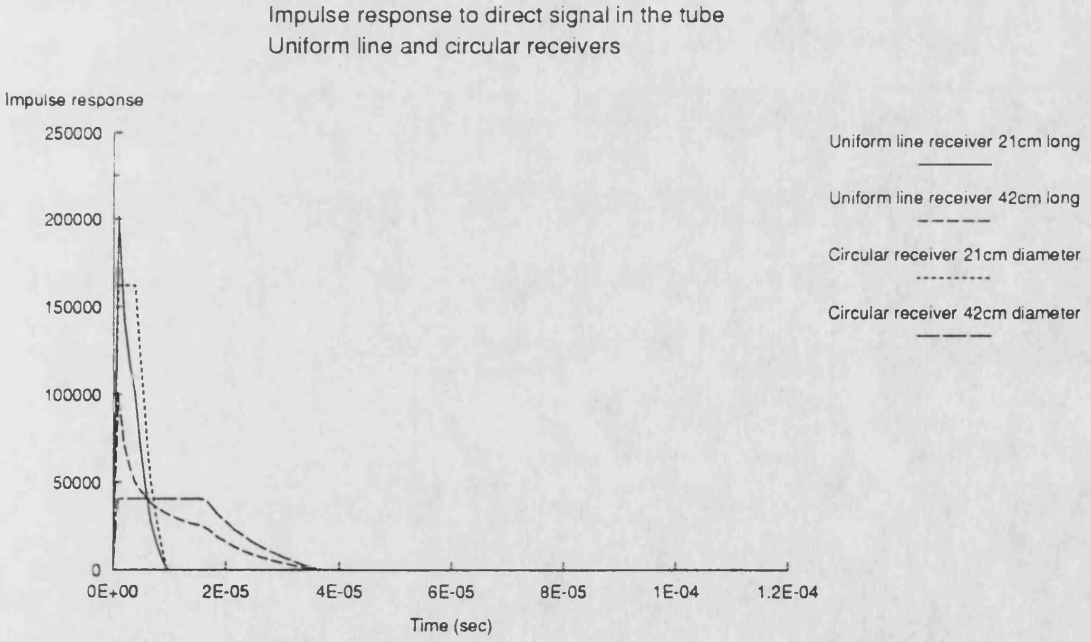

Figure 5.14. Theoretical impulse response of uniform line and circular receivers to signal from an axial end-fire source in the tube.

5.4 EXPERIMENTAL RESULTS USING RECEIVER SYNTHESIS IN THE TUBE

Experimental measurements were performed in the tube using the technique described in a chapter 3. The hydrophone was scanned along the diameter of the tube under computer control. The pressure waveform was recorded on the tube axis and in 2cm steps out to a distance of 20cm (a total of 11 measurements). Weighted summation of all or some of those waveforms enabled the synthesis of uniform line or circular area weighted receivers of various dimensions. Figure 5.15 shows the weighted sum of 6 observations used to synthesize a 22cm long (diameter) aperture. Figure 5.16 shows the weighted sum of 8 observations used to synthesize a 30cm long receiver and figure 5.17 shows the weighted sum of all 11 observations resulting in an overall receiver size of 42cm. The results of both uniform and circular weighting are shown and they are directly comparable to the axial experimental waveform shown in figure 5.1. It can be seen that spatial averaging does provide a dramatic reduction in the reflected wave strength although there is an associated reduction in the direct wave strength also. Both effects are amplified when larger receivers are synthesized.

In order to assess the accuracy of the theoretical predictions made in previous sections, the 42cm receiver (figure 5.17) and the on axis results will be used. In every case, it is possible to identify and isolate (with an appropriate time window) the direct, on axis wave. Figure 5.18 shows the direct wave spectrum obtained using and axial point receiver and a 42cm long (diameter) receiver. It can be seen that, as expected, the direct signal is reduced in amplitude when an extended receiver is used. A measure of this reduction can be obtained from the ratio of the spectra obtained with the extended receivers over the spectrum obtained with a point receiver. This ratio is essentially the transfer function of the extended receivers. Figure 5.19 shows the theoretical (equation (5.44)) and experimental transfer functions obtained for the uniform line receiver of total length of 42cm, with R=0.9m and L=0.52m. Figure 5.20 shows the theoretical (equation (5.55))

and experimental transfer functions for a circular receiver of 42cm diameter. In both cases the theoretical prediction of the transfer function of the extended receiver is quite accurate above about 10kHz; below this frequency data are unreliable due to the duration of the time window applied to the experimental data.

Experimental verification of the theoretical predictions of the frequency response of extended receivers to a ring source on the tube wall (representing reflected wave sources) is not straight forward. That is due to the difficulties encountered in distinguishing reflected wave contributions from a specific area on the tube wall especially when averaged signals are considered. It is still possible, however, to differentiate between single bounce and double bounce arrivals. Thus, the single bounce reflected wave spectrum, divided by the direct wave spectrum can be used to obtain a measure of the overall improvement offered by the two synthesized receivers when it is compared to the normalised reflected wave spectrum obtained with an axial point receiver. Figure 5.21 shows the experimental normalised reflected wave spectra obtained with an axial point receiver and synthesized uniform line and circular area receivers 42cm long. Both averaging schemes seem to offer good immunity against the reflected waves with the circular receiver marginally better at most frequencies.

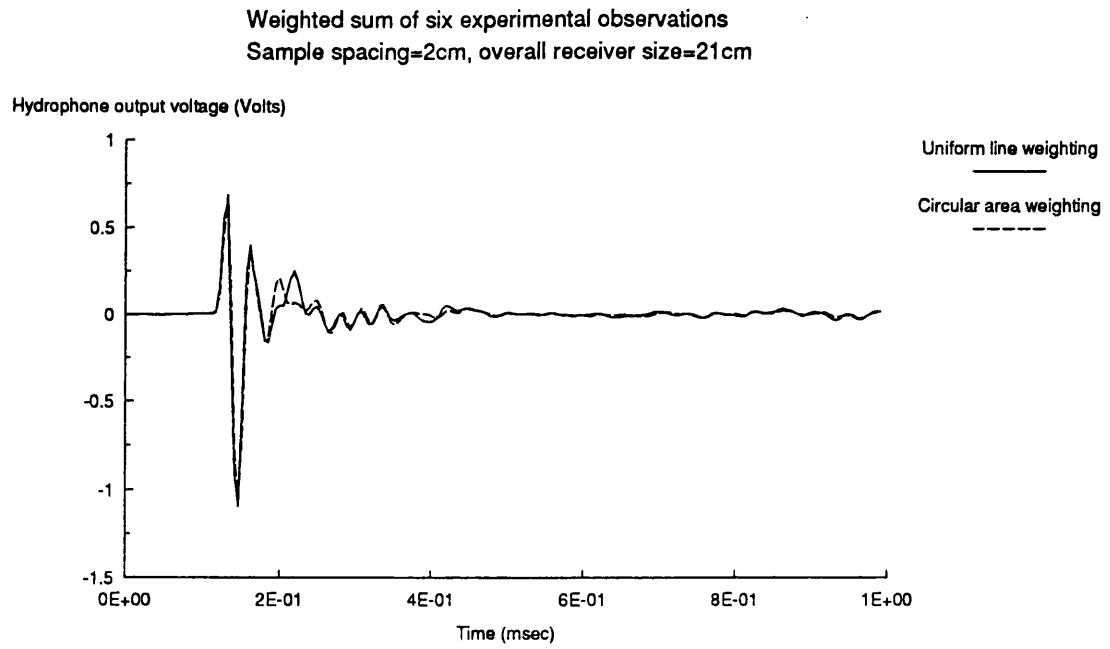

Figure 5.15. Weighted sum of 6 experimental waveforms used to synthesize a 22cm long (diameter) receiving aperture. Uniform and circular area weighting.

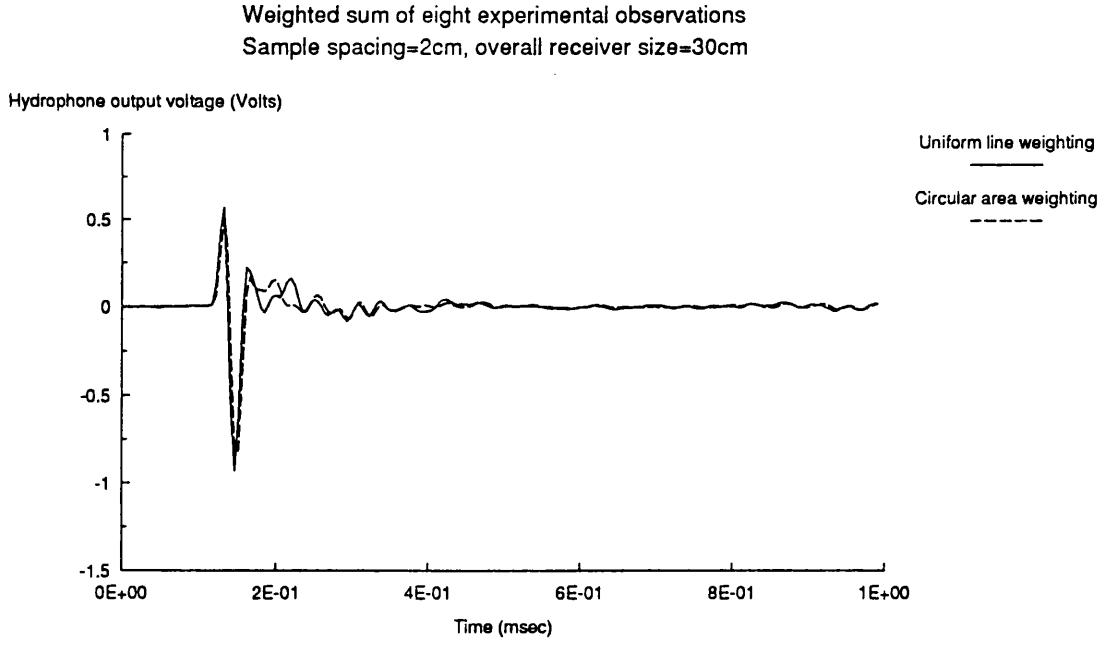

Figure 5.16. Weighted sum of 8 experimental waveforms used to synthesize a 30cm long (diameter) receiving aperture. Uniform and circular area weighting.

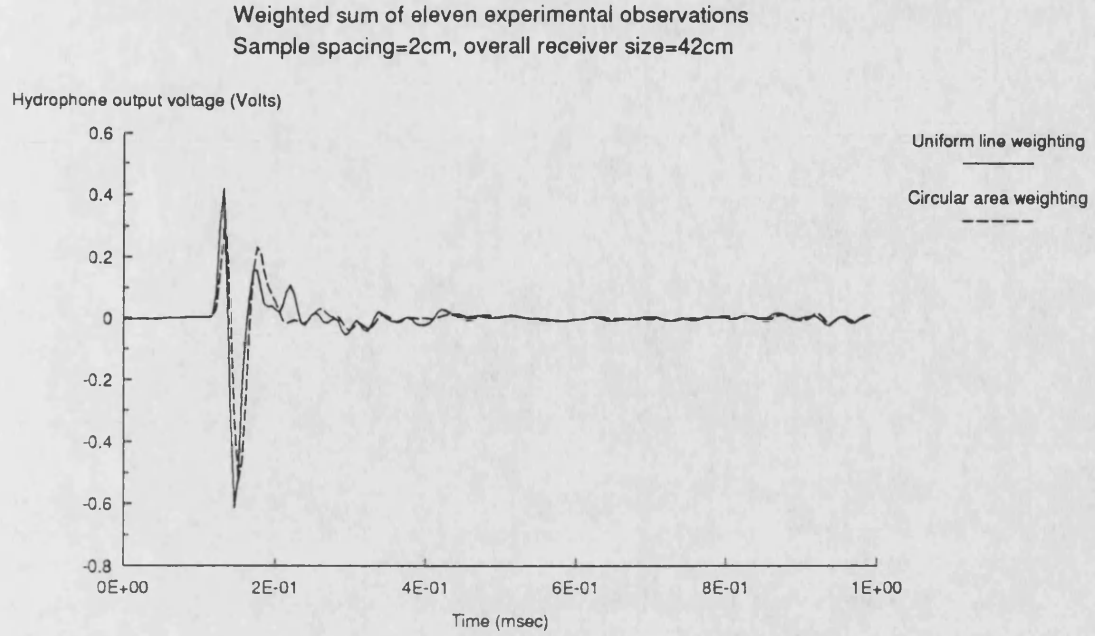

Figure 5.17. Weighted sum of 11 experimental waveforms used to synthesize a 42cm long (diameter) receiving aperture. Uniform and circular area weighting.

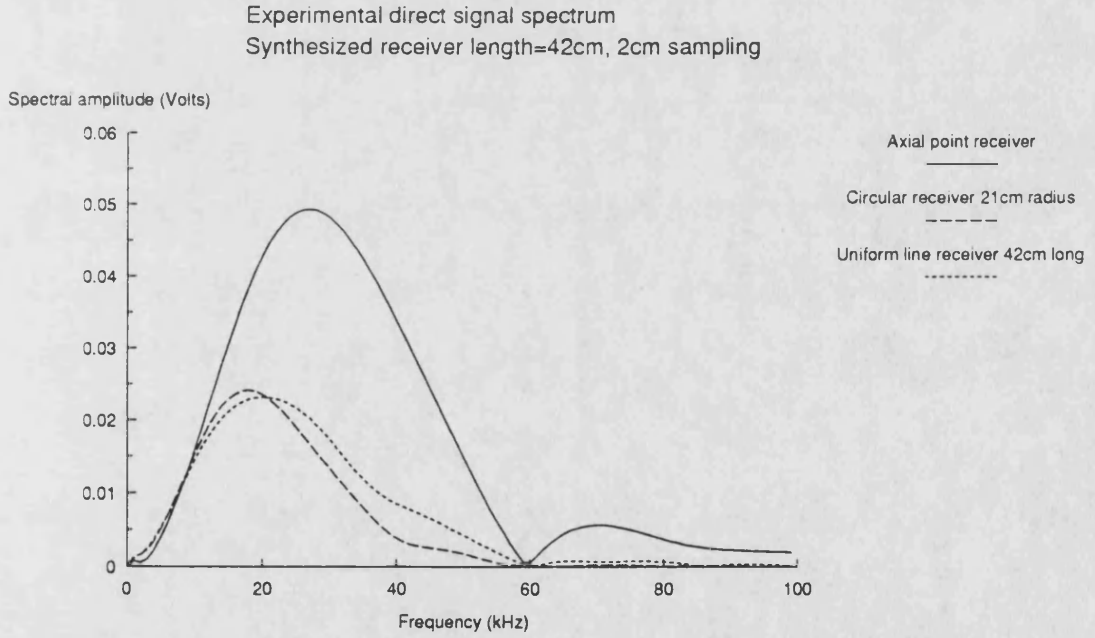

Figure 5.18. Experimental direct wave spectra. (a) point receiver on axis, (b) Synthesized line receiver 42cm long, and (c) synthesized circular receiver 21cm radius.

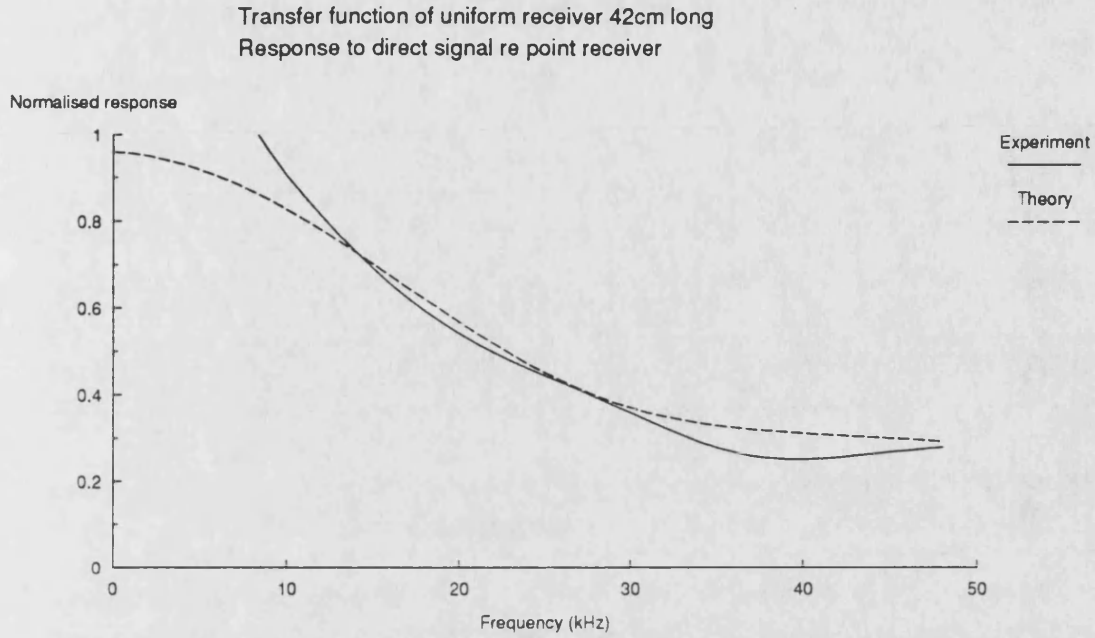

Figure 5.19. Theoretical (equation (5.44)) and experimental transfer function of uniform line receiver 42cm long.

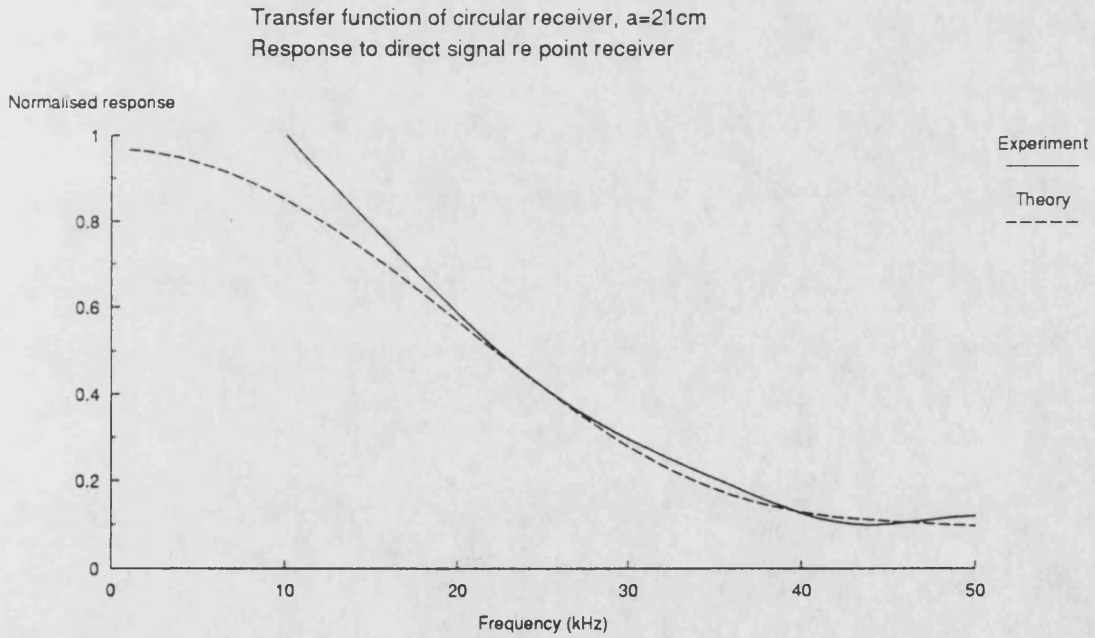

Figure 5.20. Theoretical (equation (5.55)) and experimental transfer function of circular receiver 42cm diameter.

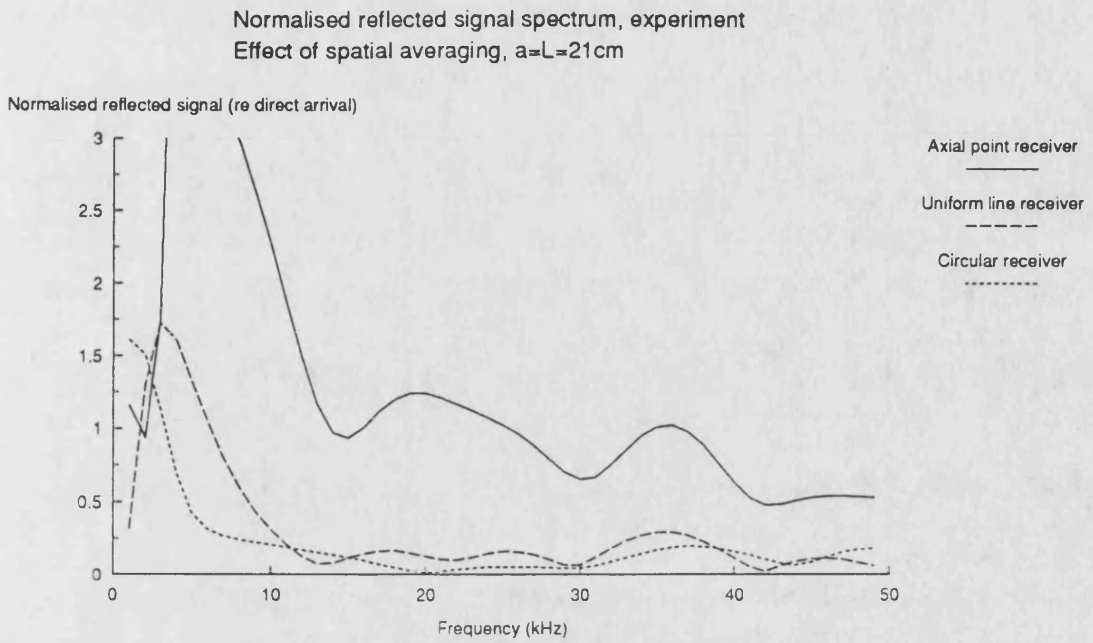

Figure 5.21. Experimental normalised reflected wave spectra obtained with a point receiver on axis and with uniform and circular synthetic receivers 42cm long (diameter) in the tube.

5.5 CONCLUSIONS REGARDING THE USE OF SYNTHETIC RECEIVING APERTURES IN THE TUBE

The aim of this chapter has been to establish the link between synthetic aperture measurements as they are commonly applied in planar wavefield situations, and the application of the technique for measurements inside the tube.

In order to determine the optimum amplitude weighting scheme for the synthesis of a receiver in the tube, we must maximise the response to the axial sources at all frequencies (equations (5.39) and (5.55)) and minimize the response to off axis sources of reflected wave from the tube wall (equation (5.30)). A direct measure of the improvement achieved using an extended receiver can be obtained if by taking the ratio of the response of the synthesized receiver to an axial end-fire line source to that for a ring source on the tube

wall representing the reflected wave. Any value over unity represents an improvement over the point receiver which has a constant response (equal to unity) irrespective of the angle of arrival of the wave.

Several amplitude weighting schemes have been used to synthesize receivers of various lengths. When a planar wavefield is considered, it is possible to find an optimum weighting scheme whereby the mainlobe beamwidth is minimized along with the sidelobe level of the receiver thus offering directive reception and immunity to off-axis interference. The synthesis of these optimum array receivers is based on the properties of Chebyshev polynomials and the technique is commonly known as the Dolph-Chebyshev array synthesis after Dolph who first suggested it. This technique gives very good results when applied in the present case but its main limitation is that it requires very close spatial sampling of the field to avoid the appearance of grating lobes within the visible region. This requirement is not acceptable because the close field sampling may lead to inter-element coupling or increased processing requirements. In practise, two amplitude weighting schemes were pursued: (a) uniform line weighting, and (b) circular area weighting. Both schemes offer similar advantages in terms of immunity to reflected wave interference, they are equally easy to implement and quite coarse spatial sampling may be used before grating lobes begin to appear in the visible region. Experimental results obtained using these weighting schemes seem to confirm theoretical predictions and offer a dramatic reduction in the strength of the reflected wave.

6 THE USE OF ABSORBING WEDGES ON THE TUBE WALL

6.1 INTRODUCTION AND PRELIMINARY RESULTS

In the effort to reduce the strength of the reflected wavefield at an axial receiver, a system of wedges was manufactured and mounted inside the tube.

The use of absorbers and/or baffles and screens for the elimination of extraneous waves is well established both in air and underwater acoustics [68].

The problems associated with the use of an absorber on the tube wall for the elimination of reflected wavefields arise from the fact that the frequencies we want to eliminate are low, cover a wide bandwidth and the angles of incidence on the absorber are quite large.

The aim of introducing the wedges was to reduce the relative strength of the reflected wave with respect to the direct wave in order to allow on-axis measurements with minimum interference. It has been shown that the reflected wave is quite strong and especially so at low frequencies. It is those frequencies, however, that are hardest to attenuate. Thus, the demands placed on the absorber are quite stringent and difficult to satisfy.

In order to maximise the energy that is actually coupled into the absorber, a wedged panel was used rather than a flat one. The wedges introduce the absorbing material gradually into the water thus enabling better impedance matching between the two media and hence better coupling.

The absorber comes in the form of panels which were machined into the right shape, folded and stuck onto the inside surface of a cylindrical shell made of 3mm thick aluminium. The outside diameter of the shell was 44cm and it fitted snugly inside the

neoprene lined tube. The overall length of the wedges was 45cm thus covering most of the tube surface were single bounce reflections of waves originating from the transducer (rather than the acoustic filter) occur.

The aluminium shell with the absorbing wedges mounted is shown in photograph 4. The panel cross-section is shown in figure 6.1.

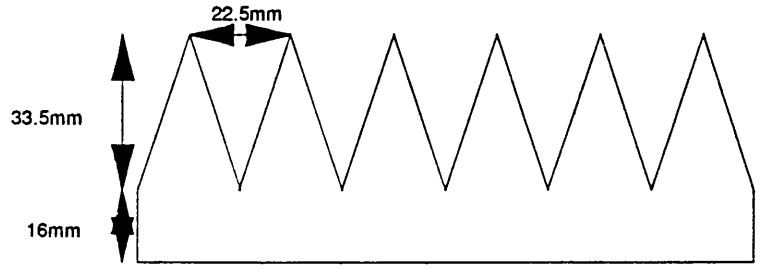

Figure 6.1. Cross section of an absorbing wedge panel.

Figure 6.2 shows the pressure waveforms on the tube axis at a range R=90cm with a parametric array L=52cm long recorded with and without the wedges on the tube wall. It can be seen that there is a significant reduction in the strength of the reflected wave with the wedges inside the tube but this reduction is by no means sufficient to enable reliable acoustical measurements on the basis of a single axial measurement without any spatial averaging. The improvement offered by the wedges is quantified in figure 6.3 which shows the normalised reflected wave spectrum on the tube axis with and without the wedges. The direct and reflected contributions are identified in figure 6.2. There is an average improvement of about 6dB over the whole frequency range with the wedges in the tube. The shift of the peaks of the normalised reflected wave spectrum in the presence of the wedges (dashed curve, figure 6.3) is attributed to a phase shift of the wave reflected by the wedges as well as the fact that the effective tube radius is reduced.

Similar results have been obtained at hydrophone ranges of R=80cm and R=70cm. In neither case is the reflected wavefield adequately suppressed.

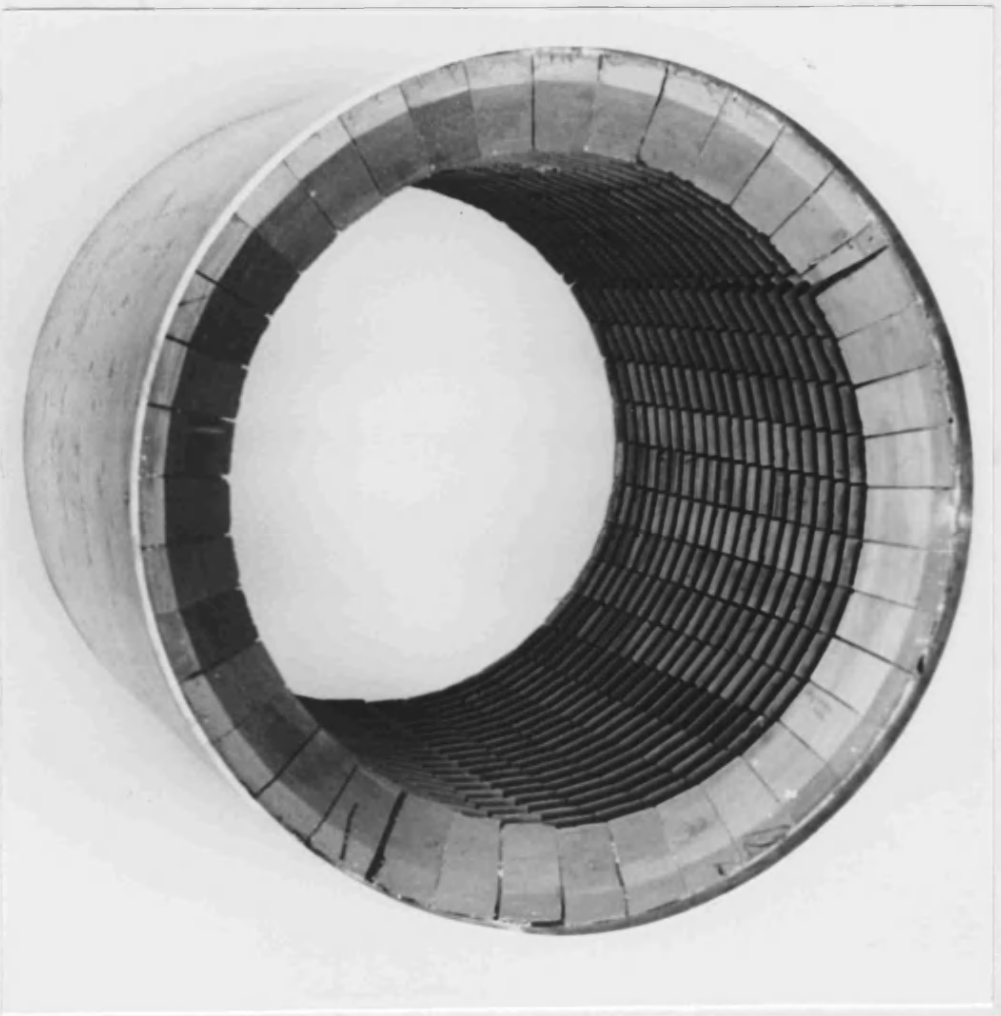

Photograph 4. The aluminium shell with the absorbing wedges mounted inside it.

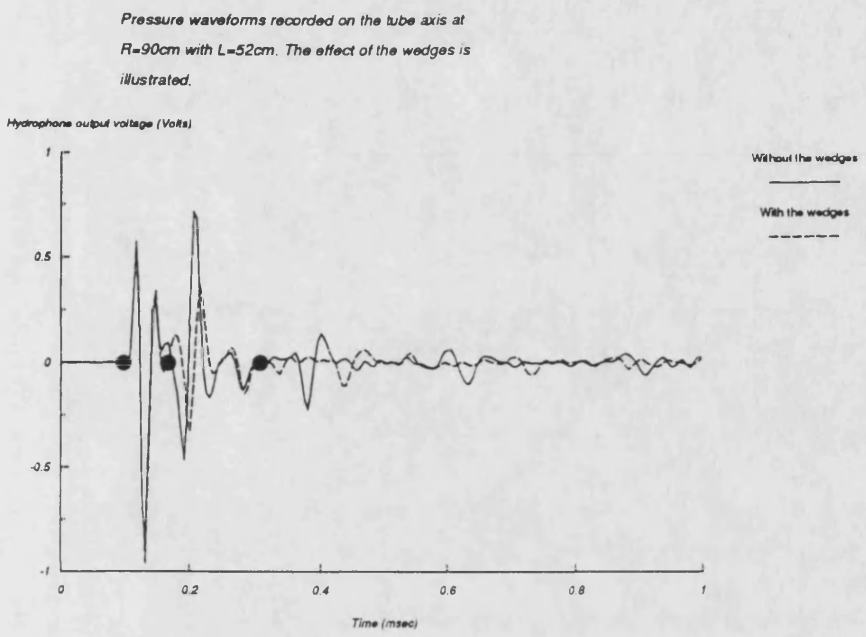

Figure 6.2. On axis pressure waveforms recorded with and without the wedges in place. The direct and reflected waves are marked.

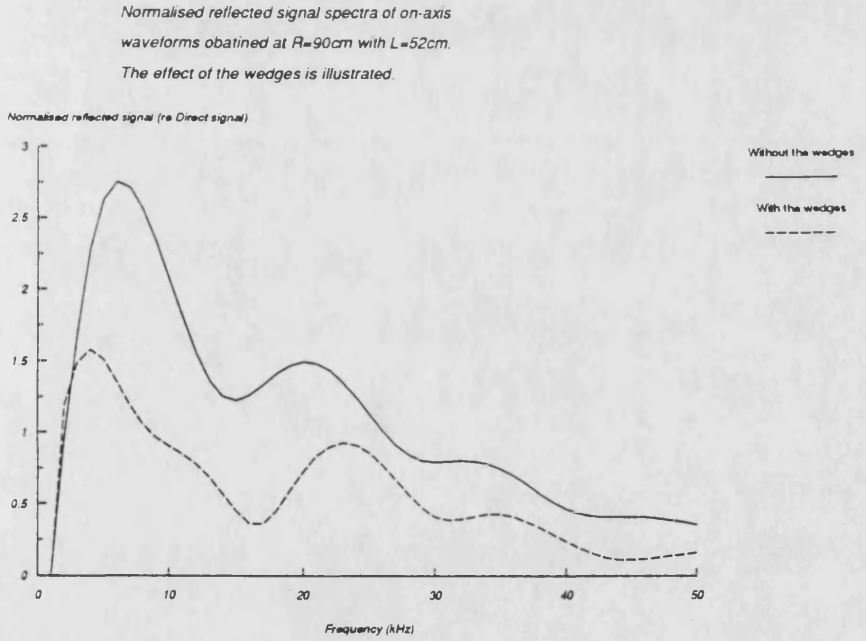

Figure 6.3. The normalised reflected wave spectra obtained with and without the wedges using the on axis waveforms shown in figure 6.2

6.2 SPATIALLY AVERAGED WAVEFORMS

In view of the advantages offered by spatial averaging (Chapter 5) measurements were performed in the tube in order to allow spatial averaging in the presence of the wedges. The waveform was recorded along the diameter of the tube in 2cm steps from an axial position out to 20cm off axis. Three hydrophone ranges were used: R=90cm, 80cm and 70cm with a parametric array L=52cm long. This set of results enables the synthesis of extended receivers of various sizes with arbitrary amplitude weighting.

For the present purposes only uniform line and circular area weighting was employed (Chapter 5) to synthesize receiving apertures of overall lengths (diameters) of 22cm and 42cm. A comparison with spatially averaged results obtained without the absorbing wedges on the tube wall enables an easy assessment of the improvement, if any, obtained with the wedges in the tube.

Figure 6.4 shows the spatially averaged waveforms obtained using circular area weighting to synthesize a receiver of 42cm diameter at ranges of R=90cm (figure 6.4a), R=80cm (figure 6.4b) and R=70cm (figure 6.4c). Each graph contains the waveform obtained with and without the wedges in the tube. It can be seen that the waveforms are virtually indistinguishable at all ranges.

Figures 6.5(a)-(c) show the same results obtained with a smaller receiver of 22cm diameter. The differences between the waveforms obtained with and without the wedges remain very small. Similar results to figures 6.4 and 6.5 can be obtained using uniform amplitude weighting to synthesize a line receiver. These shall not be shown here but insertion loss estimates obtained with uniform amplitude weighting are presented elsewhere along with those obtained with circular area weighting.

Figures 6.4 and 6.5 bear out the fact that the presence of the absorbing wedges makes virtually no difference when spatial averaging is employed. That is due to the fact that

both spatial averaging and the presence of the absorbing wedges on the tube wall offer similar benefits but their effects are not additive. The reduction in the reflected wave strength obtained with the wedges is overshadowed by the increased directionality obtained with a synthetic receiver. It is only at low frequencies that spatial averaging fails to produce a sufficiently directional receiver to reject tube wall effects but the efficiency of the absorbing wedges is also low at those frequencies thus offering very little gain over the simple pressure-release cladding of the tube wall. It should, however, be possible to obtain improved low frequency reflected wave immunity by optimizing the design of the tube wall cladding. The material used for present purposes was designed for normal incidence echo reduction and was not optimized for this particular application.

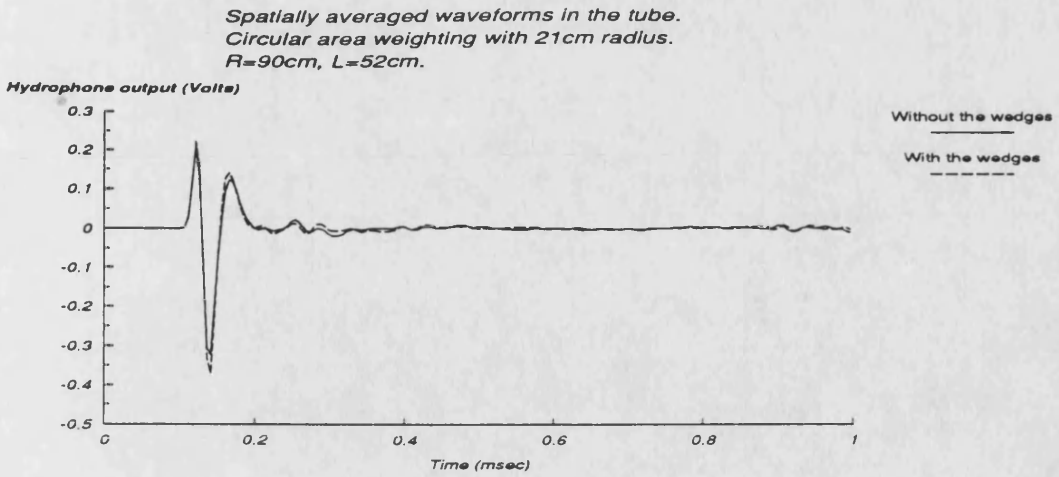

(a) R=90cm

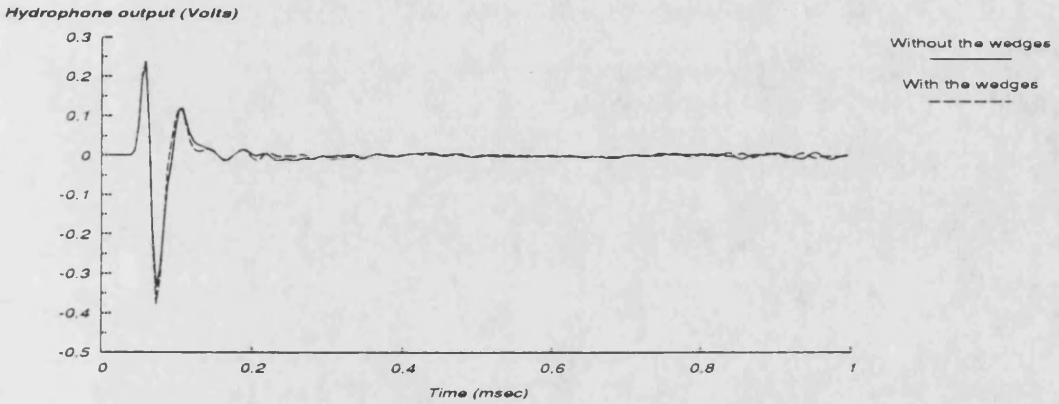

(b) R=80cm

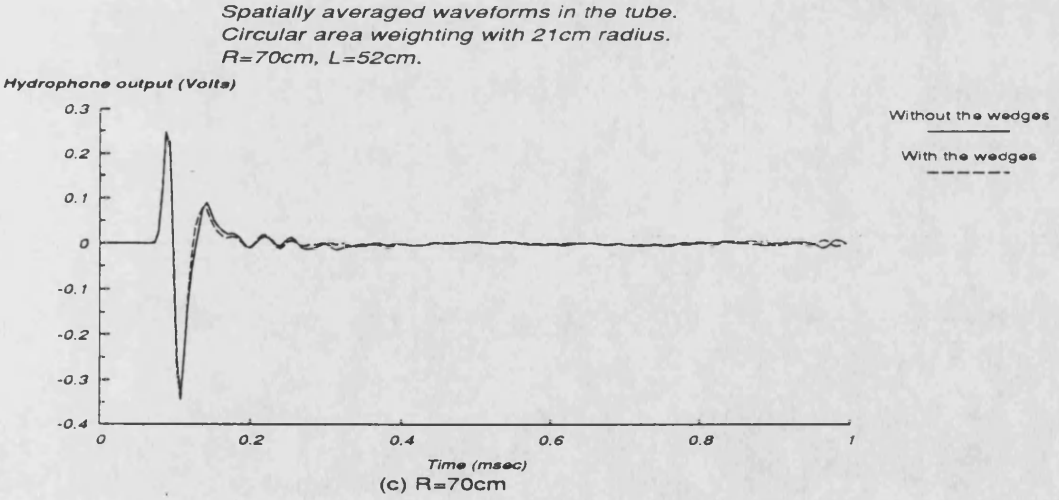

(c) R=70cm

Figure 6.4. Spatially averaged waveforms amplitude weighted for the synthesis of a 21cm radius circular receiver. Hydrophone range=70,80 & 90cm.

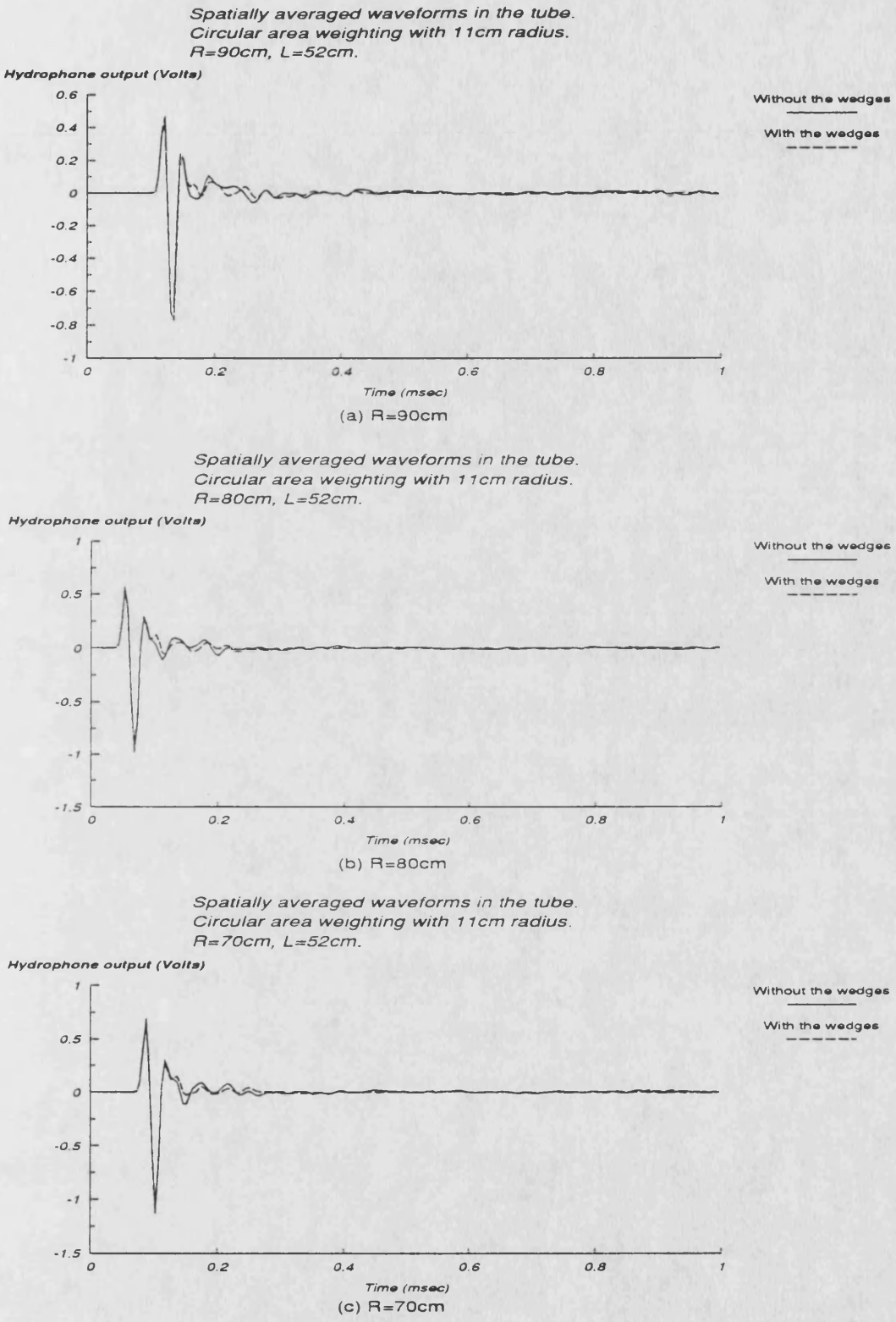

Figure 6.5. Spatially averaged waveforms amplitude weighted for the synthesis of a 11cm radius circular receiver. Hydrophone range=70,80 & 90cm.

7 INSERTION LOSS MEASUREMENTS

7.1 INTRODUCTION

The present system has been used to measure the insertion loss of samples in the form of plane sheets. The operational definition of insertion loss is:

$$\text{Insertion loss} = 20.\log_{10} \frac{\text{Incident sound pressure}}{\text{Transmitted sound pressure}}$$

Although the measurement of insertion loss is very simple in theory, it can be very difficult in practice. The above definition assumes a plane continuous wave incident on a planar sample of infinite lateral extent. The insertion loss can then be simply obtained by measuring the reduction in the acoustic signal when the sample is inserted between the source and the receiver. In practice the requirements set by the above definition of insertion loss cannot be met exactly leading to systematic errors in experimental measurements. These errors are due to: (a) the non-continuous nature of the incident wave, (b) the incident wave not being planar or of infinite extent, or (c) the finite size of the panel. Other possible sources of error include: (a) measurement errors, multiple reflections, (c) edge diffraction and (d) shear wave coupling into the plate which re-radiate into the water contiuously. When experimental measurements are performed in the tube, special care must be taken to reduce the effect of multiple reflections from the tube walls which in some cases may be stronger than the actual signal of interest. An assessment of the accuracy of the experimental results obtained with the present tube facility will be given at a later stage.

Theoretical estimation of the insertion loss of a panel is possible provided it is homogeneous, of relatively simple construction and its density and wave velocities are known [67]. The agreement between predicted and experimental results is an ideal method of measuring the performance of the measuring system. For this purpose, a

metallic plate was used to perform insertion loss measurements inside the tube as it has easily calculated properties. When more complex materials need to be investigated, the results can be compared with measurements performed in a tank under 'free field' conditions to a known accuracy. The experimental set-up used for this purpose is briefly described in chapter 3. It was first used by Humphrey [44-46,72,88] to perform insertion loss and echo reduction measurements on panels with a stated accuracy of about 1dB. Here it is used for insertion loss measurements on a rubber based panel of unknown characteristics.

Although it is possible to obtain accurate insertion loss estimates from single on axis measurements in the rectangular tank mentioned above, the same is not possible in the tube due to the large reflected wave contribution on axis. The most promising techniques for reducting the significance of this wave have been found to be the use of spatial averaging for the synthesis of an extended receiver of improved directional characteristics (chapter 5) and the use of an anechoic lining on the tube wall (chapter 6). The effectiveness of these techniques has been assessed in separate chapters. Here, the insertion loss estimates obtained with the help of the above measures are compared to theoretical results and free-field estimates.

7.2 EXPERIMENTAL INSERTION LOSS MEASUREMENTS

Experimental results were obtained for two test panels in the tank and in the tube. The first panel was a 25mm thick aluminium plate 41cmx41cm which was later cut to a circular shape of 20cm radius to fit inside the tube. This sample has a very high acoustic impedance. The density, shear and compressional wave velocities for this sample were taken from standard tables of data [103] and a corresponding estimate of theoretical insertion loss was calculated.

The other sample was a rubber based compound 1cm thick and 45cm x 45cm which was later cut into a circular shape in order to fit the tube. This sample was acoustically soft and quite different to the previous sample. The material properties of the sample were not available and thus a theoretical estimate of its insertion loss could not be obtained. In order to assess the validity of the tube results, comparative measurements were performed in the tank were a reliable insertion loss estimate could be obtained.

Insertion loss estimates were obtained with the tube for both samples using on axis measurements as well as spatial averaging of the received signal. Results for the hard and soft samples will now be presented independently.

7.2.1 THE ALUMINIUM SAMPLE

A theoretical estimate of the insertion loss at normal incidence was obtained using the following expression [68]:

$$\text{Insertion loss} \quad = \quad 10 \cdot \log_{10} \left[\frac{(1-m^2)^2}{4m^2} \sin^2 kx + 1 \right]$$

where m is the ratio of the characteristic impedance ρc of aluminium to that of water, k is the wavenumber and x the thickness of the panel.

Initially experimental results were obtained in the tank by recording the pressure waveform at a range of 86cm before and after the aluminium plate was inserted in the path of the acoustical beam at 80cm from the transmitting transducer. A parametric array 50cm long was formed using a 1MHz piston transducer transmitting a pulse with a 20kHz raised cosine envelope. The waveform at the receiver (B & K 8103) was averaged over 64 consecutive signals, using a 0.512msec time window. Figure 7.1 shows the reference waveform obtained in the tank. This waveform is free from multiple reflection arrivals or other interference. Figure 7.2 shows the waveform at the same

position with the aluminium plate inserted in the acoustical beam. The waveform has now acquired a significant tail which is attributed to diffracted waves around the sample, multipath arrivals following reflection from the sample and the tank walls or water surface, and waves that have coupled into and propagate along the sample re-radiating continuously. The fine structure of the waveform in the interval between 0.2 and 0.3msec in figure 7.2 is attributed to delayed pulse built-up due to internal reflections in the sample and multiple reflections between the sample and the hydrophone. This part of the wave would need to be included in any insertion loss estimates despite the fact that there will inevitably be a small amount of unwanted (diffracted) wave included within the window.

The same measurement was repeated in the tube with the hydrophone at a range of 90cm, a parametric array length of 52cm and the sample 10cm in front of the receiver. Figure 7.3 shows the reference waveform in the tube recorded on axis just before the plate was inserted. Figure 7.4 shows the waveform at the same position with the plate in the tube. The most striking feature of this graph is the structure of the tail of the waveform after the direct on-axis arrival.

An additional effect that influences the waveform at the receiver results from the transmission characteristics of the sample. Figure 7.5 shows a theoretical estimate of the variation of the angle of incidence of the transmission coefficient of a 25mm thick aluminium plate at 20kHz and at 40kHz (dashed line). It can be seen that the transmission coefficient is minimum at normal incidence and, consequently, any reflected wave contributions will undergo less attenuation on their way to the receiver.

It is clear that on the basis of the results shown in figures 4 and 5 we cannot make an accurate insertion loss prediction on the strength of axial waveform measurements. The diffracted wave level can be reduced and delayed by moving the hydrophone closer to the sample but this can lead to multiple reflections between the sample and the hydrophone without any reduction in the relative strength of the reflected waves.

On the basis of the results presented in previous chapters, it would appear that spatial averaging using the hydrophone to synthesize a large area receiver should be advantageous as it provides good rejection of off-axis wave arrivals.

Figure 7.6 shows the spatially averaged received signal obtained by scanning the hydrophone over a distance of 20cm, in 2cm steps, along the tube diameter. Circular area weighting was used (Chapter 6) to synthesize a circular receiving aperture of 42cm diameter. The improvement obtained over single on-axis measurements (figure 7.4) is quite significant. It is possible to use this result to obtain an estimate for the insertion loss of this sample.

Figure 7.7 shows the theoretical insertion loss of this sample at normal incidence (dotted line) as well as the experimental results obtained from free-field measurements (dashed line) and tube measurements using spatial averaging (solid line). It can be seen that the free field result gives much better agreement with theory but, tube measurements show significant deviations from theory. It must be noted that even the free field result was obtained by applying a short time window in order to avoid the influence of the diffracted wave. In the case of tube measurements, the diffracted wave is even stronger and it arrives earlier due to the circular shape of the test panel.

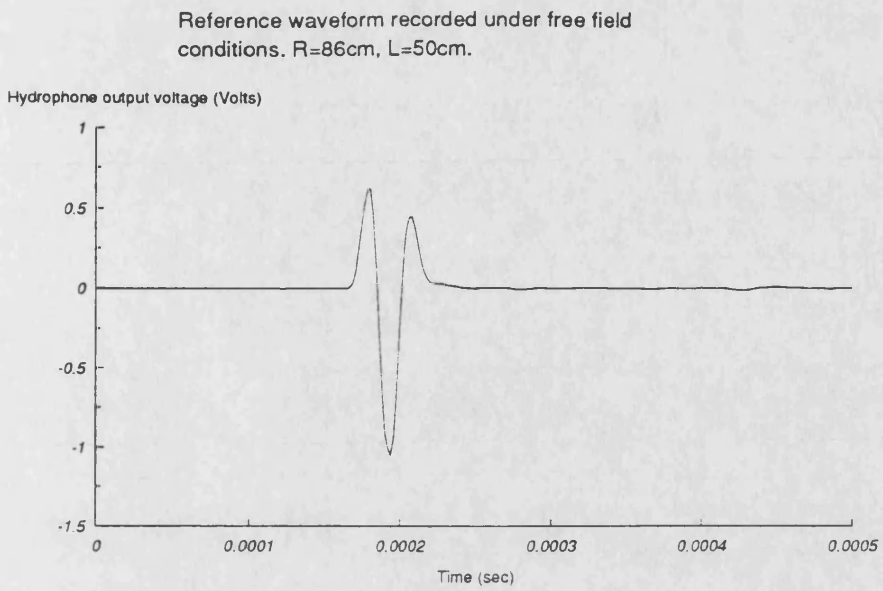

Figure 7.1. The reference pressure waveform recorded in the tank under free-field conditions. Hydrophone range R=86cm, parametric array length L=50cm.

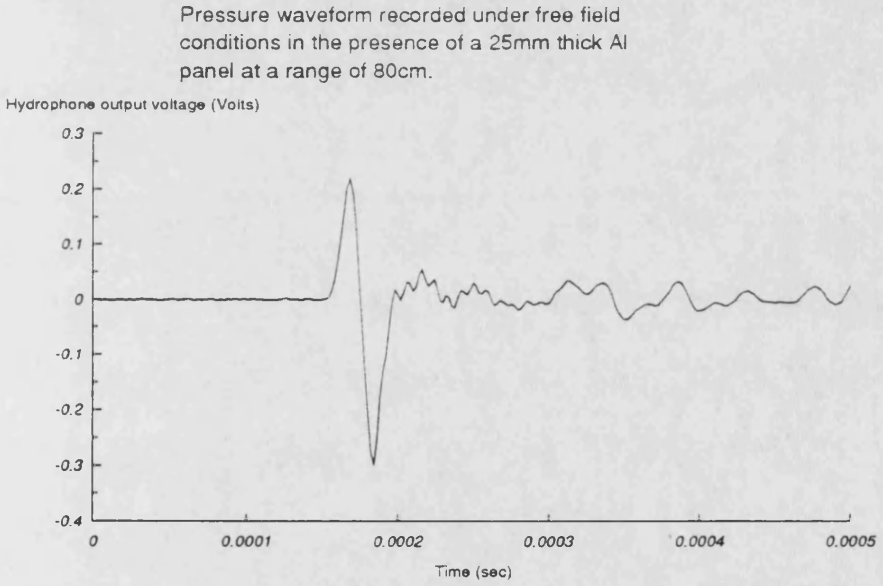

Figure 7.2. The pressure waveform recorded on the acoustic axis in the tank with the 25mm aluminium plate inserted normal to the acoustic beam at a range R=80cm (c.f. figure 7.1).

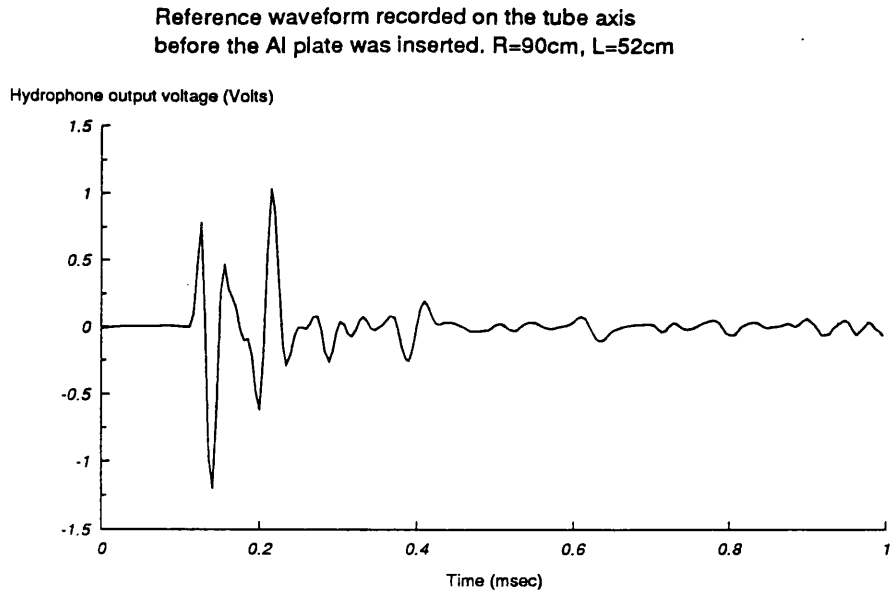

Figure 7.3. The reference pressure waveform recorded on the acoutic axis in the tube at a range R=90cm, L=52cm.

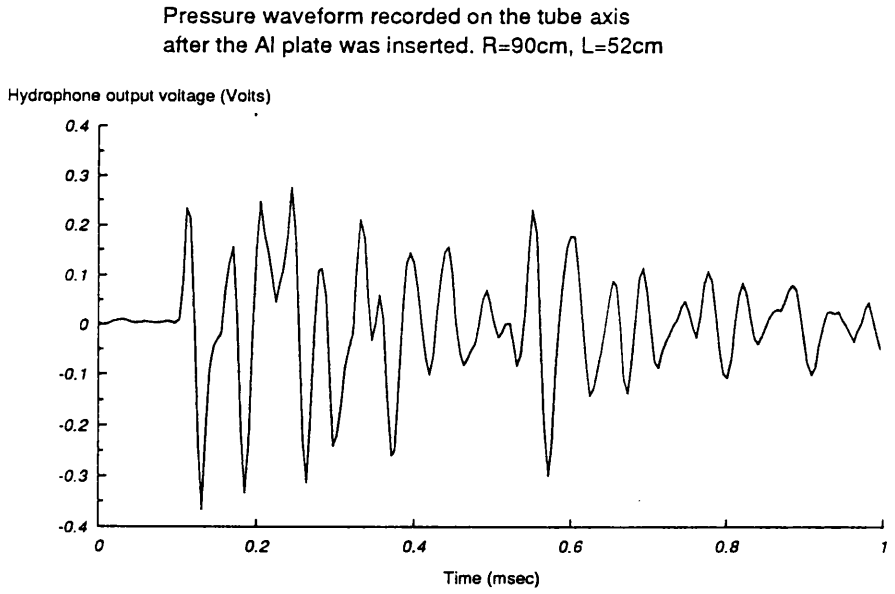

Figure 7.4. The pressure waveform recorded on the tube axis after the introduction of the 25mm thick aluminium plate at a range of 80cm.

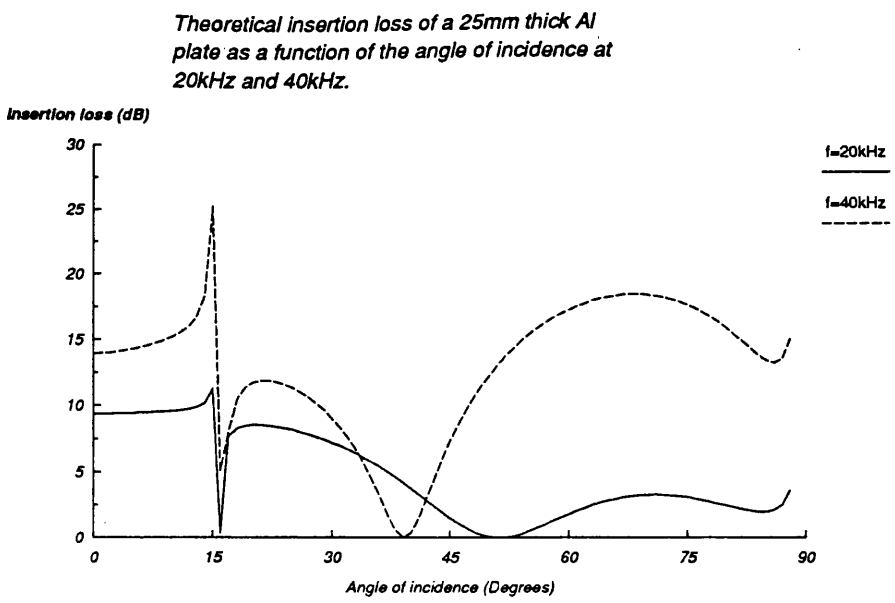

Figure 7.5. Theoretical estimate of the insertion loss of the 25mm thick aluminium plate at 20kHz and 40kHz (dashed line) as a function of the angle of incidence.

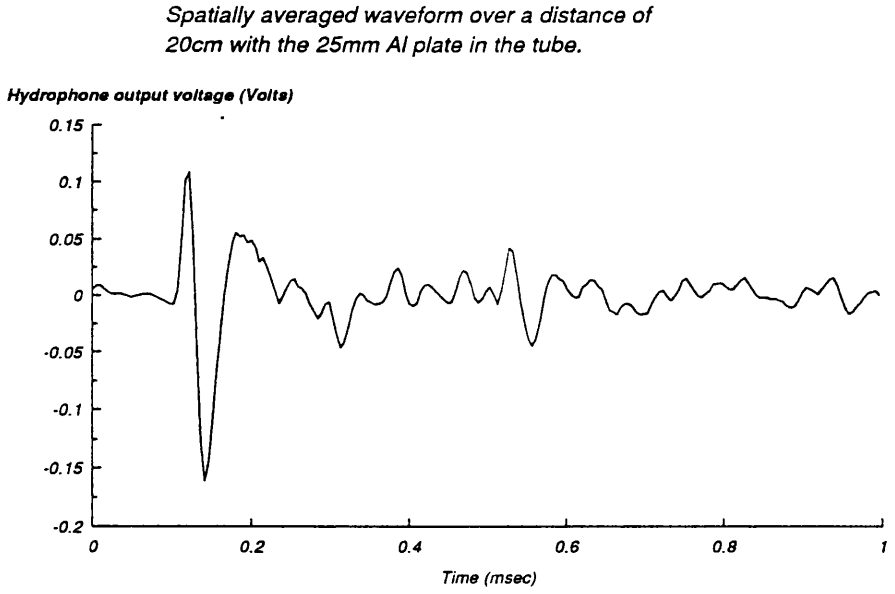

Figure 7.6. Spatially averaged received signal obtained by scanning the receiver over a distance of 20cm, in 2cm steps, along the tube diameter. Aluminium plate in the tube at a range of 80cm, R=90cm, L=52cm.

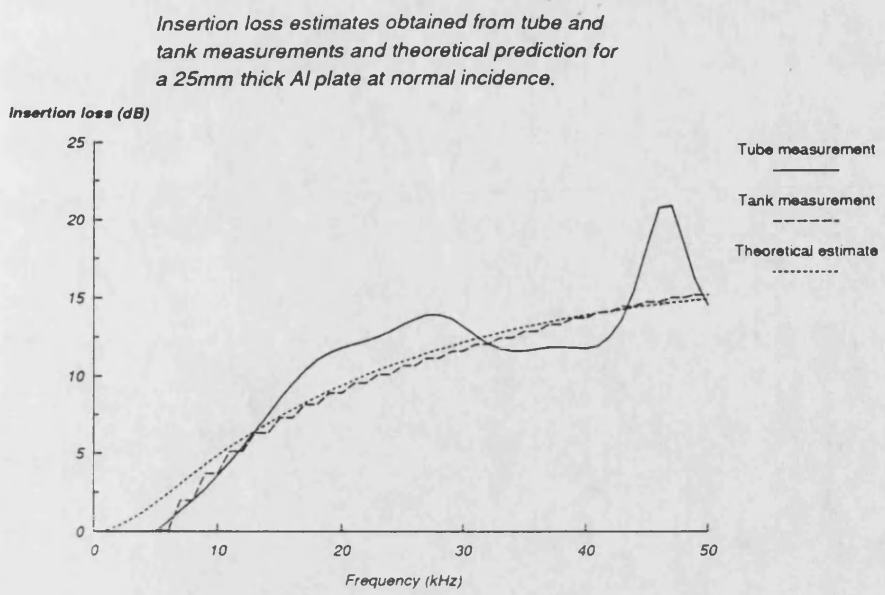

Figure 7.7. Insertion loss of the aluminium plate as a function of frequency at normal incidence. Experimental results obtained with spatially averaged tube measurements (solid line), tank measurements (dashed line) and theoretical estimate.

7.2.2 THE RUBBER COMPOUND SAMPLE

A 45cm x 45cm x 1cm rubber compound panel was also obtained for acoustical measurements. This sample is quite different to the metallic panel described previously and should provide an indication of the performance of the system for the measurement of the acoustical properties of soft samples.

Initial measurements were performed in the tank and the sample was later cut into a circular shape 22cm radius for tube measurements. A theoretical estimate of the insertion loss of this sample as a function of frequency could not be obtained since shear and compressional wave velocities were not available. Previous work [44,46,72,88] suggests that tank measurements on this kind of sample are quite reliable.

The tank measurements were performed at a range of R=90cm with a 50cm long parametric array formed by using a 20kHz raised cosine bell envelope to modulate a

920kHz primary frequency transmitted from a 5cm diameter transducer. The sample was later inserted 10cm away from the hydrophone. Figure 7.8 shows the reference waveform obtained at the hydrophone position before the test panel was introduced. This waveform is featureless apart from the direct wave arrival. Figure 7.9 shows the waveform at the receiver after the test panel was inserted. It can be seen that the effects of diffraction around the sample, multiple reflections in the tank, shear wave coupling into and re-radiation from the sample are minimal compared to these obtained with the aluminium panel.

Tube measurements with this sample were much more exhaustive than those performed on the metallic sample. The reason for this is that the present sample is much more representative of the materials that are likely to be tested with this facility whereas measurements on metallic panels are much less common.

Many sets of results were obtained with this sample in the tube at various hydrophone (and hence panel) ranges, with and without the absorbing wedges on the tube wall and with spatial averaging employing uniform and circular area weighting.

A comparative study of results obtained with and without the wedges on the tube wall will not be presented here. It should suffice to say that the results parallel those presented in chapter 6 which indicated the improvements obtainable with the wedges on the tube wall. Namely, there is a significant reduction in the reflected wave strength with on axis measurements but the additional benefit when spatial averaging is used is minimal.

The hydrophone-sample spacing was kept at 10cm. Spatial averaging was performed by scanning the hydrophone along a tube diameter in 2cm steps out to a distance of 20cm off-axis. Measurements were made with hydrophone ranges of R=90cm, 80cm and 70cm from the transmitter.

Figure 7.10 shows the axial waveform recorded at R=90cm without the sample in the tube for reference purposes. Figure 7.11 shows the waveform recorded at the same position with the panel at a range of 80cm. The result shown in figure 7.11 cannot be used to obtain a reliable insertion loss estimate due to the strong presence of reflected waves. Figure 7.12 shows a spatially averaged waveform obtained without the sample in the tube by scanning the hydrophone out to 20cm off axis, in 2cm steps, and using circular are and uniform (dashed line) weighting to synthesize a 42cm diameter (overall length) receiver. This waveform is used as a reference for comparison with that shown in figure 7.13 which was obtained in a similar manner in the presence of the test panel. The same amplitude weighting schemes were used to obtain the curves shown.

The same procedure was repeated with the hydrophone at a range of 80cm and the test panel at 70cm. Figures 7.14-7.17 show, respectively, the on axis waveform recorded for reference purposes without the test panel, the waveform at the same position with the test panel in place and the spatially averaged waveforms with uniform and circular area weighting with and without the panel.

Figures 7.18-7.21 show the same results at a hydrophone range of R=70cm and the panel at 60cm. In all cases, an appropriate trigger delay was used before recording the received waveform. At each position 1024 waveforms were averaged to improve the signal to noise ratio.

In each case, the data collected also enabled smaller receeiving apertures to be synthesized. Averaged waveforms for those are not presented here for clarity but insertion loss estimates obtained with spatial averaging over a receiver diameter of 22cm will be presented.

These results suggest that spatial averaging does reduce the level of the reflected wave at the receiver quite appreciably and does provide good results. The amplitude weighting

scheme used for receiver synthesis does not affect the averaged waveforms significantly. All averaged waveforms were windowed within a 0.2msec window following the direct wave arrival and the level of the signal was set to zero outside that window. The spectra of the windowed waveforms were then obtained with a computer and their ratios provided estimates of the insertion loss of the sample. Figures 7.22-7.24 show the insertion loss results at R=90cm, 80cm and 70cm respectively. In each case, the results obtained from the tank measurements are shown for comparison purposes (solid line). The other four curves in each graph were obtained by applying different amplitude weightings to the spatially averaged results for two different sizes of synthesized receiver. The agreement between all the tube results is very good and they are all within ±1dB of the tank result, in the 5-50kHz range, which itself is subject to that amount of uncertainty. One exception is the result obtained with the hydrophone at R=70cm. In this configuration, there is some ripple on the insertion loss results due to multiply reflected waves between the acoustic filter and the test panel.

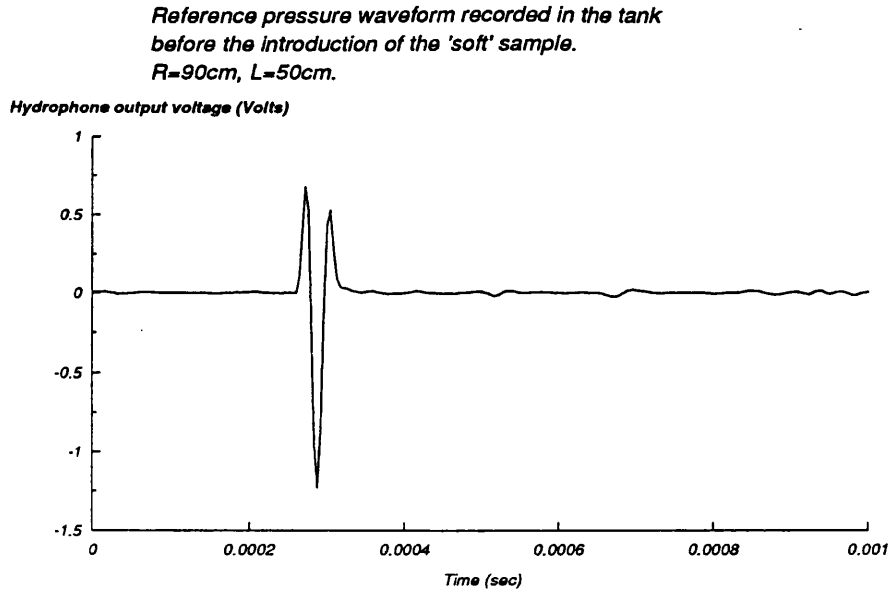

Figure 7.8. Reference pressure waveform recorded in the tank before the introduction of the 'soft' sample.

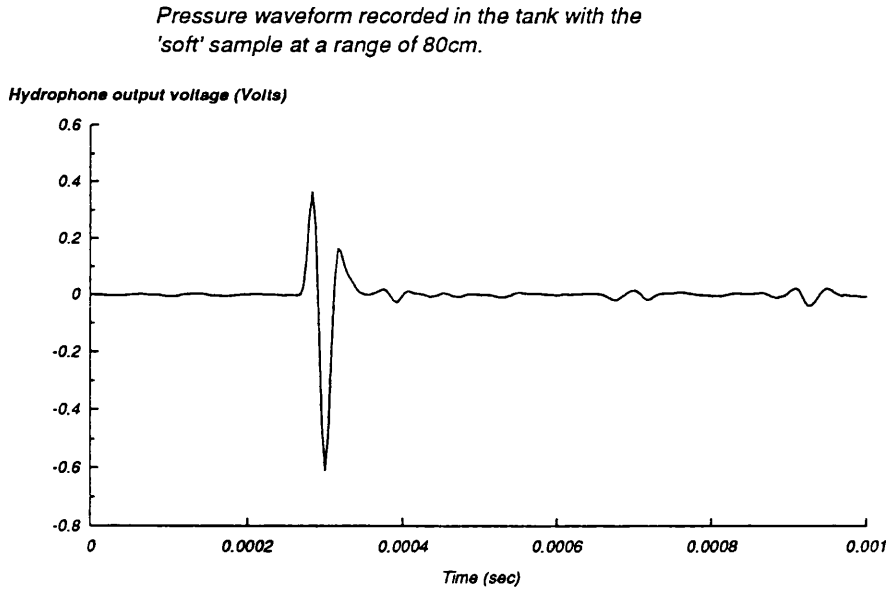

Figure 7.9. Pressure waveform obtained in the tank after the introduction of the 'soft' test panel.

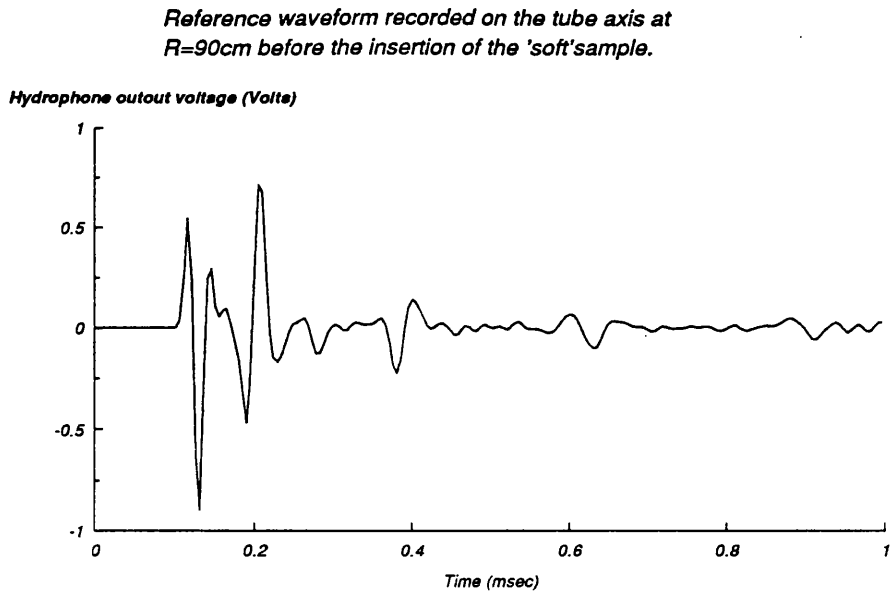

Figure 7.10. Pressure waveform recorded on the tube axis at a range R=90cm before the introduction of the 'soft' test panel for reference purposes.

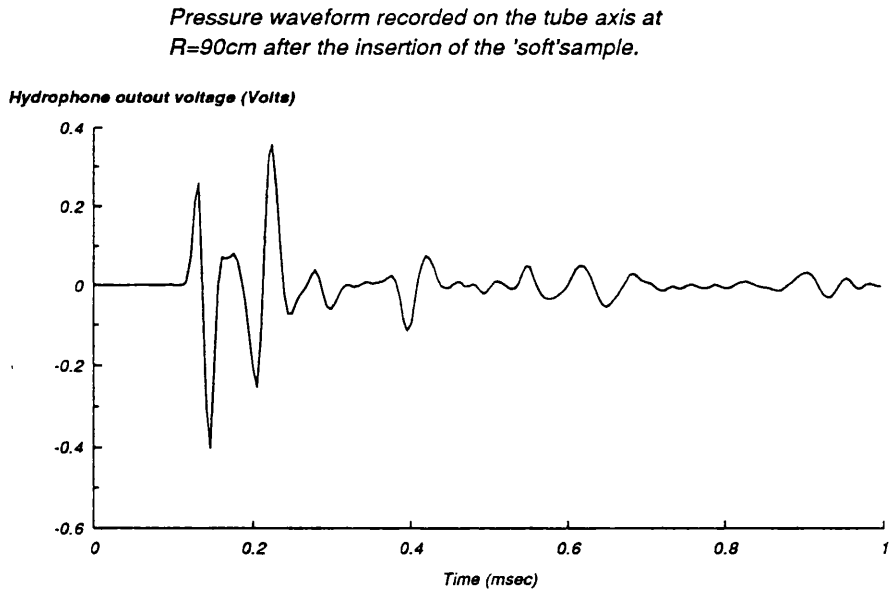

Figure 7.11. Pressure waveform recorded on the tube axis at a range R=90cm with the test panel at a range of 80cm.

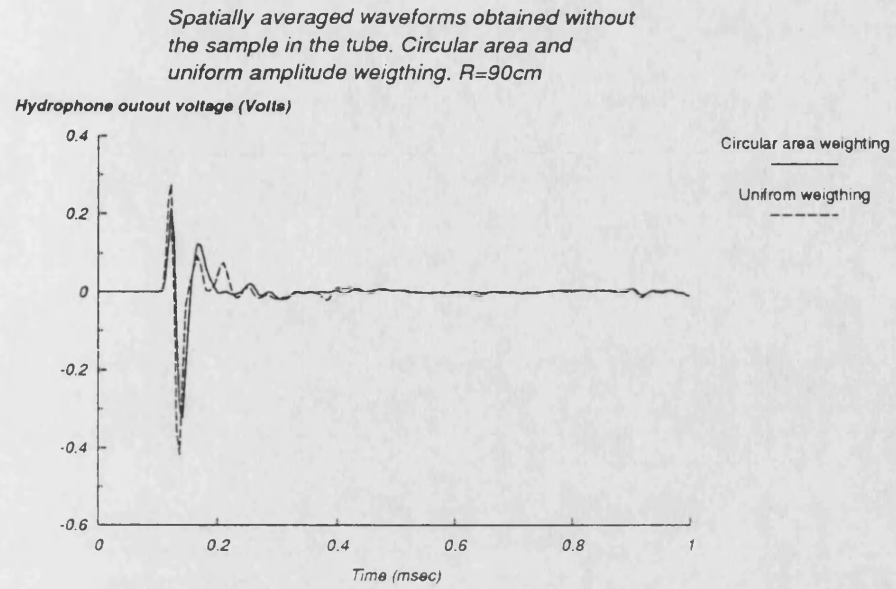

Figure 7.12. Spatially averaged receiver waveform at R=90cm without the test panel recorded for reference purposes. Circular area and uniform line amplitude weigthing.

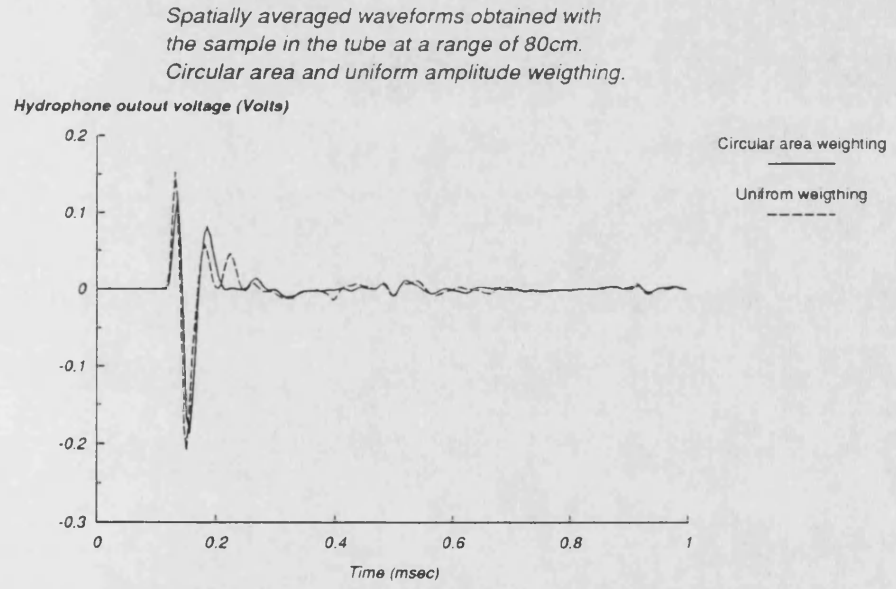

Figure 7.13. Spatially averaged receiver waveform at R=90cm with the test panel at 80cm. Circular area and uniform line amplitude weigthing.

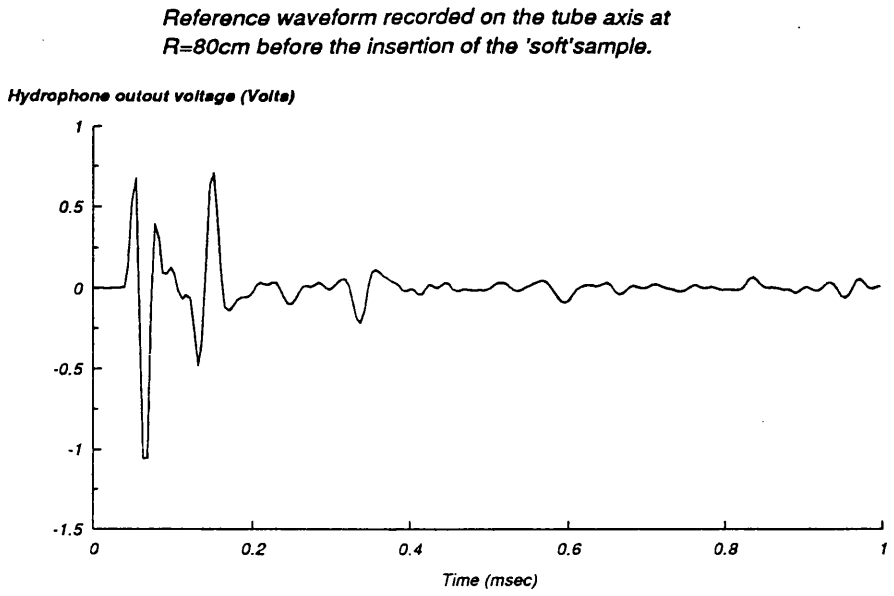

Figure 7.14. Pressure waveform recorded on the tube axis at a range R=80cm before the introduction of the 'soft' test panel for reference purposes.

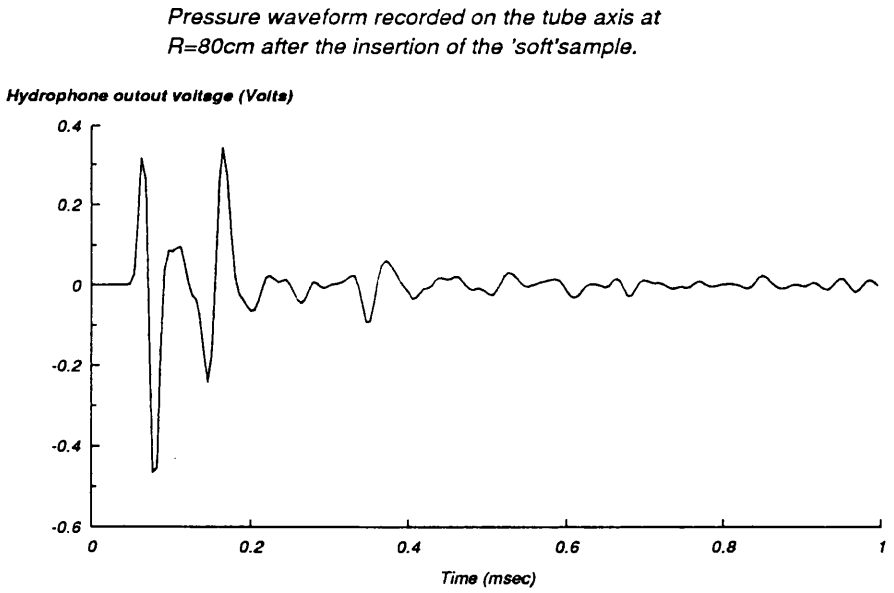

Figure 7.15. Pressure waveform recorded on the tube axis at a range R=80cm with the test panel at a range of 70cm.

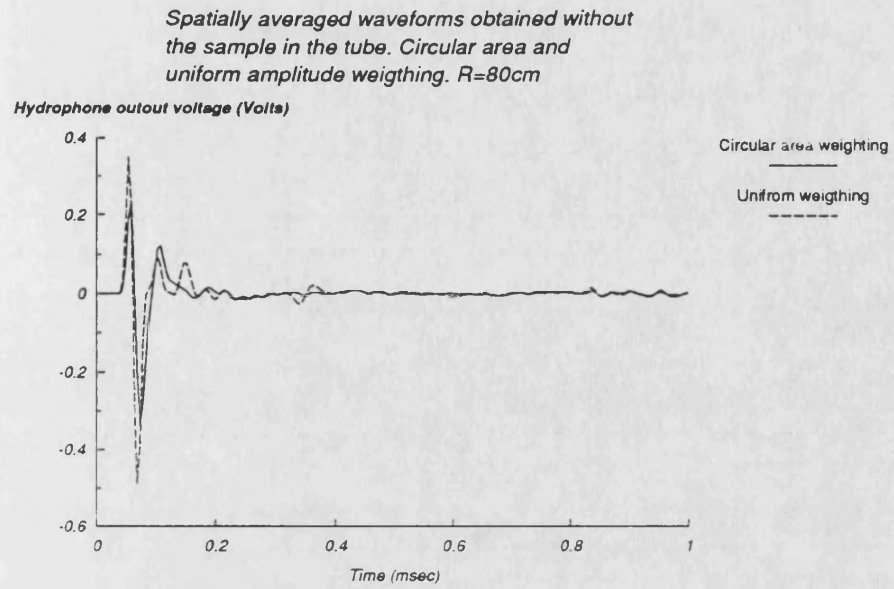

Figure 7.16. Spatially averaged receiver waveform at R=80cm without the test panel recorded for reference purposes. Circular area and uniform line amplitude weigthing.

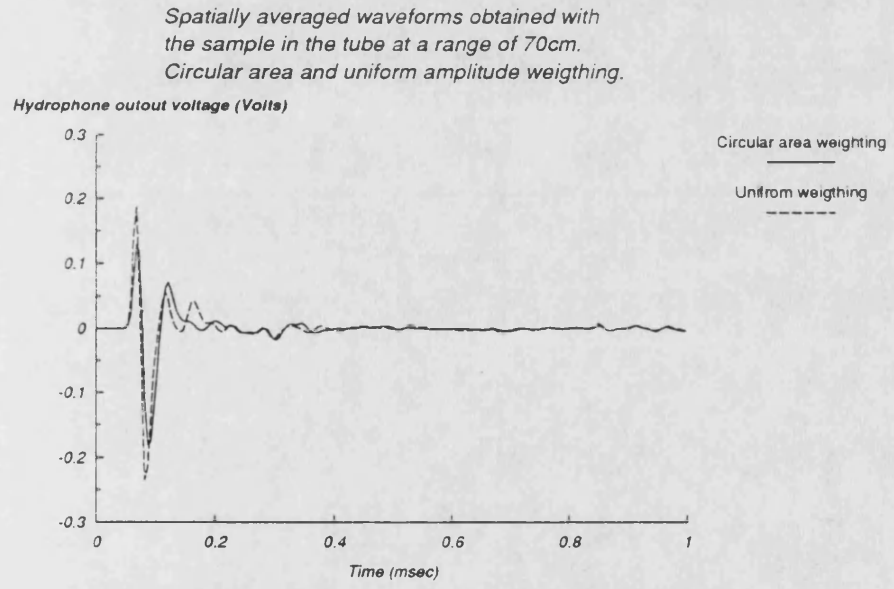

Figure 7.17. Spatially averaged receiver waveform at R=80cm with the test panel at 70cm. Circular area and uniform line amplitude weigthing.

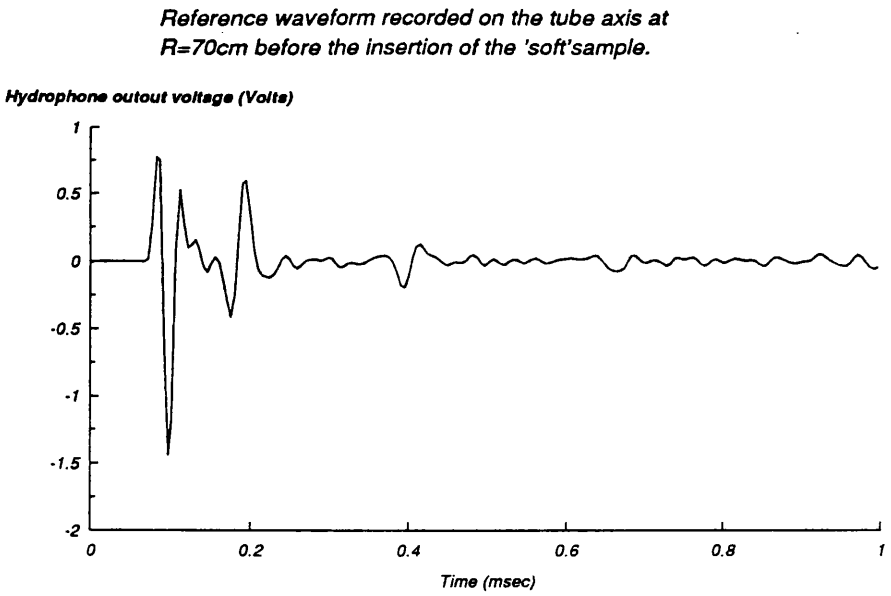

Figure 7.18. Pressure waveform recorded on the tube axis at a range R=70cm before the introduction of the 'soft' test panel for reference purposes.

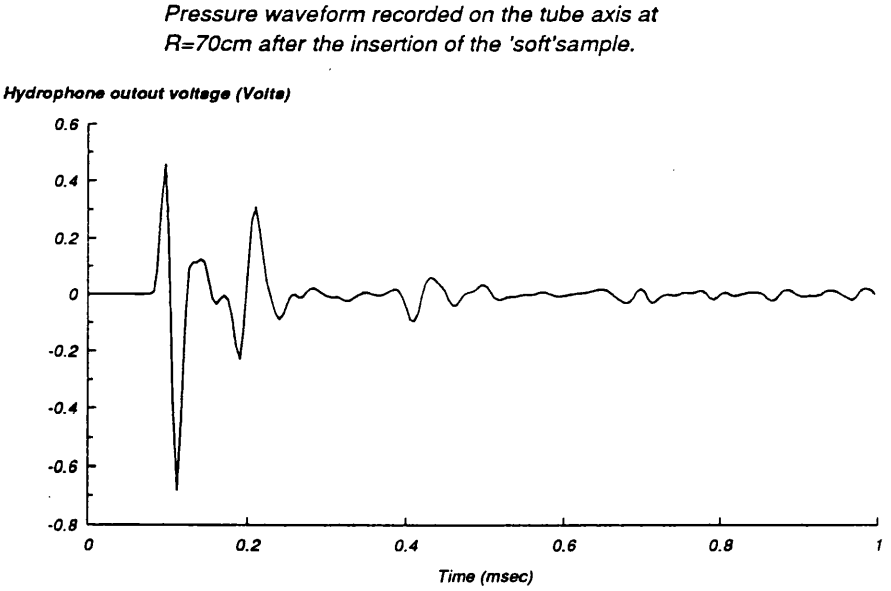

Figure 7.19. Pressure waveform recorded on the tube axis at a range R=70cm with the test panel at a range of 60cm.

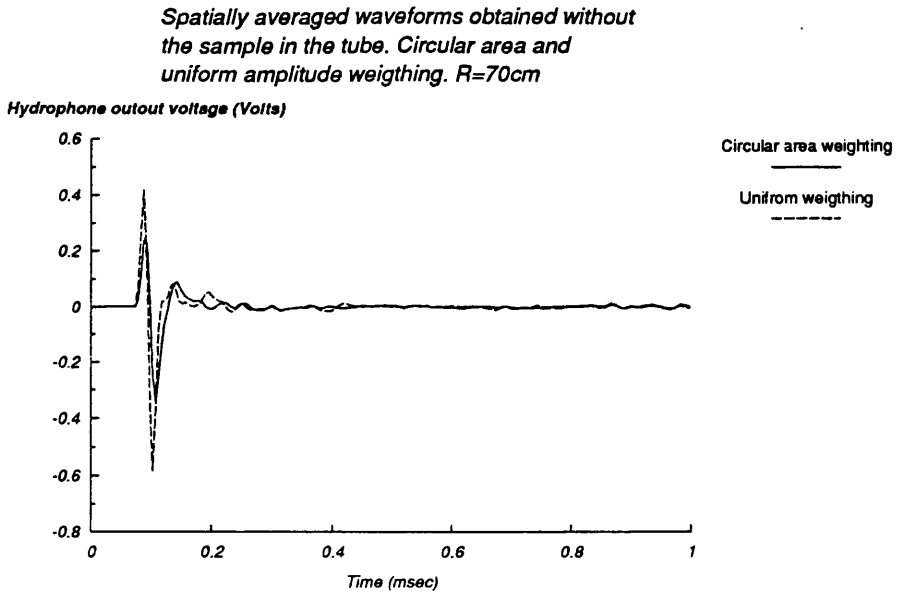

Figure 7.20. Spatially averaged receiver waveform at R=70cm without the test panel recorded for reference purposes. Circular area and uniform line amplitude weigthing.

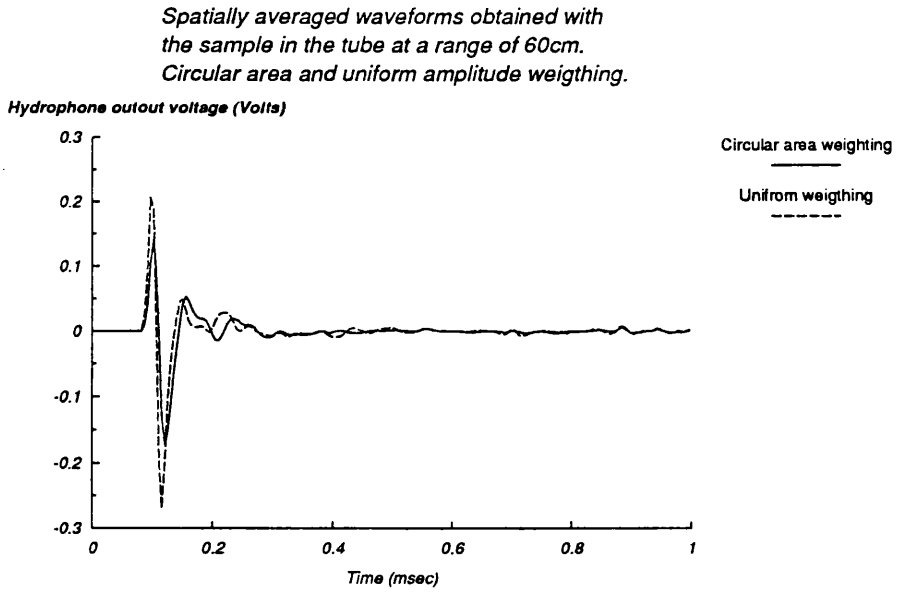

Figure 7.21. Spatially averaged receiver waveform at R=70cm with the test panel at 60cm. Circular area and uniform line amplitude weigthing.

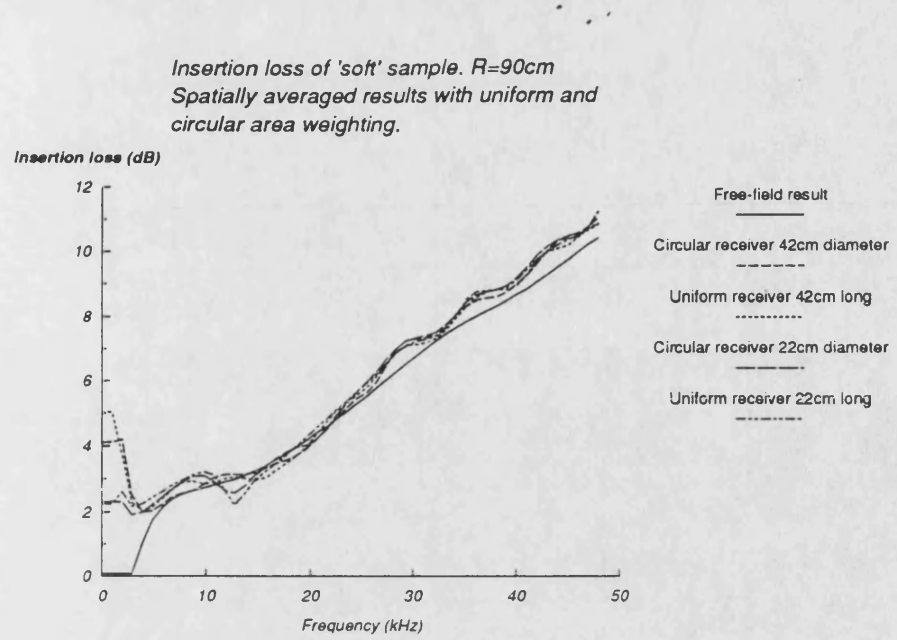

Figure 7.22. Insertion loss estimates for the 'soft' test panel obatined with measurements at R=90cm. Results with various spatial averaging schemes and the free field result.

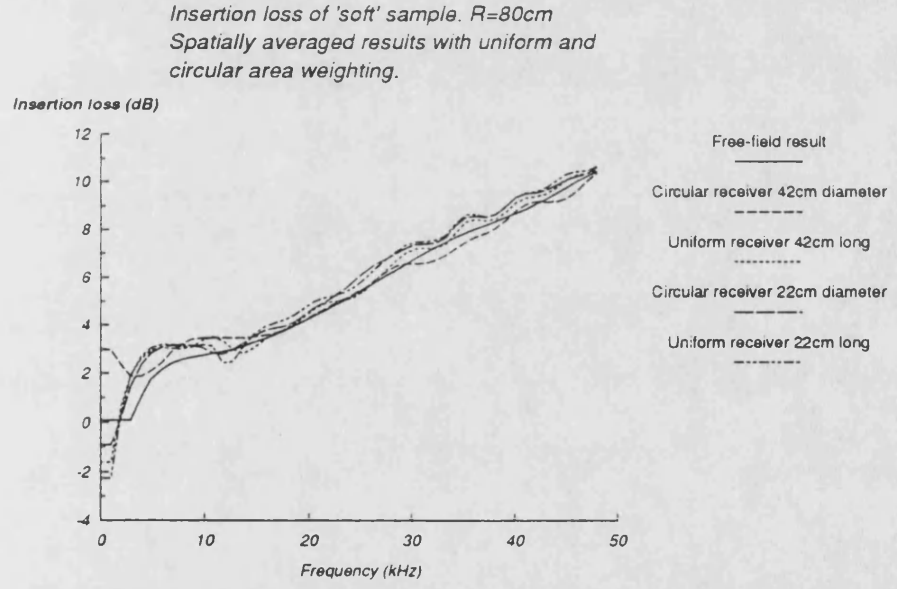

Figure 7.23. Insertion loss estimates for the 'soft' test panel obatined with measurements at R=80cm. Results with various spatial averaging schemes and the free field result.

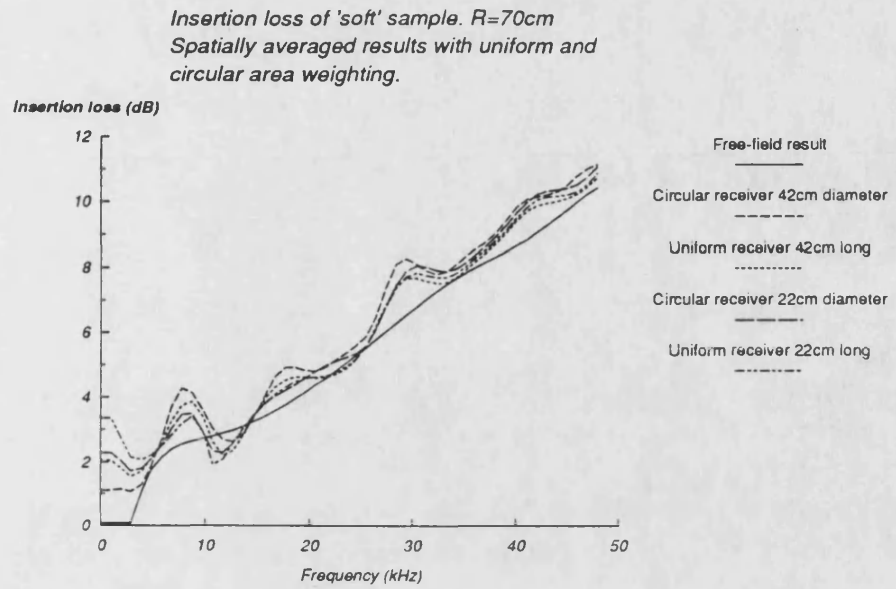

Figure 7.24. Insertion loss estimates for the 'soft' test panel obatined with measurements at R=70cm. Results with various spatial averaging schemes and the free field result.

7.3 ERRORS ASSOCIATED WITH INSERTION LOSS ESTIMATES

The results presented in the preceding sections show the potential and the limitations of the present system for insertion loss measurements at normal incidence over a wide frequency range. In this section, the factors affecting the accuracy of these results will be discussed although some have already been identified and ways of overcoming them have been suggested (i.e. spatial averaging and absorbing wedges on the tube wall).

The possible sources of error were identified in the introduction to this chapter. These can be broadly divided into systematic and non-systematic errors. Non systematic errors may occur due to:

(a) measurement errors,(b) multiple reflections, and

(c) edge diffraction.

Systematic errors occur when the conditions set in the definition of insertion loss cannot be met experimentally. These may be due to:

(1) the non-continuous nature of the incident waves,

(2) the incident waves not being planar or of infinite extent, and

(3) the finite size of the panel.

In the following subsections these possible sources of error will be discussed and their relative importance will be assessed.

7.3.1 MEASUREMENT ERRORS

These are errors associated with the measurement of the waveform amplitude. The accuracy of this measurement depends on the accuracy and linearity of the electronic devices used such as the amplifiers, oscillators, function generator, attenuators and transient recorder. The signal to noise ratio of the waveforms measured is also important although large improvements were obtained by signal averaging over many pulses (usually 1024). The effects of instrumentation error were reduced by maintaining the same instrument settings and performing insertion loss measurements as quickly as possible.

The digitisation process could also be a source of error. An 8-bit transient recorder was used leading to a digitisation error of 1:256 (0.4%) which is insignificant for full scale signal but can become significant for smaller signals. The use of signal averaging reduces this digitisation error provided there is noise present on the signal.

7.3.2 MULTIPLE REFLECTIONS

The limited size of the tube and the test panel as well as the presence of a hydrophone and an acoustic filter in the tube leads to the possibility of multiply reflected waves reaching the receiver within the recording time window. The most significant reflected wave contribution is due to difference frequency waves bouncing off the tube wall once on their way to the receiver. The estimation and elimination of this reflection has been

a main concern of this work. Other possible sources of multiple reflections shall now be considered:

(a) An additional reflection that may cause an arrival within the time window of interest occurs at the water-air interface at the top of the tube. Although this contribution may become very large, it can easily be kept outside the recording time window by adjusting the trigger delay between the transmitting and receiving electronics and keeping the tube topped-up with water in order to keep this arrival outside the time window of interest.

(b) Ideally, measurements should be made with a hydrophone that does not influence the acoustic field. In practice, There are two effects possible: (i) waves incident on the receiver may be reflected by it and then received after reflection from the test panel, and (ii) waves incident on the receiver are coupled into its mounting structure and propagate along it until they encounter a discontinuity where a reflection may occur and reach the hydrophone. In the former case, the hydrophone - test panel - hydrophone reflected wave strength may be reduced by increasing their separation and thus increasing the spherical spreading loss of this wave. The significance of this contribution also depends on the reflectivity of the test panel and the relative phase of the reflected and direct waves. In the later case, we can reduce reflections occurring in the hydrophone mounting rod by making it as long as possible and introducing few holes and slots into it. The effect of the rest of the hydrophone mounting structure is also minimal. The complexity of the mounting structure used in the tube did not allow a simple theoretical estimate to be made of the frequency response of the mounting structure. Unfortunately, the special mounting arrangement had to be modified to allow free field measurements to be made in a tank. Some results where, however, obtained in a tank with the hydrophone mounted vertically through a stainless steel tube and horizontally in a similar manner as in the tube. The aim of this measurement was to establish whether the hydrophone mounting used in the tube has any resonances in the frequency range of interest. It was found that the frequency response in the horizontal mounting position was flat compared to that in

the vertical position indicating that there were no adverse resonance effects peculiar to the new mounting arrangement. Previous results suggest [88] that the effects of the hydrophone mounting, for vertically mounted hydrophones, are minimal over the frequency range of interest.

(c) Potentially troublesome multiple reflections occur when the waves are reflected by the test panel and follow the path: test panel - acoustic filter - test panel - hydrophone. The significance of this contribution depends on the reflectivity of the test panel and that of the acoustic filter as well as their separation which controls the amount of spherical spreading suffered by the wave. The controlling factor is the reflection coefficient of the acoustic filter which is very low at all frequencies of interest. The effect of this multiple reflection became clear when insertion loss measurements were attempted at a hydrophone range R=70cm with a parametric array L=52cm long and the test panel 10cm in front of the hydrophone (see preceding section). Although this effect is small it does lead to the introduction of some ripple on the insertion loss curve which may be reduced by increasing the filter - test panel separation. The actual magnitude of this effect depends on the relative phase of the multiple reflection and the direct wave at the receiver at each frequency. Overall, this effect is smaller than 1dB.

7.3.3 EDGE DIFFRACTION

The aim of this project was to design a tube based system for the measurement of acoustical properties of limited size panels without significant errors due to edge diffraction. The fact that the test panel must be cut into a circular shape to maximise its area is an added complication as this shape maximises the diffracted wave on axis. It is clear that the diffracted wave is minimised by increasing the sample size and/or reducing the interrogating beam cross-section. The former is not possible beyond the dimensions of the tube and the latter was addressed by the use of a parametric array source rather than a conventional one.

those waves travel until they are attenuated by losses in the plate or re-radiated into the water. For a finite plate, however, those components may be reflected or re-radiated by the panel edge. The presence of obliquely incident waves due to tube wall reflections seems to accentuate this problem. It is thought that the problems in the measurement of the insertion loss of the aluminium panel arise due to a combination of diffracted waves around the panel and re-radiation from waves travelling across the plate. Overall, it seems that effects due to the finite test panel size are less significant when absorbing panels are tested.

7.4 SUMMARY

In this chapter experimental insertion loss measurements at normal incidence have been presented for an acoustically hard and an acoustically soft test panel under free-field conditions and in the tube. Comparative experimental results were thus obtained and, where possible, compared with a theoretical insertion loss estimate. In general, axial measurements in the tube were not sufficient for accurate insertion loss estimation for either sample. Spatial averaging of the field at the receiver provided a good rejection of the off-axis reflected wave arrivals and enabled an accurate insertion loss estimation to be made possible.

The most significant factors affecting the accuracy of the tube results have been discussed. It turns out that experimental measurements on rigid samples with significant insertion loss at normal incidence are harder than those performed on acoustically soft panels. That is mainly due to effects associated with the finite panel size, i.e. diffraction around the panel and waves coupled into the panel travelling radially towards the edge and continually re-radiating into the water.

The overall accuracy of the insertion loss estimates obtained with the tube for a soft panel were quite satisfactory and always within 1dB of the free field experimental result

which was itself subject to a 1dB uncertainty. Insertion loss estimates obtained for a hard panel (practically a worst case sample) were not quite as good and were only to within 3dB of the theoretical and free field experimental estimates.

8 DISCUSSION AND CONCLUSIONS

A considerable research effort has gone into the development of systems that enable underwater acoustical measurements to be made on samples of limited size. The design of these systems is mainly determined by the acoustical frequency of interest, which determines the overall size of the facility, and by the need to perform these measurements in ambient conditions or under hydrostatic pressure.

When the measurements are to be performed over a wide frequency range under ambient pressure, a rectangular tank is usually employed with a variety of transmitters at the frequencies of interest or, more recently, with a parametric acoustic source producing a continuous bandlimited wave at the frequencies of interest. These facilities are large enough to allow reflections from the tank walls to be gated out of the recorded waveforms.

Large tank facilities have also been built that allow measurements under hydrostatic pressure but these systems are not very practical or economical. For frequencies up to a few kHz measurements are performed in tubes known as impedance or pulse tubes. Their operation relies on the principle that when the tube diameter is small compared to the wavelength of the acoustic wave, only plane wave propagation is possible in the tube. These instruments are quite useful but can be limited in the frequency range that can be covered and are only practical at low frequencies; at the frequencies of interest here we would need several impedance tubes to cover the whole spectrum. In addition, the test panel would have to be cut in order to fit inside the impedance tubes and this may not give results representative of the whole sample.

It is thus obvious that a system that can combine the advantages of the two designs would be the best solution to the problem of acoustical testing of limited size panels under high hydrostatic pressure.

This thesis has described the theoretical and experimental development of a facility built around a wide bore tube (50 cm outside diameter) for performing acoustical measurements on limited size panels over the frequency range of 10-50kHz. At these frequencies single mode propagation is no longer possible and the wavefield in the tube assumes a complicated structure making it harder to estimate the strength of the acoustic field anywhere inside the tube.

8.1 REVIEW OF THE PRESENT WORK

This thesis has roughly followed the actual development of the project from the initial stages of building the system to the final testing of the material properties of actual samples in the tube.

The work will now be summarily reviewed in order to enable general conclusions to be drawn and in order to identify areas for future work.

The literature review concentrated on two areas of interest: (a) the development of parametric arrays, and (b) the use of tubes for material characterisation. The review of the parametric array indicated its advantages as a tool for acoustical measurements. The different modes of operation of the parametric array were identified and it was concluded that, for the present application, it was most appropriate to use a truncated, transient parametric array. The transient array generates a wideband beam with low sidelobe level and narrow beamwidth. By truncating it we obtain a source-free region in which the test panel can inserted.

The review of the literature on the use of tubes for material characterisation indicated that although they are very convenient for single frequency measurements on small test samples, no system is currently in use that is capable of wideband testing of larger panels.

The experimental system which is built around a plastic tube 2m high, with 50cm outside diameter and 2cm wall thickness was then described (chapter 3). The height and material of the tube were chosen for convenience. A system expected to operate under hydrostatic pressure would have to be built out of stainless steel with extra provisions to allow pressurisation and prevent water leakage. The tube could be made shorter with a suitable termination to avoid end reflections. The other characteristics of the experimental system, including the transmitting and receiving transducers and associated electronics have also been described. A discussion of the experimental procedures included an investigation into the optimum operating positions for the acoustic filter, test panel and hydrophone.

Preliminary experimental measurements performed in the tube without a test panel indicated the strong influence the waves reflected from the tube wall would have at the receiver. This was initially surprising in view of the narrow beamwidth that characterises the parametric array.

Theoretical models of various degrees of complexity were then developed for describing the propagation of the difference frequency waves inside the tube, retaining only the single bounce and direct wave contributions. The resulting integral equations could not be solved analytically and various approximations were made in order to obtain numerical or analytic results for the normalised reflected wave spectrum at an axial point receiver. The most important approximation that had to be made concerned the distribution of the difference frequency sources within the interaction volume. Three models have been considered here: (1) the line array model which considers the difference frequency sources to be uniformly distributed along the axis of the primary frequency transmitter, (2) the uniform cylindrical array model and (3) a model that takes the primary field structure into account in the difference frequency source distribution. The line array model is not suitable for the present application

since it overestimates the strength of the reflected wave due to the focussing effect of the tube wall. The uniform cylindrical array model provides accurate results quickly whereas the most rigourous model gives the best fit with experimental results.

These theoretical results confirmed the experimental observations and suggested that problems can arise due to reflections from the tube wall. In order to overcome this problem we have to: (a) reduce the sensitivity of the receiver to off axis arrivals without affecting its response to the direct wave, and (b) reduce the reflection coefficient of the tube wall by coating it with a wideband absorber. The second suggestion was pursued with limited success due to the difficulty in obtaining a wideband absorber with optimum operation at non-normal incidence. In order to reduce the sensitivity of the receiver to off-axis waves, synthetic aperture techniques were used. This method is commonly applied to planar wavefield situations but these results cannot be applied directly to measurements inside the tube. It turns out that simple uniform line weighting or circular area weighting across the synthesized aperture give better results than the Chebyshev weighting schemes commonly employed elsewhere. Experimental results seem to confirm theoretical predictions and offer a dramatic reduction in the strength of the reflected wave.

The reduction of the reflected wave obtained with spatial averaging enables experimental measurements of the insertion loss of limited size panels to be performed with good accuracy. The insertion loss of an acoustically soft panel was measured to within 1dB of the free-field measurement which is free from reflection and diffraction effects. The insertion loss estimate for an acoustically hard test panel was found to be less accurate due to more pronounced diffraction around the sample, coupling into and reradiation from the panel and reduced insertion loss at non-normal

incidence (sample-specific). In this case, when spatial averaging was performed, the insertion loss could be measured to within 3dB of the theoretical and free-field experimental values.

8.2 SUGGESTIONS FOR FUTURE WORK

It is apparent that only through the use of receiving aperture synthesis was it possible to perform insertion loss measurements in the tube. The use of a single, large area, wideband receiver would simplify the experimental system even further by doing away with the need of sampling the field at various positions and subsequent signal processing. For this purpose a large area receiver of arbitrary shape could be constructed out of a PVdF (PolyVinilidine Fluoride) piezoelectric film.

More work may also need to be done on the development of an absorber specifically designed for the present application. This is not a minimal task since we require wideband absorption at shallow angles of incidence. The thickness of the material must also be kept within reasonable limits. Non-normal incidence would probably necessitate the use of a wedged profile absorber which improves the coupling of the wave into the absorber but reduces the amount of material in which attenuation actually occurs.

If a system is actually required to perform at high hydrostatic pressures, a suitable vessel must be built capable of withstanding those pressures. It may be convenient to reduce the overall height of the tube, within the constraints set out in chapter 3, and place an absorber at the top end of the tube to avoid the return of the direct axial wave via a reflection at that end. This will lead to a compact system that will be capable of going through the process of mounting the panel, pressurising, performing the measurements, depressurising cycle much faster than with an equivalent large tank facility.

A sheet of neoprene rubber was used to line the inside surface of the tube wall to provide a reflecting interface and avoid coupling of the incident waves into the tube wall material. It is well known that pressure release materials such as the neoprene rubber used in the present work loose their properties at high hydrostatic pressure. Thus in a pressurised system, the inner tube walls would have to be coated with an absorbing material such as that described in chapter 6 or an absorber specifically designed for this application. This does not represent a prohibitive deviation from the current experimental conditions since the neoprene rubber used here was employed in order to inhibit coupling of the incident wave into the tube wall and also enable theoretical modelling without the added complication of tube wall effects.

8.3 FINAL COMMENT

A system has been developed here that enables insertion loss measurements to be performed on limited size panels. A small vessel is employed and a wideband parametric source is used to produce the probing waves. This system offers increased practicality in terms of cost and speed of use and it would be possible to incorporate it in a production line for quality control purposes. When rubber based samples are tested, the accuracy of the measurement can be better than 1dB whereas when a 'worst' case sample is tested it is possible to measure insertion loss to within 3dB.

9 REFERENCES

1) Lamb H., 'The dynamical theory of sound', London, Dover, New York, 1960

2) Strutt J.W. Lord Rayleigh, 'The theory of sound', Dover, 1945, 2nd edn.

3) Westervelt P.J., 'Parametric end-fire array', J. Acoust. Soc. Am., 32, 8, 1960

4) Westervelt P.J., 'Parametric acoustic array', J. Acoust. Soc. Am., 35, 535, 1963

5) Lighthill M.J., 'On sound generated aerodynamically. I:general theory', Proc. Roy. Soc. (London) 211A,p. 564, 1952

6) Lighthill M.J., 'On sound generated aerodynamically. II: turbulence as a source of sound', Proc. Roy. Soc. (London) 222A, p. 1, 1954

7) Lighthill M.J., Math. Revs., 19, 915, 1958. This is a review comment by M.J. Lighthill on: 'Scattering of sound by sound' by Westervelt P.J., J. Acoust. Soc. Am., 29, 199, 1957. The reviewer suggested the investigation of the scattered field in the region where the primary frequency wavefield is negligible.

8) Bellin J.L.S. And Beyer R.T., 'Experimental investigation of and end-fire array', J. Acoust. Soc. Am., 34(9), 1051-4, 1962

9) Zverev V.A. and Kalachev A.I., 'Measurement of the scattering of sound by sound in the superposition of two sound beams', Soviet Physics-Acoustics, 14, 173-8, 1968

10) Berktay H.O., 'Nonlinear interaction of two sound beams', J. Acoust. Soc. Am., 38, 480-1(L), 1965

11) Berktay H.O., 'Possible exploitation of nonlinear acoustics in underwater transmitting applications', J. Sound Vib., 2(4), 435-61, 1965

12) Berktay H.O. and Smith B.V., ' End-fire array of virtual sound sources arising from the interaction of sound waves', Elect. Lett., 1, 6, 1965

13) Naze J. and Tjotta S., 'Nonlinear interaction of two sound beams', J. Acoust. Soc. Am., 37, 174-75(L), 1965

14) Hobaek H., 'Experimental investigation of an acoustic end-fire array', J. Sound Vib., 6(3), 460-3, 1967

15) Naugol'nykh K.A., Soluyan S.I., and Khokhlov R.V., 'Nonlinear interaction of sound waves in an absorbing medium', Soviet Physics-Acoustics, 9, 155, 1963

16) Muir T.G. and Blue J.E., 'Experiments on the acoustic modulation of large-amplitude waves', J. Acoust. Soc. Am., 46(1), 227-32, 1969

17) Berktay H.O., 'Near-field effects in parametric end-fire arrays', J. Sound Vib., 20(2), 135-43, 1972

18) Berktay H.O. and Shooter J.A., 'Near-field effects in end-fire line arrays', J. Acoust. Soc. Am., 53(2), 550-6, 1973

19) Beyer R.T., Nonlinear Acoustics, Naval Ships Systems Command, 1974

20) Novikov B.K., Rudenko O.V. and Timoshenko V.I., Nonlinear Underwater Acoustics, American Institute of Physics (Translation for the Acoustical Society of America), 1987

21) Berktay H.O., 'Finite amplitude effects in acoustic propagation in fluids', New directions in Physical Acoustics, Soc. Italiana di Fisica, Bologna, Italy, p.369-408, 1976

22) Bartram J.F., 'A useful analytical model for the parametric acoustic array', J. Acoust. Soc. Am. , 52(3), 1042-4(L), 1972

23) Bartram J.B. and Westervelt P.J., 'Nonlinear attenuation and the parametric array', Program of the 83rd Meeting of the Acoustical Society of America, (abstracts only), p.28-9, 1972

24) Berktay H.O., 'Some finite amplitude effects in underwater acoustics', In Nonlinear Acoustics, Proceedings of the 1969 Symposium held at the Applied Research Laboratories, The University of Texas at Austin, (1970), p. 31-55

25) Muir T.G., 'An analysis of the parametric acoustic array for spherical wavefields', Report no. ARL-TR-71-1, The University of Texas at Austin, (May 1971)

26) Fenlon F.H., 'On the performance of a dual frequency parametric source via matched asymptotic solutions of Burgers' equations', J. Acoust. Soc. Am., 55, 35-46, 1974

27) Fenlon F.H., 'Approximate methods for predicting the performance of parametric sources at high acoustic Reynolds numbers', In L. Bjorno, (ed.), Finite Amplitude Wave Effects In Fluids, Technology Press Ltd, Guildford,(1974), p.160-7

28) Childs D.R., 'Beam pattern and directivity indices of parametric acoustic arrays', ibid, pp.156-9

29) Mellen R.H., Browning D.G. and Konrad W.L., 'Parametric sonar transmitting array measurements', Presented at the 80th Meeting of the Acoustical Society of America, Houston, Texas (1970)

30) Safar M.H., 'Propagation of acoustic waves of finite amplitude in water containing air bubbles',, In L. Bjorno (ed.), Finite Amplitude Wave Effects In Fluids, Proceedings of the 1973 Symposium, IPC Science & Technology Press, Guildford (1974), p 174-9

31) Bjorno L., Christoffersen B., Schreider M.P., 'Some experimental investigations of the parametric acoustic array', Acustica, 35(2), 99-106, 1976

32) Ryder J.D., Rogers P.H. and Jarzyncki J., 'Radiation of difference frequency sound generated by nonlinear interaction in a silicone rubber cylinder', J. Acoust. Soc. Am. , 59(5), 1077-86, 1976

33) Jongens A.W.D., 'Application of an enhanced parametric source', Ultrasonics International, 1987, Conference Proceedings, p.190-6

34) Woodsum H.C., 'Enhancement of parametric efficiency by saturation suppression', J. Sound Vib., 69(1), 27-33, 1980

35) Lockwood J.C. and Smith D.P., 'Investigation of the increase in parametric efficiency due to bubbles', AMETEK, Straza Division, Technical report No11, 1354e-74-1, 30 August 1974

36) Moffet M.B., Westervelt P.J. and Beyer R.T., Large-amplitude pulse propagation-A transient effect', J. Acoust. Soc. Am., 47(5), 1473-4(L), 1969

37) Moffet M.B., Westervelt P.J. and Beyer R.T., 'Large-amplitude pulse propagation-A transient effect II', J. Acoust. Soc. Am., 49(1), 339-43, 1971

38) Moffet M.B. and Mellen P. 'Parametric acoustic sources of transient signals', J. Acoust. Soc. Am., 66, 1182-7, 1979

39) Trivett D.H. and Rogers P.H., Pulsed parametric array', J. Acoust. Soc. Am.,, 76, 1919-22, 1984

40) Pace N.G. and Ceen R.V., 'Time study of the terminated transient parametric array', J. Acoust. Soc. Am., 73,1972-78, 1983

41) Stepanishen P.R. and Koenings P., A time formulation of the absorption limited transient parametric array', J. Acoust. Soc. Am., 82(2), 629-34, 1987

42) Nicholls B.H., 'Recent approaches to the measurement of acoustic impedance and materials characterisation', Ultrasonics, 18(2), 71-5, 1980

43) Grinberg I.E., Novikov B.K. and Timoshenko V.I., 'Parametric acoustic array in the self-demodulation regime', Soviet Physics-Acoustics, 30(2), 118-20, 1985

44) Humphrey V.F. and Berktay H.O., 'The transmission coefficient of a panel measured with a parametric source', J. Sound Vib., 101(1), 85-106, 1985

45) Humphrey V.F., Murphy C. and Moustafa A.H.A., 'Wideband back-scattering measurements using a parametric array', Ultrasonics International '87, Conference Proceedings, Butterworth Scientific Ltd, 1987, pp. 265-71

46) Humphrey V.F., 'The influence of the plane wave spectrum of a source on measurements of the transmission coefficient of a panel', J. Sound Vib., 108(2),261-72, 1986

47) Thorne P.D., 'A broad-band acoustic source for underwater laboratory applications', IEEE Trans. Son. Ultrason. Ferroelectrics and Frequency control, vol.UFFC-34, no.5, 515-23, 1987

48) Berktay H.O., 'Some proposals for underwater transmitting applications of nonlinear acoustics', J. Sound Vib., 6(2), 244-54, 1967

49) Bjorno L., 'Underwater applications of nonlinear ultrasound', Ultrasonics International '75, Conference Proceedings, pp. 238-44, 1975

50) Bjorno L., 'Parametric acoustic arrays', in 'Aspects of Signal Processing', Tacconi G. (ed), Part 1, pp.33-59, D. Reidel Publishing Company, Dordrecht-Holland, 1977

51) Bjorno L., 'Nonlinear interaction of finite amplitude sound waves', Special course on acoustic wave propagation, Report no. AGARD-R-686, pp. 17/1-17/10, August 1979

52) Timoshenko V.I., 'Applications of parametric arrays in oceanographic research', Soviet Physics-Acoustics, 27(3), 263-4, 1981

53) Konrad W.L., 'Applications of the parametric acoustic source', Proceedings of the Institute of acoustics, article 1.1, Sep. 1979

54) Bjorno L. and Grindester S., 'Parametric echoscanner for medical diagnosis', J. Phys. Colloq. (France), 41(C-8), C8/11-18,1979

55) Fenlon F.H., 'Recursive procedure for computing the nonlinear spectral interactions of progressive finite-amplitude waves in non-dispersive fluids', J. Acoust. Soc. Am., 50(5), 1299-1312, 1971

56) Muir T.G. and Willette I.G., 'Parametric acoustic transmitting arrays', J. Acoust. Soc. Am., 52(5), 1481-6, 1972

57) Berktay H.O. and Leahy D.J., 'Farfield performance of parametric transmitters', J. Acoust. Soc. Am., 55(3) 539-46, 1974

58) Moffett M.B. and Mellen R.H., 'Model for parametric acoustic sources', J. Acoust. Soc. Am., 61(3) 325-37, 1977

59) Moffett M.B. and Mellen R.H., 'A numerical model for calculating the nearfield of a parametric acoustic source', J. Acoust. Soc. Am., 63, 1622-4, 1978

60) Mellen R.H. and Moffett M.B., 'A numerical model of the parametric radiator', Proc. Inst. Acoust., 1979, 4.3/1-5

61) Moffett M.B. and Mellen R.H., 'Effective lengths of parametric acoustic sources', J. Acoust. Soc. Am., 70(5), 1424-6, 1981

62) Naze-Tjotta J. and Tjotta S., 'Nonlinear equations of acoustics with application to parametric arrays', J. Acoust. Soc. Am., 69(6), 1644-52, 1981

63) Garrett G.S., Naze-Tjotta J. and Tjotta S., 'Nearfield of a large acoustic transducer, Part II: Parametric radiation', J. Acoust. Soc. Am., 74(3), 1013-20, 1983

64) Garrett G.S., Naze-Tjotta J. and Tjotta S., 'Nearfield of a large transducer, Part III: General results', J. Acoust. Soc. Am., 75, 769-79, 1984

65) Aanonsen S.I., Barkve T., Naze-Tjotta J. and Tjotta S., 'Distortion and harmonic generation in the nearfield of a directive sound source', J. Acoust. Soc. Am., 78, 202-16, 1985

66) Foda M.A. and Ginsberg J.H., 'Finite amplitude effects in a dual frequency acoustic beam', J. Acoust. Soc. Am., 85(5)m1857-71, 1989

67) Brekhovskikh L.M., 'Waves in Layered Media', Academic Press, London, 1980, 2nd edition.

68) Bobber R.J., 'Underwater Electroacoustic Measurements', US GPO, Washington DC, pp.287-97, 1970

69) Cook R.L. and Lovejoy R.E., 'Acoustic properties of epoxy-fiberglass and epoxy-fiberglass-Pb plates in the frequency range 100-700KHz', J. Acoust. Soc. Am., 57, 1554-8, 1975

70) Barnard G.R., Bardin J.L. and Whiteley J.W., 'Acoustic reflection and transmission characteristics fro thin plates', J. Acoust. Soc. Am., 57, 577-84, 1975

71) Mikeska E.E. and Behrens J.A., 'Evaluation of transducer window materials', J. Acoust. Soc. Am., 59, 1294-8, 1976

72) Humphrey V.F., 'The measurement of acoustic properties of limited size panels by use of a parametric source', J. Sound Vib., 98(1), 67-81, 1985

73) Kinsler L.E. and Frey A.R., Fundamentals of acoustics, John Wiley and Sons Inc, 2nd edition, 1962, pp.166-183

74) Kundt , Pogg. Ann. t., cxxxv, p.337, 1868, cited in: The Theory of Sound, J.W.Strutt Lord Rayleigh, vol. II, p.57, 2nd edn.

75) Taylor H.O., 'A direct method of finding the value of materials as sound absorbers', Physics Rev., 2, pp.270-87, 1913

76) Sabine H.J., 'Notes on acoustic impedance measurement', J. Acoust. Soc. Am., 14, 143-50, 1942

77) Beranek L.L., 'Some notes on the measurement of acoustic impedance', J. Acoust. Soc. Am., 19, 420-7, 1947

78) Beranek L.L., 'Acoustic Measurements', New York: John Wiley & Son Inc, 1949

79) Melling T.H., 'An impedance tube for precision measurement of acoustic impedance and insertion loss at high sound pressure levels', J. Sound Vib., 28(1),23-54, 1973

80) Brouns A.J., 'Plane-wave tube for low-audio frequency and infrasonic acoustic measurements', J. Acoust. Soc. Am., 47(4), 1145-9, 1970

81) Sabin G.A., 'Acoustic impedance measurements at high hydrostatic pressures', J. Acoust. Soc. Am., 40(6), 1345-53, 1966

82) Born M. and Wolf E., Principles of Optics, 6th edition, 1980, Pergamon Press

83) Abramowitz M. and Stegun I. (editors), Handbook of Mathematical Functions, Dover Publications Inc, 1972

84) Zemanek J., 'Beam behaviour within the nearfield of a vibrating piston', J. Acoust. Soc. Am., 49(1), 181-191, 1971

85) Gitis M. B. and Khimunin A. S., 'Diffraction effects in ultrasonic measurements', Soviet Physics-Acoustics, 14(4), 413-431, 1969

86) Harris G. R., 'Review of transient field theory for a baffled planar piston', J. Acoust. Soc. Am., 70(1), 10-20, 1981

87) Lancaster M., 'The finite amplitude field of a circular piston', PhD Thesis, University of Bath, 1983

88) Humphrey V.F., 'The measurement of acoustic properties of specimens of limited size by use of a parametric source', Internal Report, School of Physics, University of Bath, April 1983.

89) Humphrey, V.F., and Hsu, C.H., Nonlinearity of cylindrical hydrophones used for the measurement of parametric arrays', Proceedings of the Conference on Transducers for Sonar Applications, University of Birmingham, 1980

90) Moffet, M.B. and Henriquez, T.A., 'Hydrophone nonlinearity measurements', J. Acoust. Soc. Am., 72, 1-6, 1982

91) Ryle M. and Hewish A., 'The synthesis of large radio telescopes', Monthly Nat. Roy. Astronom. Soc., Vol. 120, No. 3 , 220-230, 1960

92) Fitch J.P., Burrus C.S. (eds), 'Synthetic aperture radar', Springer-Verlag, 1988

93) Gough P.T. and Hayes M.P., 'Test results using a prototype synthetic aperture sonar', J. Acoust. Soc. Am. , 86(6), 2328-33, 1989

94) Griffiths J.W.R. and Gida A.S., 'Use of a microcomputer for synthetic aperture measurements', Proc. I.O.A., Vol. 6 , Part 5, 122-128, 1984

95) Weeks W.L., 'Antenna engineering', McGraw-Hill, 1968

96) Steinberg B.D., 'Principles of aperture and array design', John Wiley & Sons, 1976

97) Schelkunoff S.A. and Friis H.T., 'Antennas: Theory and practise', John Wiley & Sons, 1952

98) Hansen R.C., 'The handbook of antenna design', vol2, A.W.Rudge, K.Milne, A. D. Olver, P. Knight (eds), London, Peregrinus on behalf of the IEE, 1982 (IEE series on electromagnetic waves).

99) Schelkunoff S.A., 'A mathematical theory of linear arrays', Bell System Technical Journal, 22,80-107, 1943

100) Dolph C.L., 'A current distribution for broadside arrays which optimises the relationship between beamwidth and side lobe level', Proc., IRE, 34, 335-348, 1946

101) Riblet H.L., 'Discussion on "A current distribution ..." by C. L. Dolph', Proc. IRE, 35,489-492, 1947

102) Pritchard R.L., Optimum directivity patterns for linear point arrays', J. Acoust. Soc. Am., 25(5), 879-891, 1953

103) Kaye G.W.C. and Laby T.H., 'Tables of physical and chemical constants', 15th edition, Longman London New York, 1986

10 APPENDIX A

THE PLANE WAVE SPECTRUM OF A TRUNCATED COLUMN PARAMETRIC ARRAY

In the near field of a circular transducer of radius a, the primary fields can be considered to be collimated plane waves. If the parametric array is terminated at a range L within the nearfield of the transducer, then the secondary source volume can be modelled as a cylinder of radius a and length L along the axis of the transmitting transducer. The individual sources have a strength proportional to the product of the primary pressures, so the source strength is constant over the source volume.

If the transverse dimension of the parametric array is small compared to the difference frequency wavelength, the column array may be substituted by a line array of sources distributed along the acoustic axis.

Analytic results for the nearfield of the column and the line array cannot be obtained (see Theory, chapter 4) so the two models are compared in terms of their plane wave spectra.

The plane wave (or angular) spectrum of a source is a concept similar to the Fourier spectrum of a signal in the frequency domain. The wavefield is decomposed into a set of plane waves of different amplitudes and phases which, when recombined, can reconstruct the original wavefield [67].

In order to find the plane wave spectrum of the truncated uniform column parametric array consider figure 4.1. We assume planar primary waves confined within a cylinder of radius a, that of the transducer, extending from z=0 to the truncation distance z=L.

The primary waves are of the form:

$$p_{1,2}(\underline{r}) = P_{1,2}e^{j(K_{1,2}z - \omega_{1,2}t)}, \qquad \ldots(A1)$$

the secondary source strength is thus given by:

$$Q(\underline{r}) = -\frac{jk\beta}{\rho_o^2 c_o^3} p_1(\underline{r}) p_2^*(\underline{r}) \qquad \ldots(A2)$$

where the star denotes a complex conjugate and $k=K_1-K_2$ with the rest of the parameters previously defined.

The difference frequency pressure at $\underline{R}$ can be written as:

$$p(\underline{R}) = -\frac{j\omega\rho_o}{4\pi} \int \int \int_{source volume} Q(\underline{r}) \frac{e^{jks}}{s} dV. \qquad \ldots(A3)$$

Using the plane wave expansion of the spherical wave term [67]:

$$\frac{e^{jks}}{s} = \frac{j}{2\pi} \int \int_{-\infty}^{+\infty} e^{j\underline{k}(\underline{R}-\underline{r})} \frac{dk_x dk_y}{k_z} \qquad \ldots(A4)$$

where (k_x,k_y,k_z) are the components of $\underline{K}$, we can write :

$$p(\underline{R}) = \frac{j}{2\pi} \int \int_{-\infty}^{+\infty} e^{j\underline{k}.\underline{R}} \frac{dk_x dk_y}{k_z} \Lambda(\underline{k}) \qquad \ldots(A5)$$

where $\Lambda(\underline{k})$ is the plane wave spectrum of the parametric array, which can be identified as:

$$\Lambda(\underline{k}) = -\frac{k^2\beta}{4\pi\rho_o c_o^2} \int \int \int p_1(\underline{r}) p_2^*(\underline{r}) e^{-j\underline{k}.\underline{r}} dV. \qquad \ldots(A6)$$

It is more convenient, in view of the geometry of the source volume, to evaluate the volume integral in cylindrical coordinates (z, ρ, γ):

$$\sqrt{x^2+y^2}=\rho;\quad x=\rho\cos\gamma;\quad y=\rho\sin\gamma$$

$$k_r=\sqrt{k_x^2+k_y^2};\quad k_x=k_r\cos\phi;\quad k_y=k_r\sin\phi$$

$$\therefore \underline{k}.\underline{r}=k_r\rho\cos(\phi-\gamma)+k_z z \qquad \ldots(A7)$$

$$\text{and } dV=\rho d\rho d\gamma dz \qquad \ldots(A8)$$

Further, for the primary fields given by equation (A1):

$$p_1(\underline{r})p_2^*(\underline{r})=P_1P_2e^{jkz}. \qquad \ldots(A9)$$

Thus, using equations (A6)-(A9) we get:

$$\Lambda(\underline{k})=-\frac{k^2\beta P_1P_2}{4\pi\rho_o c_o^2}\int_0^L\int_0^{2\pi}\int_0^a e^{j(k-k_z)z}e^{-jkr\rho\cos(\phi-\gamma)}\rho d\rho d\gamma dz \qquad \ldots(A10)$$

after performing the γ integral:

$$\Lambda(\underline{k})=-\frac{k^2\beta P_1P_2}{2\rho_o c_o^2}\int_0^L\int_0^a e^{j(k-k_z)z}J_o(k_r\rho)\,\rho d\rho dz \qquad \ldots(A11)$$

$$\Lambda(\underline{k})=-\frac{k^2\beta P_1P_2}{2\rho_o c_o^2}a\frac{J_1(k_r a)}{k_r}\frac{e^{jkL(1-\cos\theta)}-1}{jk(1-\cos\theta)}. \qquad \ldots(A12)$$

Humphrey and Berktay [44] have performed a similar calculation to find the plane wave spectrum of a line array. They derived the following expression for the plane wave spectrum of the line array:

$$\Lambda_{line}(\underline{k})=-\frac{k^2\beta P_1P_2}{4\pi\rho_o c_o^2}\frac{e^{jkL(1-\cos\theta)}-1}{jk(1-\cos\theta)}. \qquad \ldots(A13)$$

The difference frequency field at a point ($\underline{R}$) can now be evaluated using equation (A5).

A comparison of equations (A12) and (A13) shows that the angular dependence of the plane-wave spectrum of the uniform column parametric array consists of the product of a transverse aperture function

$$\pi a^2\frac{2J_1(k_r a)}{k_r a}=\pi a^2\frac{2J_1(ka\sin\theta)}{ka\sin\theta} \qquad \ldots(A14)$$

and that due to a line array.

The contribution of the transverse aperture factor (A14) becomes more significant when a/λ is a large fraction (i.e. ka is large) and when θ is large. The second condition is not very significant since the line array plane wave spectrum at large θ becomes very small. Thus, if the cross-sectional area of the parametric array is relatively small, the line array model should be adequate. Experimental results show [44] that this is a valid approximation near the axis of the array although the beamwidth of the array is slightly overestimated.

11 APPENDIX B

THE PRESSURE AT AN AXIAL POINT RECEIVER DUE TO A POINT SOURCE A SMALL DISTANCE OFF AXIS

Consider figure 4.2. A point source S is located a small distance y off-axis. Using the notation of figure 4.2, we can write down the field at an axial point receiver at P as (equation (8) in the theory section):

$$p = -\frac{j\rho_o ckQ(S)}{2\pi} e^{j\pi} \int_0^{2\pi} \int_{-\infty}^{+\infty} \frac{e^{jk(R_1+R_2)}}{R_1 R_2} \frac{(\sin\theta_1 + \sin\theta_2)}{2} b \cdot dz d\phi, \qquad \ldots(B1)$$

where

$$R_1 = (z^2 + y^2 + b^2 - 2by\cos\phi)^{\frac{1}{2}} \qquad \ldots(B2)$$

$$R_2 = ((s-z)^2 + b^2)^{\frac{1}{2}}.$$

We can write:

$$R_1 = (z^2 + (b-y)^2 + 2by(1-\cos\phi))^{\frac{1}{2}} \qquad \ldots(B3A)$$

$$= (z^2 + (b+y)^2 - 2by(1+\cos\phi))^{\frac{1}{2}}; \qquad \ldots(B3B)$$

Let

$$R_1' = (z^2 + (b-y)^2)^{\frac{1}{2}} \qquad \ldots(B4A)$$

$$R_1'' = (z^2 + (b+y)^2)^{\frac{1}{2}}, \qquad \ldots(B4B)$$

then, substituting equations (B4) into the corresponding equations (B3) and performing a binomial expansion of the resulting expressions for R_1 gives:

$$R_1 \approx R_1' + \frac{by}{R_1'}(1-\cos\phi) \qquad \ldots(B5A)$$

$$\approx R_1'' - \frac{by}{R_1''}(1+\cos\phi). \qquad \ldots(B5B)$$

For the binomial expansion to be valid we need:

$$by << R_1^2 \qquad \ldots(B6)$$

and for yb small and z ≈ b we can write:

$$by << 2b^2$$

$$\therefore y << 2b. \qquad \ldots(B7)$$

Also, in order to perform the integration over ϕ we split the range into two parts:

$$-\frac{\pi}{2} < \phi < \frac{\pi}{2} \quad \text{and} \quad \frac{\pi}{2} < \phi < \frac{3\pi}{2}; \qquad \ldots(B8)$$

in the latter range use

$$\phi = \pi + \gamma \quad \text{with} \quad -\frac{\pi}{2} < \gamma < \frac{\pi}{2} \qquad \ldots(B9)$$

$$\text{and} \quad \cos\phi = -\cos\gamma.$$

In addition, we can write:

$$\frac{1}{R_1} \approx \frac{1}{R_1'} \approx \frac{1}{R_1''} \qquad \ldots(B10)$$

in the appropriate ϕ ranges (equation (B8)).

Finally, for y small, it can be seen from figure 4.2 that:

$$\sin\theta_1 \approx \sin\theta_2 \approx \frac{b}{R_2}. \qquad \ldots(B11)$$

Thus, using equations (B5) and (B8-B11), the field at P (equation (B1)) can be written as:

$$p = -\frac{j\rho_o ckQb^2}{2\pi} e^{j\pi} \int_{-\infty}^{+\infty} \frac{e^{jkR_2}}{R_2^2} dz \left[\frac{e^{jkR_1'}}{R_1'} \int_{-\frac{\pi}{2}}^{\frac{\pi}{2}} e^{\frac{jkyb}{R_1'}(1-\cos\phi)} d\phi + \frac{e^{jkR_1''}}{R_1''} \int_{-\frac{\pi}{2}}^{\frac{\pi}{2}} e^{\frac{-jkyb}{R_1''}(1-\cos\gamma)} d\gamma \right] \quad ...(B12)$$

Using the following standard identity [83, p.360, lemma 9.1.21]:

$$\frac{1}{\pi} \int_{-\frac{\pi}{2}}^{\frac{\pi}{2}} e^{jz\cos\phi} d\phi = J_o(z) \quad ...(B13)$$

equation (B12) becomes:

$$p = -\frac{j\rho_o ckQb^2}{2} e^{j\pi} \int_{-\infty}^{+\infty} \frac{e^{jkR_2}}{R_2^2} dz \left[\frac{e^{jk\left(R_1' + \frac{yb}{R_1'}\right)}}{R_1'} J_o\left(\frac{kyb}{R_1'}\right) + \frac{e^{jk\left(R_1'' - \frac{yb}{R_1''}\right)}}{R_1''} J_o\left(\frac{kyb}{R_1''}\right) \right]. \quad ...(B14)$$

Now, using equations (B4) we can write:

$$R_1' + \frac{yb}{R_1'} = (z^2 + (b-y)^2)^{\frac{1}{2}} + \frac{yb}{(z^2 + (b-y)^2)^{\frac{1}{2}}}$$

$$\approx (z^2 + (b-y)^2 + 2yb)^{\frac{1}{2}} \quad ...(B15A)$$

$$\approx (z^2 + b^2 + y^2)^{\frac{1}{2}}.$$

Similarly

$$R_1'' - \frac{yb}{R_1''} \approx (z^2 + b^2 + y^2)^{\frac{1}{2}}. \quad ...(B15B)$$

Therefore, each integral in equation (B14) is of the form:

$$I = \int_{-\infty}^{+\infty} \mu(z) e^{jkf(z)} dz \quad ...(B16)$$

and provided k is large, it can be evaluated approximately using the method of stationary phase. The standard result of this method for equation (B16) is:

$$I \approx \mu(z_o) e^{jkf(z_o)} \sqrt{\frac{2\pi}{k\left|\left(\frac{\partial^2 f}{\partial z^2}\right)_{z_o}\right|}} \cdot e^{\pm j\frac{\pi}{4}} \quad ...(B17)$$

where z_o is the critical point at which:

$$\left(\frac{\partial f}{\partial z}\right)_{z=z_o} = 0 \qquad \ldots(B18)$$

and the sign of the exponential being that of the second derivative of f with respect to z.

Identifying the terms of equation (B14) in the form of equation (B16):

$$\mu(z) = \frac{J_o\left(\frac{kyb}{R_1'}\right)}{R_1' R_2^2} \qquad \ldots(B19A)$$

or

$$\mu(z) = \frac{J_o\left(\frac{kyb}{R_1''}\right)}{R_1'' R_2^2} \qquad \ldots(B19B)$$

and

$$f(z) = R_2 + (z^2 + b^2 + y^2)^{\frac{1}{2}} \qquad \ldots(B20)$$

$$\begin{aligned} \therefore \frac{\partial f}{\partial z} &= \frac{1}{2}((s-z)^2 + b^2)^{-\frac{1}{2}} 2(s-z)(-1) + \frac{1}{2}(z^2 + b^2 + y^2) - \frac{1}{2}2z \\ &= \frac{z-s}{((s-z)^2 + b^2)^{\frac{1}{2}}} + \frac{z}{(z^2 + b^2 + y^2)^{\frac{1}{2}}}. \qquad \ldots(B21) \end{aligned}$$

If we let

$$\frac{\partial f}{\partial z} = 0$$

then

$$\frac{s-z}{((s-z)^2 + b^2)^{\frac{1}{2}}} = \frac{z}{(z^2 + b^2 + y^2)^{\frac{1}{2}}}.$$

$$\therefore \quad z^2 \frac{y^2}{(b^2 + y^2)} - 2sz + s^2 = 0. \qquad \ldots(B22)$$

Equation (B22) is quadratic in z and the values of z that satisfy it are given by:

$$z = \frac{2s \pm \sqrt{4s^2 - 4s^2\left(\frac{y^2}{y^2+b^2}\right)}}{\frac{2y^2}{y^2+b^2}}.$$

$$\therefore \quad z = \frac{s(b^2+y^2)}{y^2}\left(1 \pm \sqrt{1 - \frac{y^2}{y^2+b^2}}\right). \qquad \ldots(B23)$$

Using a binomial expansion to approximate the value of the square root in equation (B23):

$$z = \frac{s(b^2+y^2)}{y^2}\left(1 \pm \left(1 - \frac{y^2}{2(y^2+b^2)} - \ldots\right)\right) \qquad \ldots(B24)$$

and taking the negative sign within the parentheses,

$$\text{for} \quad \frac{\partial f}{\partial z} = 0$$

$$z_o \approx \frac{s(b^2+y^2)}{y^2}\frac{y^2}{2(b^2+y^2)} \approx \frac{s}{2}. \qquad \ldots(B25)$$

That is, a critical point for the evaluation of equation (B14) lies at a point on the tube wall half way between the source and receiver. the positive sign is taken within the parentheses in (B24) then z turns out to be much larger than s for small y and as such, the spreading loss of the wave reflected by that point will diminish its contribution quite considerably.

Using equation (B21) we can now evaluate

$$\frac{\partial^2 f}{\partial z^2} = ((s-z)^2+b^2)^{-\frac{1}{2}} + (z-s)(z-s)((s-z)^2+b^2)^{-\frac{3}{2}}$$

$$+(z^2+b^2+y^2)^{-\frac{1}{2}} - 2z^2(z^2+b^2+y^2)^{-\frac{3}{2}} \qquad \ldots(B26)$$

When z=s/2 and $y^2 << b^2$:

$$\frac{\partial^2 f}{\partial z^2} \approx \frac{2b^2}{\left(\left(\frac{s}{2}\right)^2+b^2\right)^{\frac{3}{2}}} > 0 \qquad \ldots(B27)$$

Thus, using equation (B17) to solve (B14) and substituting the relevant expressions, after some manipulation we get the following expression for the field on axis due to a generalised point source at S:

$$p = \rho_o c Q(S) \sqrt{\pi k}\, b e^{j\frac{3\pi}{4}} \frac{e^{j2k\left(b^2+\left(\frac{s}{2}\right)^2\right)^{\frac{1}{2}}}}{\left(b^2+\left(\frac{s}{2}\right)^2\right)^{\frac{3}{4}}} J_o\left(\frac{kyb}{\sqrt{\left(\frac{s}{2}\right)^2+b^2}}\right). \qquad \ldots(B28)$$

12 APPENDIX C

STATIONARY PHASE POINT OF THE INTEGRAL IN EQUATION (4.23)

Here we investigate whether the integral in equation (4.23), that gives the normalised reflected wave at an axial point receiver, has a stationary phase point and where that point is.

We start with the expression for the normalised reflected wave at an axial point receiver due to a uniform cylindrical parametric array in the tube (equation (4.23)):

$$\Phi(R)=\frac{e^{j\frac{3\pi}{4}}}{\ln\left(\frac{R}{R-L}\right)}4\sqrt{\frac{\pi}{ka}}\int_{\frac{R-L}{2}}^{\frac{R}{2}}\frac{e^{j2k\left(\sqrt{b^2+t^2}-t\right)}}{(b^2+t^2)^{\frac{3}{4}}}J_1\left(\frac{kab}{\sqrt{b^2+t^2}}\right)dt \qquad \ldots(C1)$$

with $t=\frac{R-z}{2}$

Consider the integrand in equation (C1); if the argument of the J_1 function is large, asymptotically expanding it we get [83]:

$$J_1(z)=\frac{1}{2}\{H_1^{(1)}+H_1^{(2)}\}\approx$$

$$\frac{1}{\sqrt{2\pi z}}\left\{e^{j\left(z-\frac{3\pi}{4}\right)}+e^{-j\left(z-\frac{3\pi}{4}\right)}\right\}, \qquad \ldots(C2)$$

where $H_1^{(1)}$ and $H_1^{(2)}$ are Hankel functions of the first and second kind respectively and of order one. In the second line, only the most significant terms have been used. In terms of the quantities in (C1), z in (C2) is given by:

$$z=\frac{kab}{\sqrt{b^2+t^2}}$$

Thus, the integral within (C1) becomes approximately:

$$I=\frac{1}{\sqrt{2\pi kab}}\int_{\frac{R-L}{2}}^{\frac{R}{2}}e^{j2k\left(\sqrt{b^2+t^2}-t\right)}\left[e^{j\left(\frac{kab}{\sqrt{b^2+t^2}}-\frac{3\pi}{4}\right)}+e^{-j\left(\frac{kab}{\sqrt{b^2+t^2}}-\frac{3\pi}{4}\right)}\right]dt \qquad \ldots(C3)$$

This integral has a stationary phase region around the point where the first derivative of the exponential function with respect to t is zero.

Consider

$$A = \int e^{j2k\left(\sqrt{b^2+t^2}-t\pm\frac{ab}{2\sqrt{b^2+t^2}}\right)\mp j\frac{3\pi}{4}} \qquad \ldots(C4)$$

$$= \int e^{j2k\mu_{\pm}(t)}dt. \qquad \ldots(C5)$$

The stationary phase point, if one exists within the limits of integration, is at the point where

$$\frac{\partial\mu_{\pm}}{\partial t} = 0 \qquad \ldots(C6)$$

Now

$$\frac{\partial\mu_{\pm}}{\partial t} = \frac{t}{\sqrt{b^2+t^2}} - 1 \mp \frac{ab}{2}\frac{t}{(b^2+t^2)^{\frac{3}{2}}}$$

$$= \frac{t(b^2+t^2)-(b^2+t^2)^{\frac{3}{2}} \mp (abt)/2}{(b^2+t^2)^{\frac{3}{2}}}. \qquad \ldots(C7)$$

Equation (C6) can only be satisfied when:

$$(b^2+t^2)^3 = t^2\left(b^2 \mp \frac{ab}{2} + t^2\right)^2 \qquad \ldots(C8)$$

$$\therefore t^4 + t^2\frac{b^2(3b^2-(b\mp a/2)^2)}{b^2\pm ab} + \frac{b^5}{b\pm a} = 0 \qquad \ldots(C9)$$

Equation (C9) is quadratic in t^2 and its roots are given by:

$$t^2 = \frac{-b(3b^2-(b\mp a/2)^2)}{2(b\pm a)} \pm \frac{1}{2}\sqrt{\left(\frac{b(3b^2-(b\mp a/2)^2)}{b\pm a}\right)^2 - \frac{4b^5}{b\pm a}} \qquad \ldots(C10)$$

With b>a (the tube radius is always larger than the source radius), the roots given by (C10) cannot be positive. But the left side of (C10) is always positive and equal to t^2. Therefore, the initial assumption of equation (C6) cannot be satisfied and therefore, the integral in equation (C1) does not have a stationary phase point within the region of integration.

13 APPENDIX D

STATIONARY PHASE SOLUTION OF EQUATION (4.23)

An asymptotic approximation to the solution of equation (4.23) is obtained here using the method of stationary phase.

$\Phi(R)$ is the normalised reflected wave strength at an axial point receiver distance R from the origin. Equation (4.23) is rewritten here:

$$\Phi(R) = \frac{e^{j\frac{3\pi}{4}}}{\ln\left(\frac{R}{R-L}\right)} 4\sqrt{\frac{\pi}{ka^2}} \int_{\frac{R-L}{2}}^{\frac{R}{2}} \frac{e^{j2k\left(\sqrt{b^2+t^2}-t\right)}}{(b^2+t^2)^{\frac{1}{4}}} J_1\left(\frac{kab}{\sqrt{b^2+t^2}}\right) dt. \qquad \ldots(D1)$$

The integral within (D1) is of the form:

$$I = \int_{t_1}^{t_2} F(t) e^{jk\mu(t)} dt. \qquad \ldots(D2)$$

It was shown in Appendix C that no stationary phase point exists within the region of integration of equation (D2). In this case, it is still possible to obtain an asymptotic approximation of the solution of (D2) using the standard result:

$$I = \frac{1}{jk}\left[\frac{F(t_2)e^{jk\mu(t_2)}}{\mu'(t_2)} - \frac{F(t_1)e^{jk\mu(t_1)}}{\mu'(t_1)}\right] \qquad \ldots(D3)$$

where

$$\mu(t) = 2(\sqrt{b^2+t^2}-t) \quad ; \quad \mu'(t) = 2\left(\frac{t}{\sqrt{b^2+t^2}} - 1\right), \qquad \ldots(D4A)$$

$$F(t) = J_1\left(\frac{kab}{\sqrt{b^2+t^2}}\right)\frac{1}{(b^2+t^2)^{\frac{1}{4}}}, \qquad \ldots(D4B)$$

$$\text{with} \quad t_1 = \frac{R-L}{2} \quad \text{and} \quad t_2 = \frac{R}{2}. \qquad \ldots(D4C)$$

$$\therefore \quad I=\frac{1}{jk}\left[J_1\left(\frac{kab}{\sqrt{b^2+t_2^2}}\right)\frac{1}{(b^2+t_2^2)^{\frac{1}{4}}}\frac{e^{j2k\left(\sqrt{b^2+t_2^2}-t_2\right)}}{\frac{2t_2}{\sqrt{b^2+t_2^2}}-2}-\right.$$

$$\left.-J_1\left(\frac{kab}{\sqrt{b^2+t_1^2}}\right)\frac{1}{(b^2+t_1^2)^{\frac{1}{4}}}\frac{e^{j2k\left(\sqrt{b^2+t_1^2}-t_1\right)}}{\frac{2t_1}{\sqrt{b^2+t_1^2}}-2}\right]. \qquad \ldots(D5)$$

Using $\frac{1}{j}=e^{-j\frac{\pi}{2}}$ and substituting (D5) into (D1) we get an asymptotic approximation to the solution of (D1):

$$\Phi(R)=\frac{e^{j\frac{\pi}{4}}}{\ln\left(\frac{R}{R-L}\right)}\frac{2}{ka}\sqrt{\frac{\pi}{k}}\times$$

$$\left[\frac{(b^2+t_1^2)^{\frac{1}{4}}}{\sqrt{b^2+t_1^2}-t_1}e^{j2k\left(\sqrt{b^2+t_1^2}-t_1\right)}J_1\left(\frac{kab}{\sqrt{b^2+t_1^2}}\right)\right.$$

$$\left.-\frac{(b^2+t_2^2)^{\frac{1}{4}}}{\sqrt{b^2+t_2^2}-t_2}e^{j2k\left(\sqrt{b^2+t_2^2}-t_2\right)}J_1\left(\frac{kab}{\sqrt{b^2+t_2^2}}\right)\right] \qquad \ldots(D6)$$

14 APPENDIX E

APPROXIMATE ANALYTIC SOLUTION OF EQUATION (4.23)

We start off by considering the integral expression in equation (4.23):

$$\Phi = \frac{e^{j\frac{3\pi}{4}}}{\ln\left(\frac{R}{R-L}\right)} 4\sqrt{\frac{\pi}{ka^2}}\, I \qquad \ldots(E1)$$

with

$$I = \int_{\frac{R-L}{2}}^{\frac{R}{2}} \frac{e^{j2k\left(\sqrt{b^2+t^2}-t\right)}}{(b^2+t^2)^{\frac{1}{4}}} J_1\left(\frac{kab}{\sqrt{b^2+t^2}}\right) dt. \qquad \ldots(E2)$$

We make two substitutions:

i)

$$u = \sqrt{b^2+t^2} - t. \qquad \ldots(E3)$$

$$\therefore \quad t = \frac{b^2-u^2}{2u}. \qquad \ldots(E3A)$$

$$\text{Hence} \quad \sqrt{b^2+t^2} = \frac{b^2+u^2}{2u} \qquad \ldots(E3B)$$

$$\text{and} \quad dt = -\frac{bu}{u}\frac{b^2+u^2}{2u}. \qquad \ldots(E3C)$$

Also,

$$t = \frac{R-L}{2} \quad \rightarrow \quad u = u_2 = \sqrt{b^2+\left(\frac{R-L}{2}\right)^2} - \frac{R-L}{2} \qquad \ldots(E3D)$$

$$\text{and} \quad t = \frac{R}{2} \quad \rightarrow \quad u = u_1 = \sqrt{b^2+\left(\frac{R}{2}\right)^2} - \frac{R}{2}. \qquad \ldots(E3E)$$

ii)

$$v = \frac{u}{b} \qquad \ldots(E4)$$

$$\therefore \quad v_2 = \sqrt{1+\left(\frac{R-L}{2b}\right)^2} - \frac{R-L}{2b} \qquad \ldots(E4A)$$

$$\text{and} \quad v_1 = \sqrt{1+\left(\frac{R}{2b}\right)^2} - \frac{R}{2b}. \qquad \ldots(E4B)$$

Equation (E2) thus becomes:

$$I = \sqrt{\frac{b}{2}} \int_{v_1}^{v_2} \frac{\sqrt{1+v^2}}{v^{\frac{3}{2}}} e^{j2kbv} J_1\left(\frac{2kbv}{1+v^2}\right) dv. \qquad \ldots(E5)$$

Expanding the first order Bessel function within (E5) in an asymptotic series [83] gives:

$$J_1 = \frac{1}{2}[H_1^{(1)}(z) + H_1^{(2)}(z)] \approx$$

$$\approx \frac{1}{\sqrt{2\pi z}} \left\{ e^{j\left(z-\frac{3\pi}{4}\right)} F_1(z) + e^{-j\left(z-\frac{3\pi}{4}\right)} F_2(z) \right\} \qquad \ldots(E6)$$

When $H_1^{(1)}$ and $H_1^{(2)}$ are first order Hankel functions of the first and second kind respectively. $F_1(z)$ and $F_2(z)$ are hypergeometric series which are assumed to be slowly varying in view of the large value of 2kb (≈38 at 20kHz).

With

$$z = \frac{2kav}{1+v^2}$$

we have

$$I \approx \frac{1}{2}\sqrt{\frac{b}{2\pi kb}} \int_{v_1}^{v_2} \frac{1+v^2}{v^{\frac{3}{2}}} \times$$

$$\left\{ e^{-j\frac{3\pi}{4}} F_1(z) e^{j2kb\left(v+\frac{a}{b}\frac{v}{1+v^2}\right)} + e^{j\frac{3\pi}{4}} F_2(z) e^{j2kb\left(v-\frac{a}{b}\frac{v}{1+v^2}\right)} \right\}. \qquad \ldots(E7)$$

Now use

$$I = I_1 + I_2 \qquad \ldots(E8)$$

with

$$I_1 = \frac{1}{2}\sqrt{\frac{b}{2\pi ka}} \int_{v_1}^{v_2} \frac{(1+v^2)}{v^{\frac{3}{2}}} e^{-j\frac{3\pi}{4}} F_1(z) e^{j2kb\left(v+\frac{a}{b}\frac{v}{1+v^2}\right)} dv \qquad \ldots(E9)$$

and a similar expression for I_2.

Splitting the first term in an expansion of equation (E9) in terms of equation (E9) into two:

$$\int_{v_1}^{v_2} .. = \int_{v_1}^{\infty} .. - \int_{v_2}^{\infty} .. \qquad ...(E10)$$

Consider the first term in an expansion of equation (E9) in terms of equation (E10):

$$I_3 = e^{-j\frac{3\pi}{4}} F_1(z_1) \int_{v_1}^{\infty} \left(1 + \frac{1}{v^2}\right) e^{j2kbv\left(1+\frac{a}{b}\frac{1}{1+v^2}\right)} dv. \qquad ...(E11)$$

Using

$$\Gamma_1 = 2kd\left(1 + \frac{a}{d}\frac{1}{1+v_1^2}\right) \qquad ...(E12)$$

equation (E11) becomes:

$$I_3 = e^{-j\frac{3\pi}{4}} F_1(z_1)\left\{-\frac{1}{j\Gamma_1} e^{j\Gamma_1 v_1} + \frac{1}{v_1} e^{j\Gamma_1 v_1} + j\Gamma_1 \int_{v_1}^{\infty} \frac{e^{j\Gamma_1 v}}{v} dv\right\}. \qquad ...(E12)$$

The remaining integral in (E12) is of the form:

$$\int_{\Gamma_1 v_1}^{\infty} \frac{e^{jq}}{q} dq = e^{j\Gamma_1 v_1}\{g(\Gamma_1 v_1) + jf(\Gamma_1 v_1)\} \qquad ...(E13)$$

where g and f are auxiliary Fresnel functions [83].

Thus, (E12) becomes:

$$I_3 = e^{-j\frac{3\pi}{4}} F_1(z_1) e^{j\Gamma_1 v_1}\left\{-\frac{1}{j\Gamma_1} + \frac{1}{v_1} + j\Gamma_1[g(\Gamma_1 v_1) + jf(\Gamma_1 v_1)]\right\} \qquad ...(E14)$$

with $\Gamma_1 \approx 2kb \approx 38$ at 20kHz, $\Gamma_1 v_1 \gg 1$ for most frequencies of interest, we can use the asymptotic expansion of the auxiliary functions:

$$g(z) \approx \frac{1}{z^2} \quad \text{and} \quad f(z) \approx \frac{1}{z} \qquad ...(E15)$$

giving for (E14):

$$I_3 \approx e^{-j\frac{3\pi}{4}} F_1(z_1) e^{j\Gamma_1 v_1} \frac{j}{\Gamma_1}\left(1 + \frac{1}{v_1^2}\right) \qquad ...(E16)$$

with

$$z_1 = \frac{2kav_1}{1+v_1^2}$$

and

$$e^{j\Gamma_1 v_1} = e^{j2kbv_1} e^{j2ka\frac{v_1}{1+v_1^2}}.$$

Further,

$$H_1^{(1)}(z) \approx \sqrt{\frac{2}{\pi z}} e^{j\left(z-\frac{3\pi}{4}\right)} F_1(z). \qquad \ldots(E17)$$

Thus, the result can be written in the form:

$$I_3 \approx \frac{j\left(1+\frac{1}{v_1^2}\right)}{2kb\left(1+\frac{a}{b}\frac{1}{1+v_1^2}\right)} \sqrt{\frac{\pi kav_1}{1+v_1^2}} H_1^{(1)}\left(\frac{2kav_1}{1+v_1^2}\right) e^{j2kav_1} \qquad \ldots(E18)$$

$$\therefore \quad I_3 \approx \frac{j\sqrt{\pi ka}}{2kb\left(1+\frac{a}{b}\frac{1}{1+v_1^2}\right)} \sqrt{\frac{1+v_1^2}{v_1^{\frac{3}{4}}}} H_1^{(1)}\left(\frac{2kav_1}{1+v_1^2}\right) e^{j2kav_1}. \qquad \ldots(E19)$$

Using equations (E8-E11) with (E19) to substitute for (E2) in (E1) we get:

$$\Phi \approx \frac{e^{-j\frac{\pi}{4}}}{\ln\left(\frac{R}{R-L}\right)} \sqrt{\frac{2\pi}{kb}} \frac{1}{ka}$$

$$\left[\frac{1+v_1^2}{v_1^{\frac{3}{4}}} e^{j\left(2kbv_1+\frac{\pi}{4}\right)} \left\{\frac{J_1\left(\frac{2kav_1}{1+v_1^2}\right) - j\frac{a}{b\left(1+v_1^2\right)} Y_1\left(\frac{2kav_1}{1+v_1^2}\right)}{1-\left(\frac{a}{b(1+v_1)}\right)^2}\right\} -\right.$$

$$\left. -\frac{1+v_2^2}{v_2^{\frac{3}{4}}} e^{j\left(2kbv_2+\frac{\pi}{4}\right)} \left\{\frac{J_1\left(\frac{2kav_2}{1+v_2^2}\right) - j\frac{a}{b\left(1+v_2^2\right)} Y_1\left(\frac{2kav_2}{1+v_2^2}\right)}{1-\left(\frac{a}{b(1+v_2)}\right)^2}\right\}\right]. \qquad \ldots(E20)$$

Here v_1 and v_2 are given by equations (E4A) and (E4B), and $J_1()$ and $Y_1()$ represent, respectively, Bessel and Neuman functions of the first order and first kind.